Implications of direct anthropogenic pressures on dissolved oxygen dynamics in a well-mixed estuary

Dissertation
zur Erlangung des Doktorgrades
der Mathematisch-Naturwissenschaftlichen Fakultät
der Christian-Albrechts-Universität
zu Kiel

vorgelegt von
Ingrid Holzwarth

Kiel 2018

Erster Gutachter:	Prof. Dr. Kai W. Wirtz
Zweiter Gutachter:	Prof. Dr. Andreas Oschlies

Tag der mündlichen Prüfung:	11. September 2018

We all live downstream.

Content

Summary

Dissolved oxygen (DO) is a central element in the biogeochemistry and ecology of aquatic systems. Nevertheless, severe DO deficits are increasingly observed worldwide and particularly in the coastal zone. Even vertically well-mixed estuaries are affected, despite their physically favorable condition for atmospheric oxygen input. While many well-mixed estuaries serve as marine shipping routes to large ports, they contain a shipping channel with substantially deepened bathymetry. However, the impact of man-made bathymetric modification on DO deficits is largely unknown, especially in proportion to anthropogenic nutrient enrichment which is accepted as the main cause in the coastal zone.

To fill this knowledge gap in a first step, a biogeochemical model is coupled to an idealized but effective hydrodynamic model set-up that is able to represent a vertically well-mixed estuary. The biogeochemical model configuration is tailored to the problem of DO deficits. Its results, including a parameter sensitivity analysis, clearly show that the biogeochemical system is dominated by the oxygen-consuming processes of detritus remineralization and, to a lesser extent, nitrification. Primary production within the estuary only plays a minor role due to severe light limitation. A scenario analysis indicates that a reduction in riverine nutrient and organic matter load scales down all biogeochemical processes. Furthermore, the scenarios illustrate that the interplay between water surface-to-volume ratio and the degradability state of the organic material is the most important factor to determine the severity of the DO minimum. Man-made bathymetric modifications change the surface-to-volume ratio, and thus the capacity to recover DO losses by reaeration. The modifications also change transport characteristics and with it the degradability state of the organic material at a specific position. Consequently, the study generally demonstrates the relevance of bathymetric factors during the assessment of human interference on DO dynamics and biogeochemical processes in estuaries.

The second study focusses on the physical mechanisms of bathymetric modification that were identified as critical in the first study; these mechanisms are analyzed with a more realistic three-dimensional model of the Elbe Estuary. Particularly, the impact of bathymetric deepening on the transport time scale is analyzed in detail with respect to water age. Riverine water age, as a hydrodynamic indicator for the completeness of riverine organic matter degradation, changes by about 7 % between two realistic bathymetries that differ in the effects of 40 years of man-made modification. By contrast, the impact of the natural variability in freshwater discharge can lead to a multiplication in riverine water age by the factor of four to five and thus clearly exceeds the impact of the bathymetric change. Comparable to the small impact in riverine water age, the bathymetric difference induces a moderate, 10 – 15 % change in the ratio of water surface to underlying water volume, which is a hydrodynamic indicator for the effect of reaeration on DO

concentration enrichment. Notwithstanding their small magnitude, both indicators hint at an exacerbation of DO deficits with deeper bathymetry and thus at bathymetric modification as an additional anthropogenic stressor.

As a by-product, this study provides the derivation of an empirical description for riverine water age in dependence of freshwater discharge at specific locations in the estuary. Such descriptions can be used for predictive purpose of transport time scales, and for the study on the effect of variation in river discharge and location on riverine water age.

Finally, the preliminary outcome of small impacts of bathymetric modification is further inspected in a third study. The methods developed in the previous studies are combined to create a three-dimensional hydrodynamic-biogeochemical model of the Elbe Estuary as an example for a well-mixed estuary type. Factorial analysis of simulation results explains the formation of the estuarine oxygen minimum by a sequence of oxygen-consuming processes. Among others, the small impact of the realistic bathymetric change in the order of 5 % oxygen saturation change is confirmed, while a 50 % variation in riverine load has a much larger effect on the DO deficit. Nevertheless, bathymetric modifications pose an additional stressor to the oxygen system and the cumulative effect of many bathymetric modifications over centuries may be particularly relevant, especially in combination with the human activities related to the maintenance of the artificially deeper bathymetry.

Overall, this thesis shows that the impact of man-made bathymetric modification on DO deficits in well-mixed estuaries is smaller than the eutrophication effect due to anthropogenic nutrient enrichment.

Zusammenfassung

Im Wasser gelöster Sauerstoff (DO) ist ein zentrales Element der Biogeochemie und ökologischen Funktionsfähigkeit aquatischer Systeme. Jedoch werden weltweit zunehmend massive DO Defizite beobachtet, besonders in Küstengebieten. Selbst vertikal gut durchmischte Ästuare sind betroffen, trotz ihrer physikalisch guten Voraussetzungen für die Anreicherung von Sauerstoff aus der Atmosphäre. Viele gut durchmischte Ästuare dienen als marine Schifffahrtswege zu großen Häfen und haben eine Fahrrinne mit einer erheblich vertieften Bathymetrie. Die Rolle menschlich verursachter bathymetrischer Änderungen als ein möglicher Stressor für DO Defizite ist unbekannt, insbesondere im Verhältnis zur anthropogen bedingten Nährstoffanreicherung, die allgemein als Hauptursache im Küstenraum anerkannt ist.

Um diese Wissenslücke zu füllen, wird in einem ersten Schritt ein biogeochemisches Modell mit einem hydrodynamischen Modell gekoppelt, das in der Lage ist die Bathymetrie präzise abzubilden. Eine biogeochemische Modellkonfiguration wird, auf Sauerstoffdefizite in Ästuaren angepasst, entwickelt und in einem Modell mit geometrischer Idealisierung eines vertikal gut durchmischten Ästuars angewendet. Die Ergebnisse, die auch eine Studie zur Parametersensitivität beinhalten, zeigen deutlich, dass das biogeochemische System durch die sauerstoffzehrenden Prozesse der Remineralisierung von Detritus sowie, wenn auch in geringerem Umfang, Nitrifikation dominiert ist. Primärproduktion spielt aufgrund starker Lichtlimitierung im Ästuar selbst nur eine untergeordnete Rolle. Die Analyse von Szenarien deutet darauf hin, dass eine Reduktion der flussseitigen Belastung alle biogeochemischen Prozesse vermindert. Weiterhin zeigen die Szenarien, dass das Zusammenspiel von Oberfläche/Volumen-Verhältnis und der Abbaubarkeit des organischen Materials der bestimmende Faktor für die Größe des Sauerstoffminimums ist. Bathymetrische Modifikationen verändern das Oberfläche/Volumen-Verhältnis und damit die Fähigkeit Sauerstoffverluste durch atmosphärischen Eintrag auszugleichen. Außerdem verändern sie die Transporteigenschaften und damit die Abbaubarkeit des organischen Materials. Somit zeigt diese Studie allgemein die Relevanz bathymetrischer Einflüsse durch menschliche Eingriffe auf die Sauerstoffdynamik und biogeochemische Prozesse in Ästuaren.

Der Schwerpunkt einer zweiten Studie sind die wesentlichen physikalischen Einflussmechanismen bathymetrischer Modifikationen, die in der ersten Studie erkannt wurden. Zur Untersuchung in einem realitätsnahmen, dreidimensionalen Modell des Elbeästuars wird der Einfluss bathymetrischer Vertiefungen auf die Zeitskala des Stofftransportes analysiert und dabei das Konzept des Wasseralters verwendet. Dabei dient das flussseitige Wasseralter als hydrodynamischer Indikator für die Vollständigkeit des Abbaus organischer Masse. Dieser Indikator zeigt lediglich kleine Unterschiede von etwa 7 % bei der Anwendung auf zwei realistischen Bathymetrien, die sich durch Auswirkungen von 40 Jahren menschlicher Eingriffe unterschieden. Die

natürliche Variabilität des Oberwasserzuflusses hat mit einer Vervier – bis Verfünffachung des Wasseralters einen wesentlich größeren Einfluss als die bathymetrische Änderung. Ähnlich dem kleinen Einfluss auf das flussseitige Wasseralter führt die bathymetrische Änderung auch zu einer moderaten Änderung von 10 – 15 % des Verhältnisses von Wasseroberfläche zu darunterliegendem Wasservolumen, was ein hydrodynamischer Indikator für den Einfluss des atmosphärischen Sauerstoffaustausches auf die Anreicherung der DO Konzentration ist. Ungeachtet ihrer kleinen Größenordnung deuten beide Indikatoren auf eine Verschärfung des DO Defizits mit vertiefter Bathymetrie und damit auf bathymetrische Modifikation als einen weiteren anthropogenen Stressor.

Ein Nebenprodukt dieser Studie ist die Herleitung einer empirischen Beschreibung für das flussseitige Wasseralter in Abhängigkeit des Oberwasserzuflusses für einzelne Orte entlang des Ästuars. Solche Beschreibungen können für Vorhersagen von Transportzeit verwendet werden.

Schließlich wird der vermutlich kleine Einfluss einer realistischen bathymetrischen Veränderung in einer dritten Studie genauer untersucht. Dazu werden die in den vorangegangenen Studien entwickelten Methoden zu einem dreidimensionalen hydrodynamisch-biogeochemischen Modell des Elbeästuars als Beispiel eines gut durchmischten Systems kombiniert. Die Ergebnisse für die Simulation des aktuellen Zustandes erklären die Entstehung des ästuarinen Sauerstoffminimums durch aufeinanderfolgende sauerstoffzehrende Prozesse. Die Analyse von Szenarien bestätigt den kleinen Einfluss der realistischen bathymetrischen Änderung auf die DO Dynamik in einer Größenordnung von 5 % und zeigt darüber hinaus, dass eine Halbierung der flussseitigen Belastung eine deutlich größere Auswirkung auf das DO Defizit hat. Dennoch stellen bathymetrische Modifikationen einen weiteren Stressor für den Sauerstoffhaushalt dar und die kumulative Wirkung vieler bathymetrischer Modifikationen über Jahrhunderte kann relevant sein, insbesondere im Zusammenhang mit menschlichen Eingriffen zur Unterhaltung der künstlich hergestellten Wassertiefen.

Insgesamt zeigt diese Arbeit, dass die Auswirkungen einer menschengemachten bathymetrischen Modifikation auf Sauerstoffdefizite in gut durchmischten Ästuaren geringer sind als der Einfluss der Eutrophierung durch anthropogene Nährstoffanreicherung.

1. Introduction

1.1. Oxygen deficits in estuarine environments

Dissolved oxygen (DO) is a central element in the biogeochemistry and ecology of aquatic systems. The availability of DO is substantial for most aquatic animals and low DO concentrations affect aquatic life on various levels, from molecular responses inside an individual organism to entire ecosystem changes [*Diaz and Rosenberg,* 1995; *Wu,* 2002; *Breitburg,* 2002; *Ekau et al.,* 2010; *Roman et al.,* 2012; *Wang et al.,* 2016; *McCormick and Levin,* 2017]. At the same time, DO takes passive and active roles in various biogeochemical processes: DO concentration is influenced by e.g. primary production, organic matter respiration and nitrification while it controls several redox-reaction that determine the nitrogen, manganese, iron, sulphur and phosphorous cycling [*Testa and Kemp,* 2011]. Notwithstanding the key role of DO in aquatic environments, clear indication exists that low oxygen conditions in surface waters have increased due to anthropogenic influences [*Diaz,* 2001; *Diaz and Rosenberg,* 2008; *Rabalais et al.,* 2010; *Jenny et al.,* 2016] and will continue to exacerbate under non-reduced nutrient input and anthropogenic climate change conditions [*Meier et al.,* 2011; *Rabalais et al.,* 2014].

Under equilibrium condition, the DO concentration in surface water is equal to its saturation concentration, or solubility, which ranges from 456 µmol l^{-1} (14.6 mg l^{-1}) at 0 °C and 0 psu to 194 µmol l^{-1} (6.2 mg l^{-1}) at 30 °C and 35 psu, respectively [*Weiss,* 1970; *Benson and Krause Jr.,* 1984]. Physical or biogeochemical processes in the water may produce an actual oxygen concentration that deviates from saturation concentration. In case the actual DO concentration is lower than saturation concentration, the water is oxygen undersaturated and the difference between actual and saturation concentrations is termed oxygen deficit. The inverse may exist as well with water being oversaturated, carrying an oxygen surplus.

The definition of a threshold value at which low DO concentration, DO deficits or undersaturation become problematic in surface waters is difficult as it strongly depends on the process, specie or ecosystem under consideration [*Eby and Crowder,* 2002; *Vaquer-Sunyer and Duarte,* 2008]. When dealing with problematically low oxygen concentrations in estuarine and coastal systems, the most frequently used term in literature is hypoxia, e.g. in [*Kuo and Neilson,* 1987; *Justić et al.,* 1993; *Diaz and Rosenberg,* 1995; *Hagy et al.,* 2004; *Baird et al.,* 2004; *Paerl,* 2006; *Talke et al.,* 2009; *Zhu et al.,* 2011; *Howarth et al.,* 2011; *Lanoux et al.,* 2013; *Lajaunie-Salla et al.,* 2017] and many others. 2 mg l^{-1} (63 µmol l^{-1}) is the common threshold value below which conditions are termed hypoxic [*Diaz,* 2001; *Rabalais et al.,* 2010], though sometimes slightly different values are used, e.g in *Diaz and Rosenberg* [1995].

In this thesis the term “estuarine oxygen minimum zone (eOMZ)” will be used; it describes a DO deficit that can be clearly identified either in a time series at one specific position or on a longitudinal profile at a specific date, see Figure 1. Thereby, the eOMZ does not depend on a defined threshold value.

Generally, oxygen deficits develop where DO consumption exceeds DO gain from production and atmospheric enrichment. The DO consuming processes are mainly heterotrophic remineralization of organic matter, and nitrification, whereas DO is produced by primary production. The oxygen exchange with the atmosphere is a compensation process in case of an oxygen deficit (or surplus).

There is rare evidence of natural – in the meaning of not anthropogenically caused – oxygen minima in estuarine systems; if at all, natural oxygen minima may occur in coastal areas close to upwelling of deeper oceanic waters [*Rabalais et al.,* 2010; *Zhang et al.,* 2010; *Roegner et al.,* 2011] or enclosed/semi-enclosed basins like fjords or the Black Sea [*Rabalais et al.,* 2010]. The observed increase in severe oxygen deficits in estuaries is attributed to human-caused eutrophication, in the definition of *Nixon* [1995], with increased supply of organic matter. Whereas historically the oxidation of organic matter from untreated sewage caused oxygen deficits in rivers and estuaries [*Streeter and Phelps,* 1925; *Sharp et al.,* 1982; *Harremoës,* 1982; *Parker and O'Reilly,* 1991; *O'Shea and Brosnan,* 2000], it is nowadays due to massive nutrient enrichment, particularly nitrogen, from agricultural fertilizers, which generates nutrient-fueled primary production with subsequent oxygen-consuming microbial respiration of its detritus [*Nixon,* 1995; *Cloern,* 2001; *Diaz and Rosenberg,* 2008; *Howarth et al.,* 2011; *Fulweiler et al.,* 2012].

Classically, low oxygen conditions have been mainly reported from systems subjected to vertical stratification, like the ocean, lakes and stratified estuaries [*Wyrtki,* 1962; *Legović et al.,* 1991; *Stanley and Nixon,* 1992; *Wiseman et al.,* 1997; *Fujiwara et al.,* 2002; *Diaz and Breitburg,* 2007; *Wei et al.,* 2007; *Murphy et al.,* 2011; *Müller et al.,* 2012; *Bruce et al.,* 2014; *Qian et al.,* 2018]. In vertically well-mixed systems, low oxygen conditions are less frequent but they are increasingly observed, also in systems that were thought to be immune to hypoxia [*Verity et al.,* 2006].

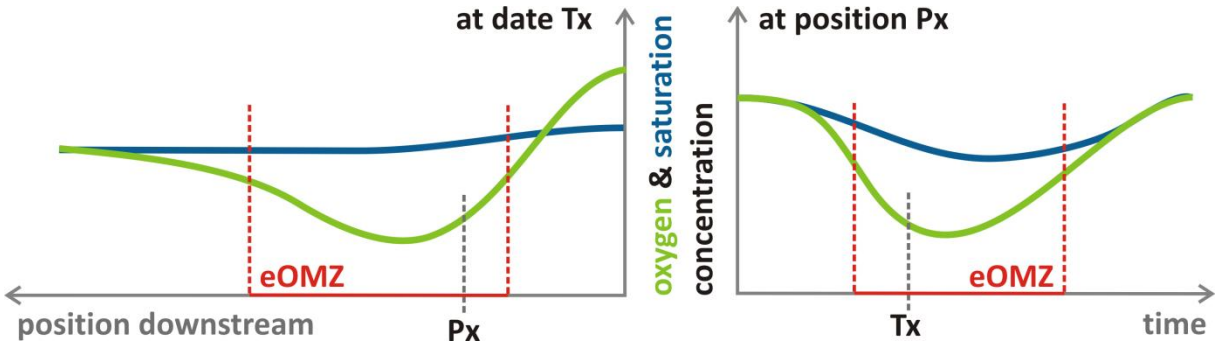

Figure 1: Sketch of an eOMZ in space (left) and time (right). Green lines show actual dissolved oxygen concentration, blue lines represent oxygen saturation concentration. The oxygen deficit is the gap between actual concentration and saturation, between green and blue line, respectively.

Though sometimes, it is located in the estuarine turbidity maximum [*Abril et al.,* 2003; *Etcheber et al.,* 2007], the eOMZ mainly occurs in the freshwater tidal river section [*Álvarez-Salgado and Miller,* 1999; *Amann et al.,* 2012] which is governed by both strong river inflow and tidal range. There, the eOMZ vertically extends over the entire water column of usually 5 to 15m and is characterized by a seasonal persistency of several months, typically summer [*Verity et al.,* 2006; *Kemp et al.,* 2009; *Zhang et al.,* 2010].

In well-mixed estuaries, the direction of the eOMZ formation is horizontal, following the decrease in light availability which is due to an increase in water depth and mineral suspended sediment concentration. One can distinguish between three different sections (see Figure 2 right), as described in *Schroeder* [1997] and *Amann et al.* [2012]: first, in the most upstream section, primary production prevails over heterotrophic processes. Second, primary production ceases downstream because of severe light limitation. Detritus degradation depletes more oxygen than can be supplied through the water surface, generating the eOMZ. In the third section further downstream, most (fresh) material is degraded and reaeration balances the oxygen deficit. Those three zones are similar to the classical picture of the DO sag formation in rivers downstream of a point of sewage discharge [*Streeter and Phelps,* 1925; *Chapra,* 2008].

In stratified systems, the relevant direction for the formation of oxygen minimum zones is vertical. In the open ocean, as an example for stratified systems, distinct zones of oxygen minima can be found at depths between 400 m and 1200 m [*Wyrtki,* 1962; *Keeling et al.,* 2010]. In ocean research, the term oxygen minimum zone refers to areas where these concentration minima are particularly low, like less than 20 µmol l^{-1}, though an universally valid threshold is difficult to define [*Paulmier and Ruiz-Pino,* 2009]. Here, general patterns of eOMZs are compared to their oceanic counterparts and, thus, the term oceanic oxygen minimum zone (oOMZ) is refered to ocean oxygen minimum layers at depths mentioned above, regardless of a limiting value. When considering the commonly used value of 63 µmol l^{-1}, or 2 mg l^{-1}, to characterize coastal and estuarine hypoxia [*Rabalais et al.,* 2010], the oxygen minimum layer in the entire North Pacific and Equatorial Indian Ocean as well as in parts of the Equatorial Atlantic falls within this hypoxia criterion [*Keeling et al.,* 2010; *Schmidtko et al.,* 2017]. For oOMZs, *Wyrtki* [1962] gives a simplified picture which describes the formation in the vertical, also based on three layers. The first vertical layer is well ventilated. In addition, light availability allows for primary production. The second layer below is less well ventilated due to thermal stratification, less well illuminated, and oxygen consumption is high due to sinking of degradable material, leading to low oxygen concentrations. The lowermost third layer has higher oxygen content because of lateral advection of oxygen-rich waters.

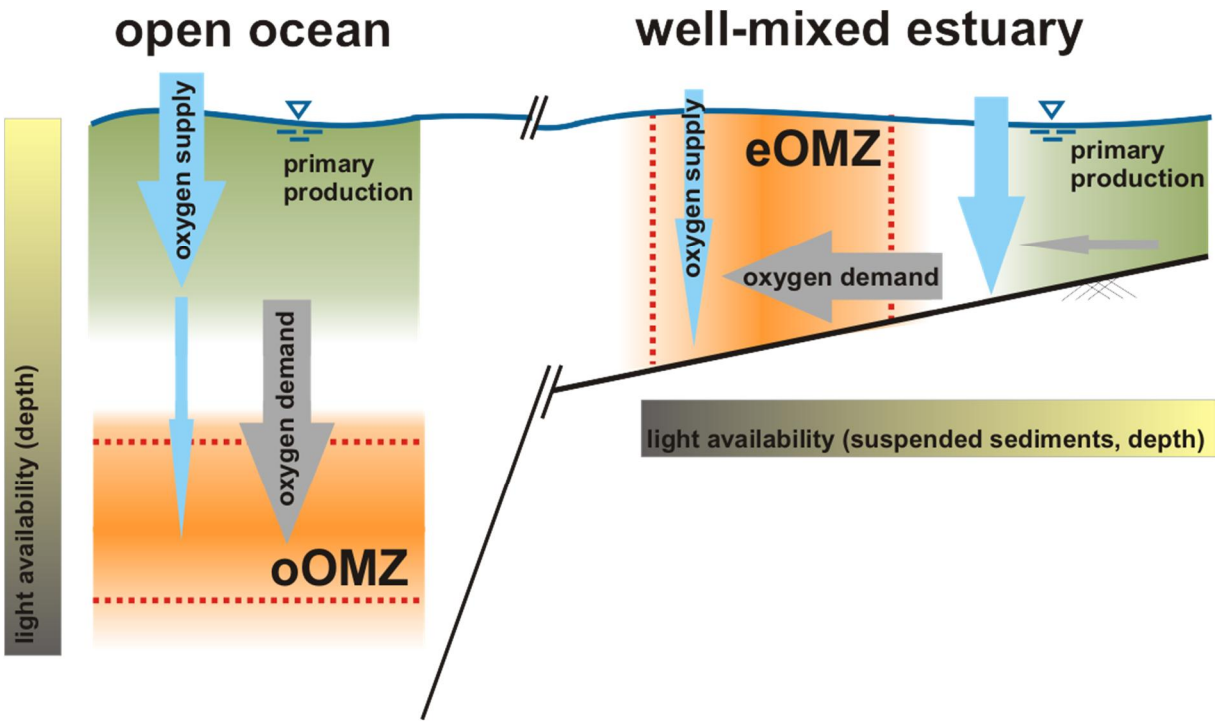

Figure 2: Conceptual picture of the oxygen minimum formation in a well-mixed estuary (eOMZ – estuarine oxygen minimum zone) and in the open ocean (oOMZ – ocean oxygen minimum zone). The direction of the oxygen minimum formation in both systems is along the direction of declining light availability and therefore horizontal in estuaries and vertical in the ocean.

In his work on the importance of biogeochemical processes and circulation forming oOMZs, *Wyrtki* [1962] concluded that "…biogeochemical processes are responsible for the existence of oxygen minima, but circulation is responsible for the position." This statement, when transferred to estuaries, also includes the interplay with geometry, because geometry strongly influences circulation (which are the hydrodynamics/physical processes) and biogeochemical processes in estuaries.

Figure 2 conceptually shows the oxygen minimum formation (oxygen demand outweighs oxygen supply) in a vertically well-mixed estuary and in the open ocean. In both cases, the physical control on oxygen demand in the minimum zone is determined by the transport processes of degradable organic matter: in the vertically well-mixed case organic matter is predominantly transported by horizontal advection, whereas in the stratified system, the relevant transportation direction for the oxygen minimum formation is vertical by sinking and vertical mixing. The physical control on oxygen supply (reaeration) in the stratified system is given by the intensity of vertical mixing and thus determined by the strength of the stratification, while in the vertically well-mixed estuary oxygen supply is determined by the amount of oxygen flux through the water-atmosphere interface.

1.2. Human impact

The influence of human activities on earth shows effects on a large scale so that sometimes the current geological epoch is termed the Anthropocene, see e.g. *Zalasiewicz et al.* [2010] for a discussion. The perception of the actual world as human-dominated [*Vitousek,* 1997] is mostly linked to global phenomena, particularly anthropogenic climate change [*Oreskes,* 2004; *Rosenzweig et al.,* 2008], which is expected to affect surface waters mainly by an increase in water temperature, changes in river discharge [*van Vliet et al.,* 2013] , and sea level rise [*Nicholls and Cazenave,* 2010]. These effects and their consequences for DO are a topic of ongoing research in estuarine and coastal science [*Najjar et al.,* 2000; *Justić et al.,* 2005; *Whitehead et al.,* 2009; *Najjar et al.,* 2010], anticipating lower DO concentrations mainly due to lower oxygen solubility and higher organic matter mineralization rates.

Another anthropogenically induced, worldwide impact on DO in estuaries is eutrophication: the enrichment of nutrients, particularly nitrogen and phosphorous, stimulates primary production and therefore increases organic matter production [*Nixon,* 1995; *Smith,* 1998; *Fulweiler et al.,* 2012]. Nutrient enrichment can be conceived as a global phenomenon [*Seitzinger et al.,* 2010], especially with regard to its effect on the world's oceans, e.g. [*Duce et al.,* 2008]. In contrast, the eutrophication impact on a specific estuary solely arises from its own catchment. One can therefore consider estuarine eutrophication as a global anthropogenic change with local and direct impact. Likewise, more anthropogenically driven changes with direct impacts in estuaries exist and occur worldwide [*Bianchi,* 2007; *Halpern et al.,* 2008; *Cloern et al.,* 2016].

Bathymetric modification is a man-made change that has attracted little attention in the context of eOMZs. Though, most estuaries are waterways for ships, and many estuaries host large ports in their upper regions; to ensure navigability, also for large container vessels, a shipping channel is developed and maintained in these estuaries, like in the Columbia River Estuary [*Sherwood et al.,* 1990], the Scheldt [*Meire et al.,* 2005], the Yangtze [*Wu et al.,* 2016], the Elbe [*Boehlich and Strotmann,* 2008], the Seine [*Marmin et al.,* 2014], the Guadalquivir [*Ruiz et al.,* 2015], the Loire [*Brossard et al.,* 1990], San Francisco Bay [*Dallas and Barnard,* 2011] and many more.

While the combined contributions of climate change and eutrophication on eOMZs are widely studied, e.g. in [*Rabalais et al.,* 2009; *Gilbert et al.,* 2010], there is less research on the contributions of other local human interventions. In well-mixed systems, the effects of a deepened bathymetry are particularly interesting because the physical factors of eOMZ formation are affected: deepening (i) influences hydrodynamics including the transport of degradable organic matter and thus the pathway of oxygen demand (see Figure 2), and (ii) reduces the ratio of water surface to water volume, therefore the atmospheric interface for reaeration and thus the pathway of oxygen supply.

1.3. Modeling coupled hydrodynamic – biogeochemical processes in estuaries

The estuarine environment is usually characterized by high-energy hydrodynamic processes induced by the tides, water density differences and river inflow. The complexity and variability of the resulting hydrodynamic processes usually requires a three-dimensional simulation of water movement, including the transport of salinity and sometimes also water temperature [*Warner,* 2005; *Zhang and Baptista,* 2008; *Gross et al.,* 2010; *Sehili et al.,* 2014; *Kärnä and Baptista,* 2016a; *MacWilliams et al.,* 2016]. The simulation of 3D hydrodynamics has become a standard method during the last decades. An overall trend to increase the complexity in hydrodynamic models, indicated by an increase in the number of computational cells and decrease in maximum grid resolution, is shown by *Ganju et al.* [2016]. This trend is straightforward given the broad consensus on the mathematical description of water flow. In contrast, the modeling of ecological processes is complicated by the inherent complexity of biological systems, limited understanding of several processes and sparse availability of observational data, leading to over-parameterization, high model uncertainty and error propagation [*Ganju et al.,* 2016]. These difficulties, together with the wish to develop models that are as general as possible to be easily transferable [*Evans et al.,* 2013], retarded the establishment of 3D, high resolution estuarine biogeochemical models in a way similar to hydrodynamic models. Nevertheless, several coupled hydrodynamic-biogeochemical models exist with applications mainly in coastal areas, shelf seas and stratified estuaries [*Wool et al.,* 2003; *Cerco and Noel,* 2004; *Webster and Harris,* 2004; *Xu and Hood,* 2006; *Neumann and Schernewski,* 2008; *Fennel et al.,* 2011; *Khangaonkar et al.,* 2012; *Testa et al.,* 2014; *Wild-Allen and Andrewartha,* 2016; *Kerimoglu et al.,* 2017; *Lajaunie-Salla et al.,* 2017]. These estuarine 3D models vary greatly in their complexity, both in terms of geometric resolution and process description, but their common aim is the assessment of eutrophication effects on either DO concentrations or nutrient, particularly nitrogen, cycling. Bathymetric deepening as a widespread local human intervention has not yet been analyzed.

For this thesis I applied the mathematical model Untrim for hydrodynamic simulation in a version that enables the description of the bathymetry on subgrid level [*Casulli,* 2009; *Casulli and Stelling,* 2010] and thus also a precise representation of water volume. Another advantage of this method for subgrid scale bathymetry is the possibility to also model the water surface area on subgrid scale and thus in great detail: whereas in classical approaches to wetting and drying grid cell can be only handled as either wet or dry, in the method for subgrid bathymetry of *Casulli* [2009] grid cells in the intertidal area can also be partially wet.

For the simulation of biogeochemical processes in this thesis, the Deltares Water Quality Model [*Postma et al.,* 2003; *Blauw et al.,* 2009; *Smits and van Beek,* 2013] was coupled to the hydrodynamic model Untrim in offline mode and in a mass-conserving way [*Lang,* 2012]. I configured

the biogeochemical processes (see Chapter 2 and Appendix A) with state variables for DO, inorganic macronutrients, phytoplankton and several pools of degradable organic material to describe the processes of phytoplankton growth, respiration, mortality, organic matter degradation, remineralization, nitrification and denitrification.

1.4. The Elbe Estuary as test site

The Elbe Estuary is the tidally influenced, approximately 140 km long part of the Elbe River which today has a total length of 1 094 km. The catchment of the Elbe River is fourth largest in Middle Europe with about 148 000 km², thereof 2/3 belonging to Germany, and 24.5 Mio inhabitants. The Elbe is a lowland river with only about ½ of its length lying 200 m above mean sea level. The temperate climate includes average air temperatures of 8-9 °C in the lowland and a hydrographic regime with highest discharges usually in spring. These figures on the Elbe Estuary are cited from *IKSE* [2005] and more detailed information, especially on the catchment, can be found therein.

Long-term mean freshwater discharge at the last gauging station upstream of the tidal limit at Geesthacht Weir is 713 $m^3 s^{-1}$; mean summer low discharge is 301 $m^3 s^{-1}$, and mean winter high discharge is 1870 $m^3 s^{-1}$, respectively [*FHH and HPA,* 2014]. The estuary is a well-mixed mesotidal/macrotidal coastal plain estuary [*Kappenberg and Grabemann,* 2001; *Middelburg and Herman,* 2007] with an inland delta at about 20 – 40 km downstream of the tidal weir. In the area of this inland delta, the Port of Hamburg is located; it is Germany's largest seaport and currently rank three among the largest container ports in Europe (rank eighteen worldwide). Next to natural changes, the estuary has been subjected to man-made modifications for centuries - if not millennia - by diking, land reclamation, realignment, riverine water quantity management and navigation channel deepening [*IKSE,* 2005]. Thus, the geometry of the Elbe Estuary today looks very different from what one might see in case of no human modification.

In addition to the geometric impacts, humans have impacted water quality, with highest organic, phosphorus and contaminant pollution before the 1990s (before the German reunification). Since then, water quality has improved, except for nitrate and certain heavy metals [*Pusch,* 2006]. However, concentrations in nutrients (as total nitrogen and total phosphorous) are still high [*IKSE,* 2016]. They promote, in combination with favorable light climate and high retention times in the riverine section, limnic primary production leading to maximum concentrations as high as 300 µg Chla l^{-1} [*Pusch,* 2006; *Quiel et al.,* 2011; *IKSE,* 2016]. Eventually, this phytoplankton burden charges the turbid estuary where adverse conditions, especially in terms of light availability, lead to rapidly decreasing phytoplankton concentration (measured in terms of chlorophyll-a) with heterotrophic degradation of its detritus resulting in a regularly occurring eOMZ

in the estuarine freshwater section in summer [*Bergemann et al.,* 1996; *Schroeder,* 1997; *Amann et al.,* 2012].

The severity of both, the bathymetric and the water quality impact by human intervention, make the Elbe Estuary an example for heavy anthropogenic influence on the local scale.

1.5. Motivation, chapter overview and author contributions

This dissertation deals with the impact of man-made bathymetric modification on low oxygen conditions in an anthropogenically influenced and vertically well-mixed estuary, and compares them to the impact of a change in eutrophication.

In the first chapter, I give an overall introduction to oxygen deficits, human impact, modelling methods, the study site and the main objectives of the work. The work's core body is contained in the following three chapters, each being a separate manuscript, of which the first is an already published article, the second is submitted for publication, and the third is in preparation. These manuscripts describe the developed method including numerical model set-up and biogeochemical model configuration, the key processes driving oxygen dynamics, different model applications with bathymetric and riverine load scenarios, and a detailed analysis and discussion of results. I finally draw overall conclusions in the last chapter. Overall, I address the following questions in this thesis:

- What are the key processes driving an eOMZ in a vertically well-mixed system and is there a bathymetric impact on DO dynamics? (Chapter 2)
- What are possible physical influences of a realistic man-made bathymetric modification on an eOMZ, and are they potentially relevant? (Chapter 3)
- How large is the effect of man-made bathymetric modification in relation to changes in nutrient enrichment? (Chapter 4)

Chapter 2 introduces a biogeochemical model configuration for DO dynamics in anthropogenically impacted estuaries, and an idealized 1D model domain for a well-mixed estuary. Results clearly show the dominance of oxygen consuming processes in the estuary, and demonstrate that oxygen reaeration is the only process notably counteracting the eOMZ. A scenario analysis including a bathymetric variation and a reduction in riverine nutrient load underpins the effectiveness of riverine load reduction in mitigating eOMZ conditions; it furthermore reveals that the relationship between the amount of easily degradable material and the conditions for reaeration, given by the availability of sufficient water surface area and expressed as surface-to-volume ratio, determine the severity of the eOMZ. Chapter 2 is from the article: Holzwarth, I. and Wirtz, K. (2018): Anthropogenic impacts on estuarine oxygen dynamics: A model based evaluation. *Estuarine, Coastal and Shelf Science,* doi:10.1016/j.ecss.2018.01.020, 2018.

I. Holzwarth and K. Wirtz conceived the idea, and developed the idealized set-up and the model configuration. I. Holzwarth coupled the models, performed and analyzed the simulations, and wrote the manuscript with comments provided by K. Wirtz

Chapter 3 focuses on a realistic man-made bathymetric change and related hydrodynamic effects that potentially influence an eOMZ. Results indicate that the physical impacts of multi-decadal, man-made bathymetric modifications are moderate and pose one among multiple, possibly stronger, stressors. Methodically, this chapter promotes the approach to identify and apply suitable hydrodynamic indicators to describe the influence of physical changes on the eOMZ. This indicator-based approach allows distinguishing between bathymetric modifications with potentially low or high impact on eOMZs. As by-product, it is shown that the derivation of an empirical description for riverine water age in dependence of freshwater discharge at a specific location in the estuary is possible. Chapter 3 is from the submitted manuscript: Holzwarth, I.; Weilbeer, H. and Wirtz, K. (2018): The effect of bathymetric modification on water age in the Elbe Estuary. *Submitted to Estuarine, Coastal and Shelf Science*.

All authors contributed to the idea. I. Holzwarth performed the simulations and analysis, and wrote the manuscript with comments provided by K. Wirtz and H. Weilbeer.

Chapter 4 quantifies the impact of a man-made bathymetric modification on an eOMZ compared to a change in anthropogenic nutrient loading. Results confirm the finding from Chapter 3: the impact of a multi-decadal, realistic change in bathymetry is low. In contrast, a change in riverine load has a much severe impact on the eOMZ. In this chapter, the model configurations and model applications developed in the previous Chapters 2 and 3 are combined to a 3D process-based hydrodynamic-biogeochemical model. Chapter 4 is from the manuscript: Holzwarth, I. and Wirtz, K. (2018) A 3D estuarine biogeochemical model to evaluate the impact of man-made bathymetric modification and nutrient reduction on dissolved oxygen. *In preparation*.

I. Holzwarth developed the idea with contributions of K. Wirtz. I. Holzwarth performed the simulations and analysis, and wrote the manuscript with comment provided by K. Wirtz.

2. Anthropogenic impacts on estuarine oxygen dynamics: a model based evaluation

This chapter is based on the paper "Anthropogenic impacts on estuarine oxygen dynamics: a model based evaluation", which is in press and published online in the journal Estuarine, Coastal and Shelf Science.

Citation: Holzwarth I, Wirtz K (2018). Anthropogenic impacts on estuarine oxygen dynamics: A model based evaluation. Estuarine, Coastal and Shelf Science. doi: 10.1016/j.ecss.2018.01.020

Abstract Direct human interference has been shaping todays estuaries for centuries, and depletion of dissolved oxygen (DO) frequently occurs in such anthropogenically impacted estuaries. Whereas the role of nutrient input as a major human impact driving DO depletion is clear, the effect of bathymetric modifications as another human impact is less well-known.

Here, we aim at a better understanding of how DO dynamics are influenced by bathymetric modifications and changed nutrient input. Therefore, we introduce a coupled hydrodynamic-biogeochemical model (Untrim-Delwaq) and develop an idealized one-dimensional set-up of a vertically well-mixed, funnel-shaped estuary with strong human impact. The set-up dimensions are inspired by the Elbe Estuary (Germany) and model results show good agreement in comparison to observational hydrodynamic and water quality data. In particular, the model reproduces the dynamics of the summer oxygen minimum which regularly develops in the estuarine freshwater part.

Analysis of our model runs shows that the estuarine biogeochemistry is dominated by heterotrophic degradation processes rather than primary production because of severe light limitation. A scenario analysis indicates that a reduction in input load scales down all biogeochemical processes. In contrast, a bathymetric change affects the estuarine system and its DO in a more complex way. In particular, the interplay between surface-to-volume ratio and the degradability state of the organic material is the most important factor which determines the capacity to recover high DO mineralization losses by atmospheric input.

Thus, our study demonstrates the relevance of bathymetric factors during the assessment of human interference on DO dynamics and biogeochemical processes in estuaries.

Keywords: biogeochemical model; human impact; dissolved oxygen; bathymetry; well-mixed estuary

2.1. Introduction

Constituting the interface between riverine and marine water bodies, estuaries are areas of intense biogeochemical activities. In the center of these activities, dissolved oxygen (DO) plays a prominent role: most of the transformation processes involve DO, and a lack of oxygen impacts the ecological functioning of an estuary, see *Testa and Kemp* [2011] and references therein.

Oxygen-depleted conditions are frequently reported for estuaries worldwide, like the Yangtze Estuary [*Zhu et al.,* 2011], Chesapeake Bay [*Hagy et al.,* 2004], the Scheldt Estuary [*Meire et al.,* 2005] and the Elbe Estuary [*Amann et al.,* 2012]. The human influence on DO depletion ranges from globally acting anthropogenic climate change to local human interventions. Climate change impacts on estuarine ecosystems have been extensively studied during the past two decades [*Najjar et al.,* 2000; *Scavia et al.,* 2002; *Robins et al.,* 2016], and an exacerbation of estuarine DO depletion due to large scale changes in e.g. water temperature and freshwater discharge is expected [*Rabalais et al.,* 2009]. In contrast, the effects of direct human interventions appear more regional and versatile [*Wakelin et al.,* 2015]. Such direct effects basically arise from, e.g., changing the input of substances like nutrients, trace metals and organic contaminants [*Bianchi,* 2007] or from modifying the estuarine geometry by e.g. land reclamation, realignment, barriers and channel deepening. Like climate change effects, the human-induced change of substance input has received much attention, especially the increased nutrient load of nitrogen and phosphorous, which was put on a level with the human-induced rise of carbon dioxide by *Fulweiler et al.* [2012]. The increase in nutrient input, which fuels primary production and subsequent oxygen-consuming microbial respiration of its detritus, is commonly believed to be the predominant driver of exacerbated low oxygen conditions in estuarine and coastal areas worldwide [*Diaz and Rosenberg,* 2008; *Howarth et al.,* 2011; *Statham,* 2012].

However, geometric influences on biogeochemical processes in estuaries have not been examined to the same extend, though the geometry fundamentally influences all processes in an estuarine water body. Generally, geometric changes interact with the biogeochemical system by several interrelations. Most basically, geometric changes induce changes in hydrodynamic characteristics. Furthermore, changes in hydrodynamics influence advective transport characteristics and biogeochemistry [*Volta et al.,* 2014]. Recent research explored the influences of differences in horizontal size and shape to control biogeochemical processes: whereas *Jickells et al.* [2014] focused on the area size of an estuary independent of its shape, *Volta et al.* [2016a] included different types of lateral shapes in their investigation. Yet, the influence of variations in depth, and thus the vertical dimension, is of special interest because in many estuaries worldwide human activities have altered the bathymetry to deepen the shipping channel for navigational purposes. Prominent examples are the Scheldt [*Meire et al.,* 2005], the Yangtze [*Wu et al.,* 2016], the Columbia River [*Sherwood et al.,* 1990], the Seine [*Marmin et al.,* 2014], the Ems [*Jonge et al.,* 2014;

van Maren et al., 2015a] and the Elbe [*Boehlich and Strotmann,* 2008]. Nevertheless, scientific knowledge on the effect of changes in bathymetry to the biogeochemical system, and to DO dynamics in particular, is missing.

This study aims at understanding estuarine DO dynamics in response to the direct human impacts of riverine nutrient load and depth change. Therefore, we developed an integrated hydrodynamic-biogeochemical model and an idealized model domain to provide an easier understanding of the processes under consideration. The model is a prototype of a vertically well-mixed, alluvial estuary that includes artificial modifications. The domain dimensions and proportions are inspired by the Elbe Estuary (Northern Germany) and the geometric idealization enables transferability of the results to other estuaries.

The Elbe Estuary extends between the tidal barrier in Geesthacht and the seaward end of the maintained shipping channel in the German Bight. The tidal limit, a weir, completely reflects the incoming tidal wave and constitutes a clear landward end of the estuary. The Port of Hamburg is located about 30 km downstream of the weir. There, the maintained marine shipping channel starts by a clear drop in bottom bathymetry to facilitate the navigation of large container ships between the port and the sea. Geometry and water quality of the Elbe Estuary were changed considerably compared to pristine conditions, making it a characteristic example of an anthropogenically influenced estuary.

In this study, we first develop our model and increase confidence in it by comparing model results to observational data. A subsequent parameter sensitivity study identifies the key processes of DO dynamics. After that we model different scenarios to investigate changes in DO dynamics due to changes in human impact. Besides a nutrient reduction scenario, we especially focus on a bathymetric change and thus provide deep insight into the interplay between bathymetry and estuarine DO dynamics.

2.2. Methods

We coupled the mathematical models Untrim [*Casulli and Stelling,* 2010] and Delwaq [*Postma et al.,* 2003; *Smits and van Beek,* 2013]. Details on both models can be found in e.g. *Casulli* [2009] and *Sehili et al.* [2014] for Untrim, and in *Blauw et al.* [2009] and *Deltares* [2014] for Delwaq. Untrim calculates hydrodynamic characteristics in tidal environments by solving the Reynolds-averaged Navier Stokes equations in a semi-implicit way. Based on these information, Delwaq simulates biogeochemical processes in the water column by solving the advection-diffusion-reaction equation for each state variable with a mass-conserving finite-volume method, but needs to be configured individually (see section 2.2.1 for our configuration) in terms of resolved processes and state variables. Our coupling of the mass-conserving models Untrim and Delwaq is realized by a coupling module that retrieves the exact water fluxes through the edges of each

computational volume [*Lang,* 2012]; the coupling itself is, thus, mass-conserving. In this study, we use the models in 1D mode and for water column processes only.

2.2.1. Biogeochemical model

Our configuration of the biogeochemical model Delwaq simulates the dynamics of nutrients, phytoplankton, particulate organic matter, dissolved organic matter and DO. In this section we summarize important interactions between the state variables (see Figure 3). Appendix A lists the mathematical formulations of the biogeochemical model configuration in tabular form.

Our model resolves nitrogen, ortho-phosphate (PO4) and free silicate (Si) as inorganic nutrients. Dissolved inorganic nitrogen is further subdivided into ammonium (NH4) and nitrate (NO3). The attenuation of light on its way through the water column is linked to suspended mineral and organic material. The model parameterization bases on the Beer-Lambert law and includes a general background attenuation, specific attenuation coefficients for inorganic suspended matter (SPMI) and particulate organic matter, and self-shading effects from phytoplankton.

Phytoplankton is in the model distinguished between freshwater diatoms (DIAT) and freshwater non-diatoms (NON-DIAT). Changes in their biomass arise from three processes: net primary production, mortality and settling – as also documented in detail in Appendix A. Our approach ignores higher trophic levels but conceptually includes grazing in the pelagic zone through a higher mortality rate constant, and grazing by benthic filter feeders through settling.

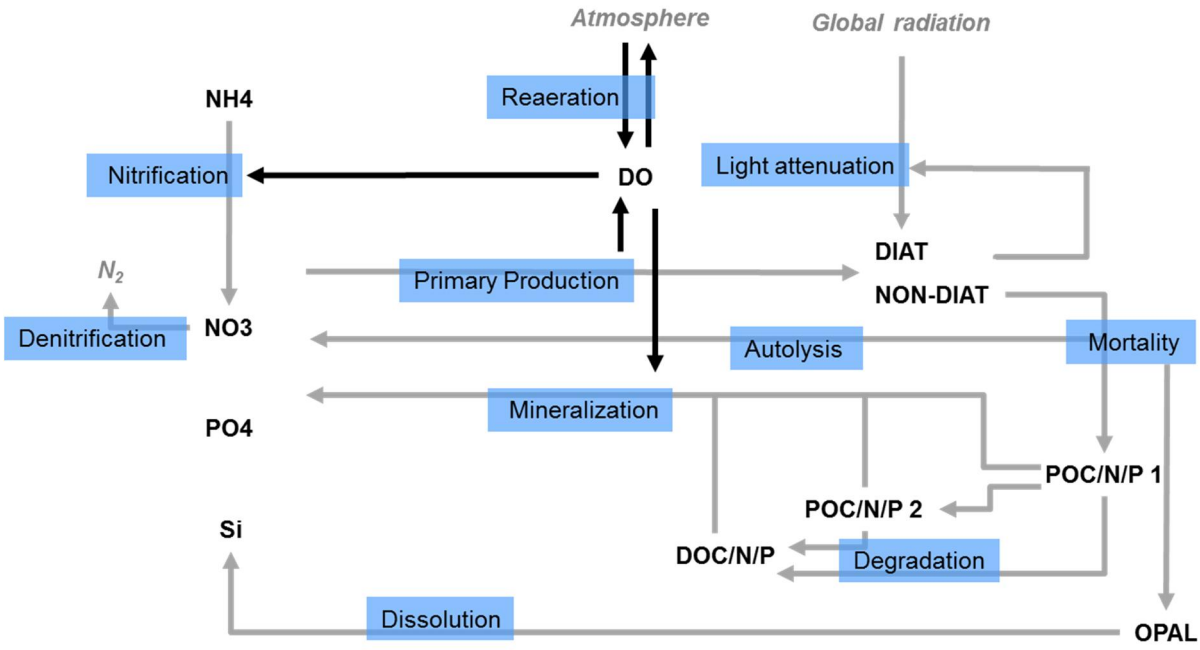

Figure 3: Sketch of the model configuration. Bold abbreviations denote state variables, blue boxes the most important model processes. Arrows indicate process-related influences on state variables. For a complete formulation of all model processes refer to Appendix A.

Mortality of phytoplankton results in two shares: an autolysis share is directly remineralized into inorganic nutrients without any influence on the DO budget. The share fuels the detritus pool, which comprises carbonaceous, nitrogenous and phosphorous fractions. The degradation of detritus happens in several steps: the most easily degradable particulate organic matter for carbon (POC1), nitrogen (PON1) and phosphorous (POP1) is decomposed into inorganic nutrients, and in slowly degradable particulate organic matter with corresponding particulate nutrient fractions (POC2, PON2 and POP2), and dissolved organic matter (DOC, DON and DOP), respectively. The decomposition of the slowly degradable particulate matter also yields remineralized inorganic nutrients and dissolved organic matter. The dissolved organic matter pool is remineralized to inorganic nutrients.

The inorganic nitrogen cycling in our model configuration includes nitrification and denitrification, both dependent on the oxygen level. By remineralization, organic nitrogen is transformed into ammonium. In case of sufficient DO, ammonium is nitrified. In case of low DO condition, nitrate can be denitrified which effectively is a nitrate sink to the model. By mortality, the silicate that is incorporated into diatoms feeds an opal silicate pool (OPAL). This opal silicate is transformed to free silicate by dissolution.

Our configuration does not directly simulate processes at the sediment-water interface and in the bottom sediment, but uses enhanced rates of organic matter sedimentation and mineralization, as well as nitrification and denitrification in order to emulate effects of benthic biogeochemistry.

The concentration of DO depends on the solubility of oxygen, which decreases with increasing water temperature and increasing salinity [*Weiss,* 1970], and may range roughly between 200 and 460 mmol DO m^{-3}. Most of the biogeochemical processes mentioned above influence DO in our model configuration, as summarized in Equation 1. A more detailed mathematical formulation of the DO balance equation is given in Table A1 in Appendix A. DO decreases due to mineralization and nitrification, and increases through primary production. Reaeration, the exchange of oxygen with the atmosphere at the water surface, can act in both ways, depending on the difference between the actual dissolved oxygen concentration and oxygen saturation concentration.

$$\frac{\mathrm{d}}{\mathrm{dt}}\mathrm{DO} = \text{Primary Production} - \text{Mineralization} - \text{Nitrification} + \text{Reaeration} \qquad (1)$$

2.2.2. Model domain

Focusing on well-mixed, alluvial estuaries we simplified the complex estuarine geometry to an idealized funnel-shaped model domain as illustrated in Figure 4. Mathematical formulations that describe the cross sectional area, width and depth of a natural estuarine funnel are, for example, provided by *Prandle* [1986] and *Savenije* [2005]. Anthropogenically modified estuarine geometries mainly differ from naturally developed geometries by (i) an artificial tidal limit instead of

an upstream dissipating tidal wave and (ii) an adjusted, deepened bathymetry to meet navigational purposes instead of a water depth generated in a morphological equilibrium. To include the artificial tidal limit, we modified a power law formulation [*Prandle,* 1986] of the estuarine width, resulting in Equation 2. The model cross section is rectangular.

$$B = B_0 + a_n \cdot x^a \quad (2)$$

with B: estuarine width, B0: width at the (artificial) tidal limit, an: coefficient, x: distance from tidal limit, and a: shape factor for funnel curvature.

The dimensions of the model reference domain are inspired by the Elbe Estuary. For detailed information on the geography and hydrodynamics of the Elbe Estuary see *Boehlich and Strotmann* [2008]. The total length of the domain is 172 km, the depth1 of the first 30 km downstream of the weir and upstream of the bottom step is 6 m, and then depth is increasing downstream to depth2 of 14 m throughout the rest of the model domain. The initial width B0 at the tidal barrier (km-0) is 200 m and the width BL at the mouth (km-172) is 10 000 m. All dimensions are summarized in the column for scenario R of Table 1. The coefficient a_n and the shape factor a were chosen in such a way that the resulting width best fits the width of the Elbe Estuary at four evenly distributed locations along the total length of the estuary and under the constraint that the volume of the model domain corresponds to the Elbe Estuary volume. The computational mesh consisted of 344 elements with an equal length of 500 m lined up in longitudinal direction.

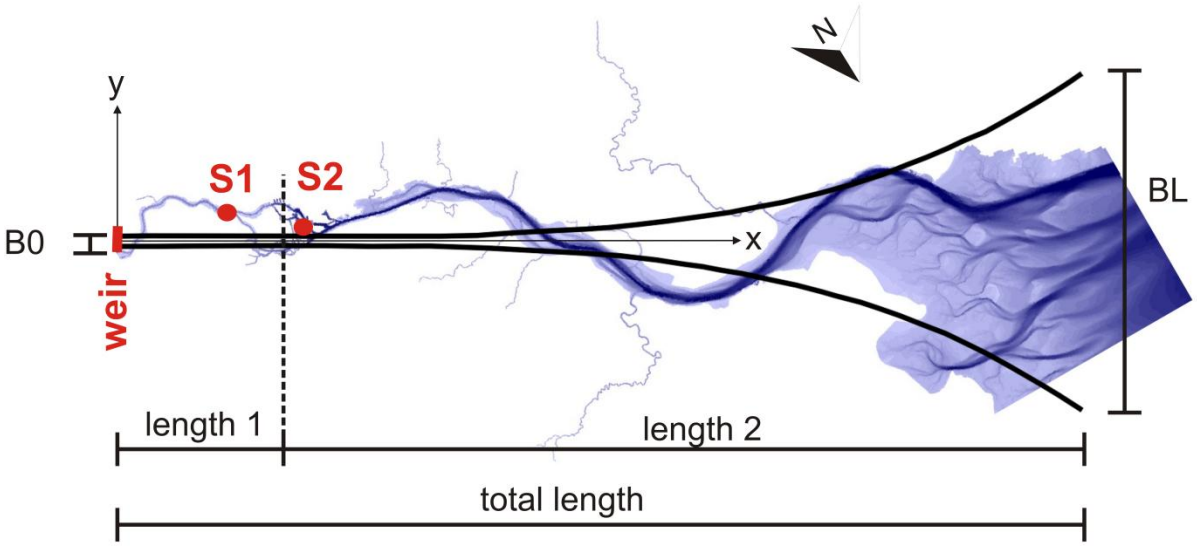

Figure 4: Plan view sketch of the idealized estuary geometry in black; length1 is the length of the shallow estuarine section upstream of the bottom step with depth1, and length2 is the length of the deep section downstream of the bottom step with depth2. B0 is the width of the estuary at the tidal limit and BL is the width at the seaward end. The dimensions are given in Table 1. Two continuous monitoring stations are marked: Bunthaus (S1) upstream of the bottom step and Seemannshöft (S2) in the port area directly downstream of the bottom step. The background picture shows the high resolution topography of the Elbe Estuary [*Sehili et al.,* 2014].

2.2.3. Data for hydrodynamic model forcing and evaluation

The hydrodynamic model simulates flow conditions and transport of salt and water temperature. Tides at the seaward model boundary and freshwater inflow at the landward model boundary mainly govern water levels and current velocities inside the model domain. We force the hydrodynamic model with the following values: (i) measured daily mean freshwater discharge at the gauging station Neu Darchau (last gauging station upstream of the weir, data available on www.portaltideelbe.de), (ii) water temperature of freshwater discharge from gauging station Cumlosen, about 115 km upstream of the weir (provided by Landesumweltamt Brandenburg, available on www.fgg-elbe.de), (iii) air temperature measurements from the station Hamburg-Fuhlsbüttel as representative values for the entire model domain (provided by Germany's National Meteorological Service DWD) to model heat exchange at the water surface using the excess-temperature model [*Sweers,* 1976], (iv) simplified values at the open, seaward boundary: an artificial, single semidiurnal tide with an amplitude of 1.0 m, constant salinity of 32 psu and observed water temperatures at 'Tonne 5' (www.fgg-elbe.de) in the estuary mouth.

The energy of the water motion in the model domain is partly dissipated by bottom friction. We use Nikuradse bottom friction roughness and apply a constant value of 0.1 m for the entire domain. This relatively high value accounts for the geometric smoothness of the idealized system.

To evaluate the hydrodynamic model, water level measurements at several gauging stations along the estuary are available on www.pegelonline.wsv.de, provided by the Water and Shipping Administration (WSV).

We ran the model for the entire period 2010 to 2011 and used the results from 2011 for our analysis because the year 2011 can be regarded as representative in terms of freshwater discharge into the estuary: there was a high flooding event in January with a peak value of about 3500 $m^3 s^{-1}$. Discharge subsequently declined to commonly low summer values between 500 $m^3 s^{-1}$ and 300 $m^3 s^{-1}$ until August. For the rest of the year, the discharge stayed between 400 $m^3 s^{-1}$ to 800 $m^3 s^{-1}$ and therefore in the range of the long-term mean discharge of 712 $m^3 s^{-1}$ (long-term characteristic hydrographic numbers, published in *FHH and HPA,* [2014]).

2.2.4. Data for biogeochemical model forcing and evaluation

Observational boundary values are generally scarce. A valuable source of data for model forcing and evaluation originates from regular helicopter flights on the longitudinal transect of the Elbe Estuary. The FGG Elbe (www.fgg-elbe.de) carried out these flights, starting in the estuarine mouth at fully developed ebb current, keeping the tidal phase when flying upstream and thereby taking measurements at specific locations. The resulting profiles are therefore no synoptic views but representations at a comparable tidal phase with a time difference of about 3 h between the most downstream and the most upstream position. In 2011, 5 flights on 8th of March, 3rd of May, 4th of July, 2nd of August and 1st of November took place and provide concentration data

of DO, chlorophyll-a, ammonium, nitrate, silicate, ortho-phosphate and particulate organic carbon.

Seaward biogeochemical boundary values originate from the data of the outermost helicopter sampling point. The landward boundary values are more critical for the biogeochemical processes in the estuarine freshwater part and we compiled landward boundary values (see Figure B1 in Appendix B) from three sources: (1) data from the helicopter sampling directly upstream of the weir, continuous/biweekly observational data at the stations (2) Cumlosen and (3) Schnackenburg. The two stations are located more than 100 km upstream of the weir (data from www.fgg-elbe.de). We therefore adjusted their data to fit the temporally sparse helicopter measurements directly upstream of the weir.

To convert the phytoplankton concentration, measured as chlorophyll-a, into units of carbon, we used a constant conversion factor of 0.05 g Chl-a g^{-1} C. For the boundary values of degradable organic matter, we assumed: (i) particulate organic carbon, reduced by carbon biomass, is equally distributed among POC1 and POC2, (ii) inorganic nutrient concentrations upstream of the weir are made of NH4, NO3, and PO4, (iii) algal stoichiometry agrees to the Redfield Ratio (as given in *Bianchi* [2007]), (iv) also the ratio of POC1, PON1 and POP1 conforms to Redfield Ratio, and (v) slowly degradable particulate organic matter is poorer in nutrients so PON2 and POP2 relate to POC2 only by half of the Redfield Ratio.

Global radiation and wind speed are required as meteorological boundary data at the water surface. We used monthly areal averages of global radiation from maps, accessible on www.dwd.de, and daily values of wind speed, directly provided by DWD.

Due to the idealized domain, the geometric ratio between water surface area and underlying water volume (surface-to-volume ratio, sv-ratio) is, on average, 0.5 times smaller in the model compared to the real estuary. This ratio is important for the impact of the oxygen exchange with the atmosphere on the water volume below. We therefore enhanced the oxygen transfer coefficient (see Table A2 in Appendix A) with a factor of 2.

For the comparison of model results with observations we used the above mentioned helicopter sampling data. In addition, time series measurements of biogeochemical data in the Elbe Estuary are available for two stations: (1) Bunthaus, located upstream of the bottom step and marked as S1 on Fig. 2, and (2) Seemannshöft, which is located downstream of the bottom step and marked as S2 (data provided by the Institut für Hygiene und Umwelt Hamburg, www.wgmn.hamburg.de, license dl-de/by-2-0).

2.2.5. Biogeochemical parameter sensitivity study

We adopted most parameter values for the biogeochemical model from similar models [*Soetaert et al.,* 1994; *Schroeder,* 1997; *Wild-Allen et al.,* 2013; *Schöl et al.,* 2014]. In addition we performed a sensitivity study in which key process rates were systematically varied based on parameter

values from literature. *Volta et al.* [2016b] provide a comprehensive overview for estuarine model parameters such as phytoplankton mortality rate and nitrification rate, though, partly, the use of different parameterizations complicates the transferability. This is especially the case for organic matter degradation rates where varying organic matter pool partitions additionally impede direct comparability. Thus we investigated a larger range for organic matter mineralization rates than described in the above mentioned compilation. The range for maximum autotrophic growth rates was taken from *Wirtz* [2011] and literature therein.

Sensitivity of DO levels to light availability was evaluated by changing the concentration of SPMI in a range typically found in the estuarine freshwater part of the Elbe, see e.g. measurements in *Weilbeer* [2015] for the transect Hamburg.

2.2.6. Change scenarios

We defined three scenarios which represent changes of human impact on the estuary, see Table 1. These three change scenarios are variations of the reference scenario (R) which has been described in the previous sections.

The first change scenario (L) corresponds to the call of reducing the human nutrient footprint. This scenario L contains a reduced riverine input load of nutrients, dissolved and particulate organic matter including phytoplankton. To obtain a clear signal in the results we realized scenario L by halving all landward boundary values in the biogeochemical simulation, except the one for DO. In the second change scenario (D) we implemented a bathymetric change: the bottom step is located 50 km further downstream. Thus, the 6 m deep section length1, see Figure 4, is 80 km long in D compared to 30 km in the reference case R. The third change scenario (LD) is a combination of L and D including reduced riverine input load and a downstream relocation of the bottom step. Whereas the hydrodynamic base is the same for scenarios R and L, a rerun of the hydrodynamic model was necessary for scenarios D and LD because of the change in bathymetry.

Table 1: Definition of the change scenarios. For terms which describe the model domain see Figure 4. In all scenarios, the total length of the domain is 172 km, the initial width B_0 is 200 m, and the seaward width B_L is 10 000 m.

Scenario	R	L	D	LD
long name	reference	load reduction	depth change	load & depth change
length1 (depth1 6m)	30 km	30 km	80 km	80 km
length2 (depth2 14m)	142 km	142 km	92 km	92 km
riverine load (nutrients, phytoplankton, POC, DOC)	measured	½ measured	measured	½ measured

2.3. Results

2.3.1. Hydrodynamic results for the reference scenario **R**

Along the estuary, the model skill in simulating large-scale hydrodynamic processes is evident from a reproduction of the tidal range and its symptomatic changes including maximum values directly downstream of the bottom step at km-30. Furthermore, the model simulates realistic water temperatures in the freshwater zone. This is indicated by correspondence of observed and simulated water temperature at position S2 on Figure 5b). Though simulated results tend to overrate observed temperatures during peak events with up to 3 K for short periods, the difference is less than 0.5 K during most of the year.

Altogether, the hydrodynamic model captures the main features of water elevation and related water movements, which is apparent from comparing modeled and measured mean high and means low water levels, see Figure 5a).

As a proxy for residence time, we calculate flushing time t_{flush} along the estuary with $t_{flush} = V_{mean}/Q_{const}$, based on the time-averaged water volume Vmean in the hydrodynamic results, and constant freshwater discharge Q_{const}. Flushing time values from our model qualitatively agree with values from *Bergemann et al.* [1996], see Figure B2 in Appendix B. It has to be noticed, that the values in *Bergemann et al.* [1996] base on a 30 year older bathymetry and on water volume below half tide level.

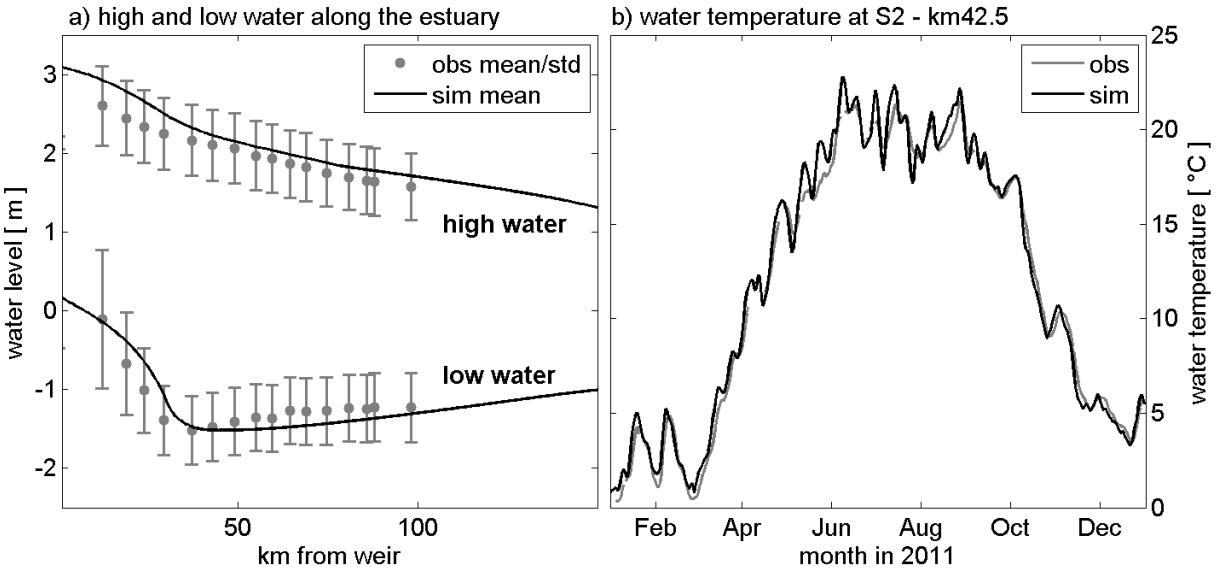

Figure 5: Comparison of measured and simulated hydrodynamic states. a): mean high and low water in 2011 along the estuary. Black, solid lines represent simulation results. Grey circles mark mean high and low water at gauging stations along the Elbe estuary in 2011, bars indicate standard deviation. Mean values and standard deviation calculated from water level records. b): observed water temperature (grey line) in 2011 at station S2 and modeled water temperature (black line) in the corresponding computational element at km-42.5.

2.3.2. Biogeochemical results for the reference scenario

Computed longitudinal transects of major biogeochemical variables at least qualitatively agree with most observational data from helicopter flights in 2011, see Figure 6. The first profiling date at the beginning of March reflects a typical end-of-winter/early-spring situation. In this situation, concentration levels of DO and inorganic nutrients correspond to typical winter values. Merely phytoplankton (as chlorophyll-a) concentrations are already elevated compared to common winter values. This initial state is almost exactly reproduced by the model. Largest deviations result in NO3 and Si concentrations at the section more than 100 km downstream of the weir.

At the sampling dates in summer, July and August, see Figure 6, model results exhibit large changes in DO, chlorophyll-a, NH4, PO4 and POC concentration along the longitudinal axes of the estuary. We observe a fast decline of the high upstream freshwater phytoplankton concentrations. Simultaneously, POC increases and DO decreases downstream of km-30 to a distinct minimum zone which is followed by subsequent oxygen enrichment. Right before the oxygen minimum zone, a zone with elevated ammonium concentrations is observed. The largest differences between observed data and modeled results are apparent in the exact position of the oxygen minimum zone and in NH4 and PO4 concentration level.

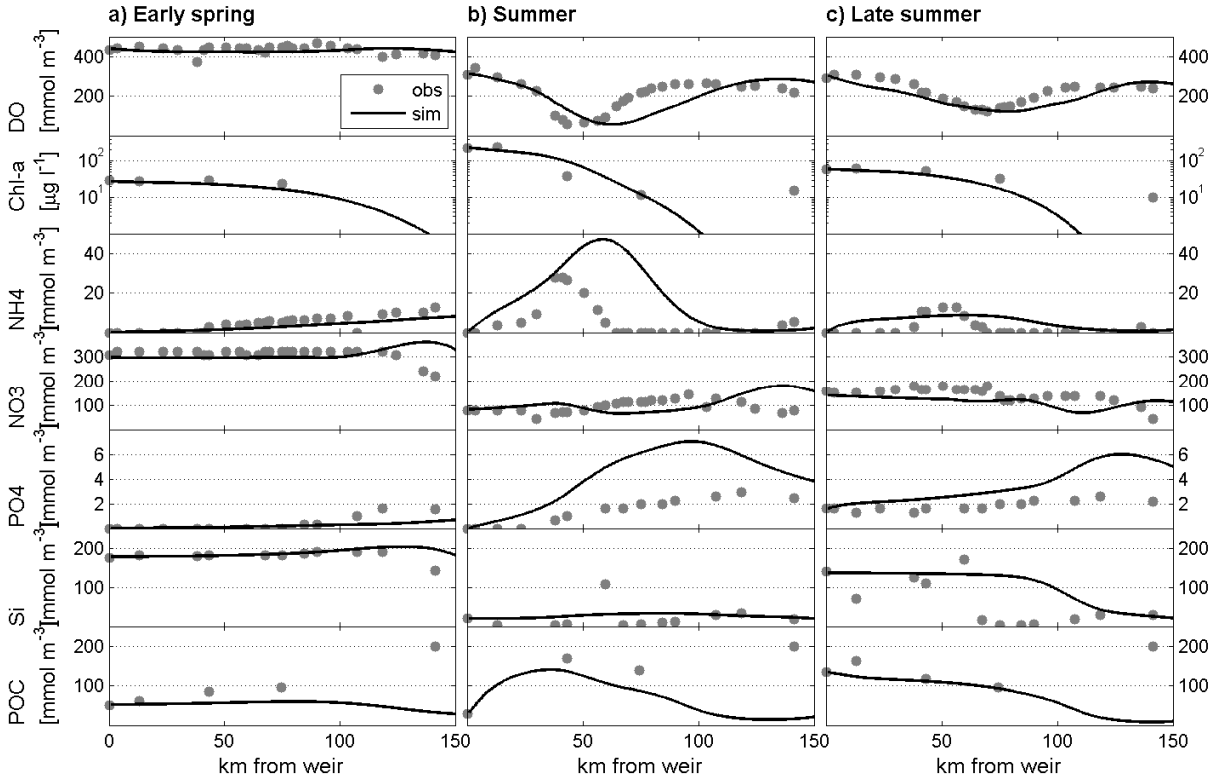

Figure 6: Comparison of observed (grey points) and simulated (black continuous lines) values for DO, freshwater chlorophyll-a, NH4, NO3, PO4, Si and POC (with POC ¼ POC1 þ POC2) along the longitudinal axes of the estuary. Panel a) shows transects for 8-March-2011, b) for 4-July-2011 and c) for 2-August-2011. Km-0 denotes the tidal barrier at the landward end.

The last sampling date (not shown) denotes a beginning of winter situation with low biogeochemical activity and substance concentrations returning to winter levels. Apart from NH4 concentrations and minor deviations in DO in the upper estuarine part, the model reproduces this situation.

A qualitatively good agreement between observed and simulated biogeochemical state variables also follows from the comparison with long-term continuous measurements at the stations S1 and S2. In Figure 7 we compare their DO data with model results in the corresponding computational grid cell at km-23 and km-42.5, respectively. The comparison shows a generally good correspondence between observed and modeled values. At the position upstream of the bottom step (S1, upper panel), model results are consistently too low during some periods in May and August to October, with deviations up to 130 mmol DO m^{-3}. These deviations match the trend visible during the late summer profile on Figure 6 with DO decreasing too fast downstream of the weir. At the position downstream of the bottom step (S2, lower panel) the model well simulates the DO seasonality though periodically, model results are too high. Again, these systematic deviations are already indicated in Figure 6 by the position of the minimum zone not being captured exactly but further downstream.

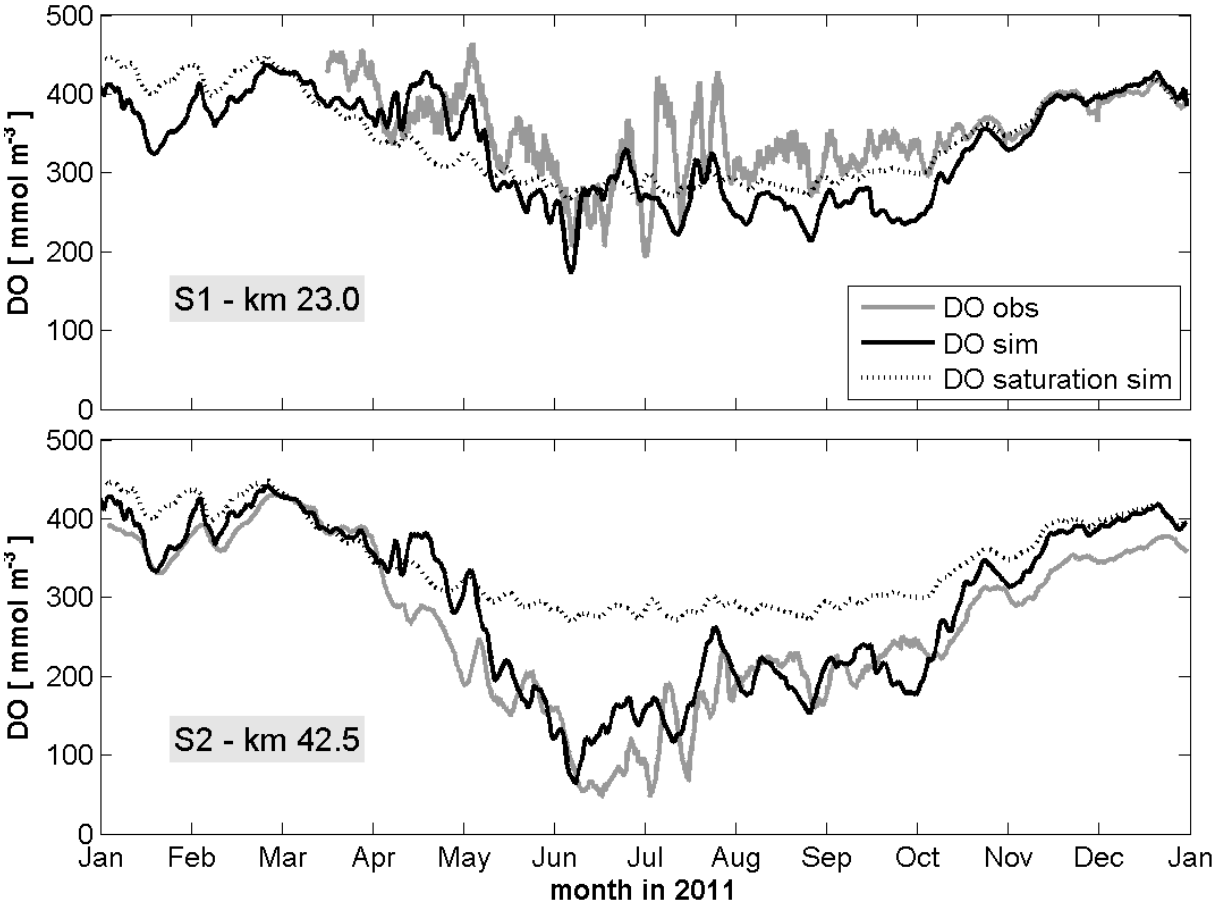

Figure 7: Comparison of observed DO (grey line) at the two permanent measuring stations S1 (upstream of the bottom step) and S2 (directly downstream of the bottom step) with simulated DO (black line) at their corresponding model locations for the entire year 2011. The dashed black line shows the calculated oxygen saturation concentration.

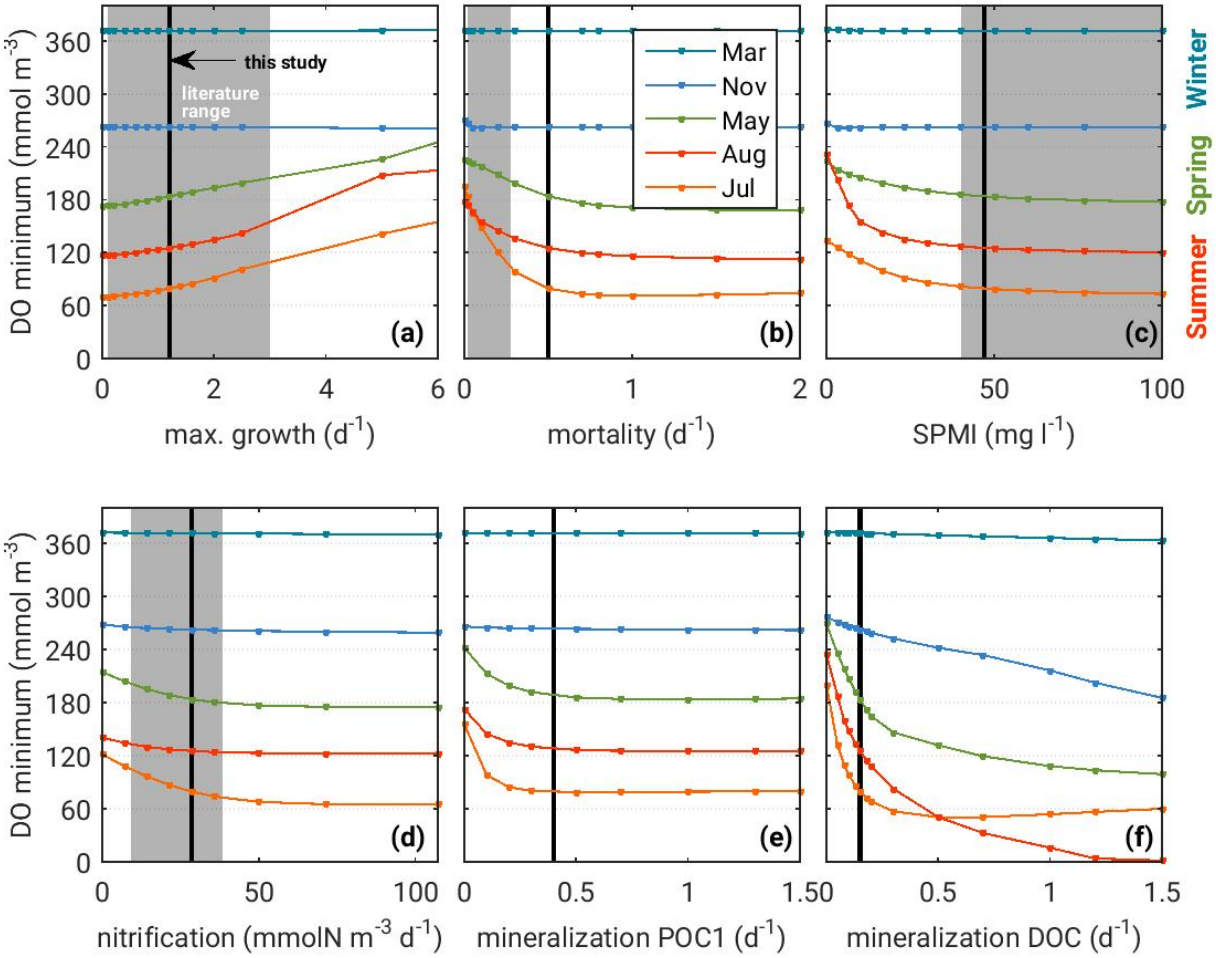

Figure 8: Sensitivity of the DO minimum to changes in model parameters during different seasons. a) Maximum phytoplankton growth rate constant. b) Phytoplankton mortality rate constant. c) Concentration of inorganic suspended particulate matter. d) Nitrification rate constant. e) Mineralization rate constant of easily degradable particulate organic matter. f) Mineralization rate constant of dissolved organic matter. The black bar marks the standard reference value used in this study. The grey shaded areas indicate parameter ranges available in the literature.

2.3.3. Dependence of the oxygen minimum on process parameters

How does the intensity of the oxygen minimum depend on the model imposed biogeochemical process parameters? From the parameter sensitivity study described in section 2.2.5, we derive the change in absolute DO minimum with systematically varied parameter values, see Figure 8. Consistent with the biogeochemical reference run, no sensitivity is found during winter. Only the DOC mineralization rate constant influences the absolute DO minimum during late autumn (Nov). However, during spring and summer (May-Jul-Aug), all rate constants and light attenuation parameter (SPMI) affect the oxygen minimum, at least for small value ranges. Minimum DO concentrations increase with increasing maximum phytoplankton growth rate constant (panel a), whereas an increase in other important rate constants and SPMI concentration leads to a decrease in minimum DO. These results of the sensitivity study display an expected and coherent model behavior. The comparison to literature parameter ranges shows that our parameter

reference values lie within the common magnitude. Within this range, the model reacts most sensitive to the mineralization rate constant, phytoplankton mortality rate constant and light attenuation during summer.

2.3.4. Analysis of process-based changes in DO

We calculate mean volume-based bulk changes of DO by averaging the process rates over periods of two months, see Table 2. Small DO-related bulk changes in January and February (Table 2), DO concentrations at 90 – 100 % saturation level (Figure 7), and winter DO values remaining almost unaffected from large parameter variations (Figure 8), consistently show that biogeochemical activity is low during winter. Note that the high value for winter reaeration in Jan/Feb results from the input of riverine water with only about 80 % DO saturation. This undersaturated water forces atmospheric DO enrichment in the upper part of the estuary. In the years before and after 2011 the riverine DO saturation lay between 90 and 100 % during this season. Explaining the unusual situation in 2011 is beyond the scope of this study. Though the reaeration value appears high, it has no further influence on our results and on the following analysis.

Active processes in early spring are mineralization, reaeration and primary production (scenario R in Figure 9; note, that Table 2 contains volume-based bulk changes but Figure 9 shows depth-integrated change rates). Primary production is slightly active with, at most, 24 mmol DO m^{-2}. Upstream of the weir, primary production also starts becoming active at this time of the year, and the incoming water is DO oversaturated. Therefore, outgassing causes reaeration losses from up to 250 mmol DO m^{-2} directly downstream of the weir. Organic matter mineralization produces depth-integrated change rates between 40 and 70 mmol DO m^{-2} in the entire model domain leading to compensation rates with positive reaeration values downstream of km-50.

Table 2: Mean DO bulk changes in the freshwater zone between km-0 and km-120 for reference scenario R in mmol DO m^{-3} d^{-1}. 'Sum of all' contains all depth-integrated change rates and transport-related DO exchanges.

	primary production	mineralization	nitrification	reaeration	sum of all
Jan/Feb	0.1	-5.8	-0.2	40.0	48.5
Mar/Apr	5.7	-24.3	-4.0	0.7	-11.2
May/Jun	16.7	-66.3	-15.4	25.7	-34.1
Jul/Aug	9.5	-67.1	-10.7	28.4	-35.7
Sep/Oct	1.6	-40.4	-6.3	25.9	-18.3
Nov/Dec	0.1	-11.7	-2.6	8.0	-2.7

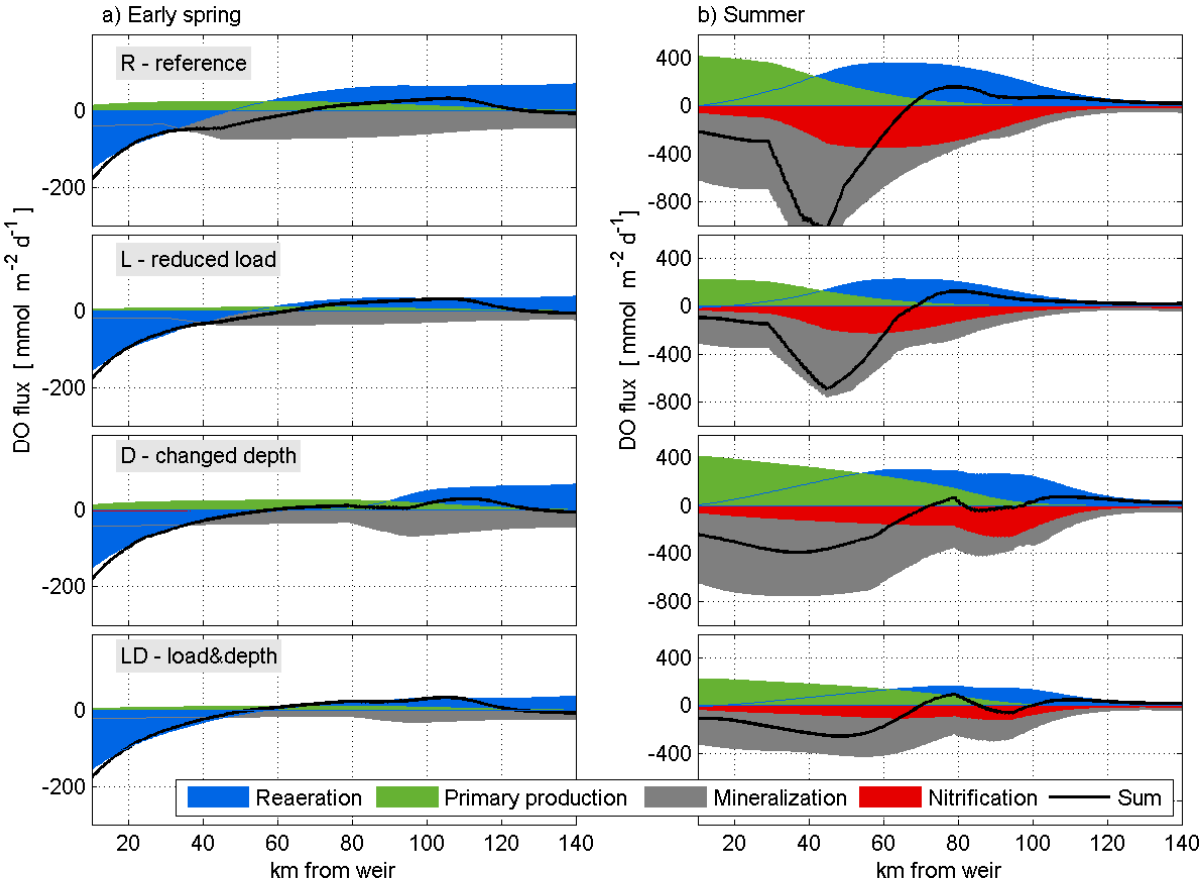

Figure 9: Simulated daily depth-integrated oxygen change rates per process for the two situations a) early spring on 08-March-2011 and b) summer on 4-July-2011, for the four scenarios R, L, D and LD. 'Sum of all' also includes transport which are not depicted separately in the plots.

During the following spring and summer seasons the depth-integrated rates and bulk changes in DO are substantially larger (Figure 9, Table 2). In summer, peak boundary values for phytoplankton generate highly active primary production upstream of the bottom step with peak values of +415 mmol DO m^{-2} (Figure 9). Photosynthetic oxygen production decreases to +2 mmol DO m^{-2} at km-120. Mineralization produces a high DO loss of -500 to -700 mmol DO m^{-2} upstream of the bottom step which strongly rises to a maximum of -1200 mmol DO m^{-2} at the bottom step. Downstream of the bottom step, depth-integrated oxygen change due to mineralization subsequently declines to 1/8 of the maximum at km-100.

Nitrification, not significant in winter, also accounts for substantial DO loss during summer when NH4 concentration augments through mineralization. Related depth-integrated oxygen changes due to nitrification already increase downstream of the weir. They quickly grow to values around -300 mmol DO m^{-2} downstream of the peak mineralization zone and, then, constantly decrease towards the estuarine mouth.

Intense mineralization and nitrification deplete available DO and lead to strong oxygen undersaturation which generates a compensating depth-integrated reaeration rate with a maximum of +360 mmol DO m^{-2}. The sum of all depth-integrated oxygen changes (Figure 9), including

transport induced changes, peaks directly downstream of the bottom step with approx. 900 mmol DO m^{-2} in July.

Throughout late summer mineralization remains high (Table 2), because of high water temperatures promoting decomposition and mineralization. In contrast, primary production and the related DO production reduces by about 50 % due to much lower upstream phytoplankton input population. Production further declines during autumn and almost ceases at the beginning of winter. Mineralization and nitrification activity decrease more gradual from late summer towards the end of the year following the falling water temperature and reduction of easy degradable material delivered by primary production.

2.3.5. Impacts of anthropogenic interventions

Compared to the reference scenario R, the concentration levels in scenario L are substantially lower for nutrients, phytoplankton and organic matter, and the DO deficit is not as severe as in R, see Figure 10. The depth-integrated oxygen change rates in the freshwater zone, especially the ones for mineralization, nearly scale down linear to the reduction by 0.5 in boundary values, see Figure 9 a) and b) for L - reduced load, and Table 3. Locally, we observe main deviations from this linearity for summer DO changes due to nitrification with higher relative changes upstream of km-70 benefiting from higher DO levels in L. Consequently lower relative depth-integrated oxygen change rates due to nitrification result further downstream because of exhausted NH4 substrate by the enhanced upstream consumption. The resulting upstream offset of maximum DO change due to nitrification does not affect the position of the DO peak loss, which has a value of about 700 mmol DO m^{-2} in scenario L.

In scenario D, the introduced bathymetric change leads to a more complex feedback in the biogeochemical system. The situation in July displays the resulting characteristics most clearly. The downstream decrease in phytoplankton biomass, indicated as chlorophyll-a, happens more gradual (Figure 10) because of primary production being slightly less light limited by the shallower water depth. As a consequence, oxygen production by primary production is higher compared to R, Figure 9. Mineralization remains the process with the strongest influence on the oxygen budget though it acts more uniformly distributed along the estuary. Mineralization rates are as high as in scenario R directly downstream of the weir and cause DO depletion because they are not completely counter- balanced by primary production and reaeration. In the downstream course of the estuary, DO bulk changes due to mineralization (Figure 9) remain almost constant till km-55, and thus smaller than in scenario R, and then slowly decline connected to diminishing easily degradable organic matter, see Figure 11. Conversely, NH4 concentration (not shown) grows through mineralization, and the influence of nitrification on DO increases. Peak DO loss in July occurs around km-35 with values close to 400 mmol DO m^{-2} d^{-1} and thus clearly smaller than in R and L.

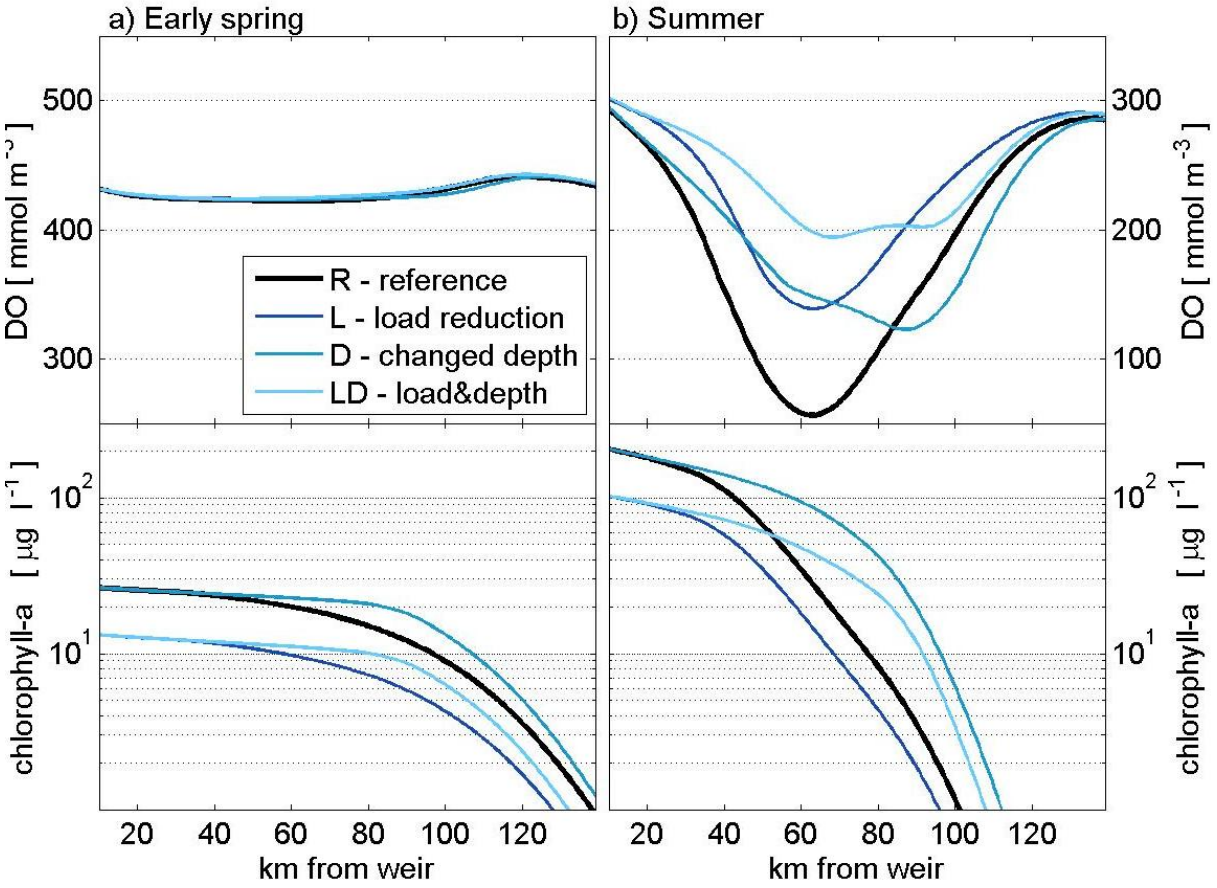

Figure 10: Simulated DO (notice the different range of y-axis values) and freshwater chlorophyll-a concentrations along the estuary for the two situations a) early spring on 08-March-2011 and b) summer on 4-July-2011, for the four change scenarios R, L, D and LD.

Directly upstream of the bottom step at km-80, positive and negative depth-integrated oxygen change rates almost completely level out. Downstream of the bottom step the influence of DO consumption processes again increase whereas primary production almost ceases.

These processes cause DO to continuously decrease downstream of the weir with a minimum zone at the position of the bottom step and thus further downstream than in R and L. The resulting minimum DO is consistently higher in D compared to R. This is noteworthy because detritus production due to the higher estuarine primary production is bigger in D. The resulting total DO loss in the freshwater zone by mineralization is up to 25 % higher in D than in R, see Table 3.

Regardless of the bigger global loss, DO remains higher in the upstream section of the estuary, due to a higher contribution of primary production (see Figure 9 b) D) and due to larger surface-to-volume ratio (sv-ratio). To illustrate the latter relationship, Figure 11 shows the sv-ratio for scenarios R and D together with the concentrations of POC1, POC2 and DOC at the position of the respective bottom step. The drop in bottom bathymetry causes the sv-ratio to decrease. Thereby, the relative importance of water surface processes, such as reaeration, also decreases. In contrast, we expect flushing time to increase which in turn favors local DO depletion. In R, the

decrease of sv-ratio coincides with high concentrations of easily degradable material, leading to a strong decline in DO. In D, the sv-ratio starts declining further downstream at km-80. There, the concentration of easily degradable material is considerable smaller because much of the organic material has already been degraded and mineralized further upstream where the more favorable sv-ratio better counterbalances DO losses. The remaining degradable material downstream of km-80 does not generate similar DO depletion compared to R.

In scenario LD, the combination of reduced boundary input load and downstream relocated bottom step results in an almost linear superposition of the effects observed in L and D, leading to considerable lower DO depletion during summer, see Figure 10. The water-column change rates are influenced proportionally to those in D and we do not observe an additional feedback mechanism. An instructive measure to compare the different scenarios with regard to DO-relevant processes is the ratio between producing and consuming processes (prod/cons-ratio, Table 3). This ratio is an equivalent to the carbon-based P:R ratio, i.e. in *Garnier et al.* [2001], in terms of oxygen. The prod/cons-ratio is calculated by dividing the bulk changes of DO-producing processes (in our case: primary production) by the bulk changes of the consuming processes (in our case: mineralization and nitrification). We disregard the oxygen exchange with the atmosphere in the calculation of this ratio because the exchange basically is a reaction process in the biogeochemical system. The resulting prod/cons-ratios reveal that the DO-consuming processes always clearly outweigh the DO-producing processes in all scenarios and in all seasons in the estuarine freshwater zone. An annual cycle is common to all scenarios with highest ratios resulting in spring and early summer and decreasing to low ratios in winter. Comparing the prod/cons-ratios between the different scenarios clearly shows that the relation of DO-producing to DO-consuming processes is similar for R and L, and for D and LD, respectively. The prod/cons-ratio thus confirms that the reduction in riverine loads almost linearly scales down the biogeochemical system whereas the change in geometry introduces more complex responses.

Table 3: Mean DO bulk changes for primary production, mineralization and nitrification in the freshwater zone between km-0 and km-120 for scenarios R, L, D and LD in mmol DO m^{-2} d^{-1}. The prod/cons-ratio describes the relation between the bulk changes of the DO-producing (here: primary production) and the DO-consuming processes (here: mineralization and nitrification).

	primary production				mineralization				nitrification				prod/cons - ratio			
	R	L	D	LD	R	L	D	LD	R	L	D	LD	R	L	D	LD
Jan/Feb	0	0	0	0	-6	-3	-6	-3	0	0	0	0	0.02	0.01	0.03	0.02
Mar/Apr	6	3	9	4	-24	-12	-25	-13	-4	-2	-4	-2	0.20	0.18	0.30	0.27
May/Jun	17	9	26	14	-66	-37	-79	-43	-15	-9	-17	-9	0.20	0.19	0.27	0.26
Jul/Aug	10	5	15	8	-67	-38	-79	-43	-11	-6	-11	-6	0.12	0.12	0.17	0.17
Sep/Oct	2	1	3	1	-40	-21	-44	-23	-6	-3	-7	-3	0.03	0.04	0.05	0.05
Nov/Dec	0	0	0	0	-12	-6	-12	-6	-3	-1	-3	-1	0.01	0.01	0.01	0.01

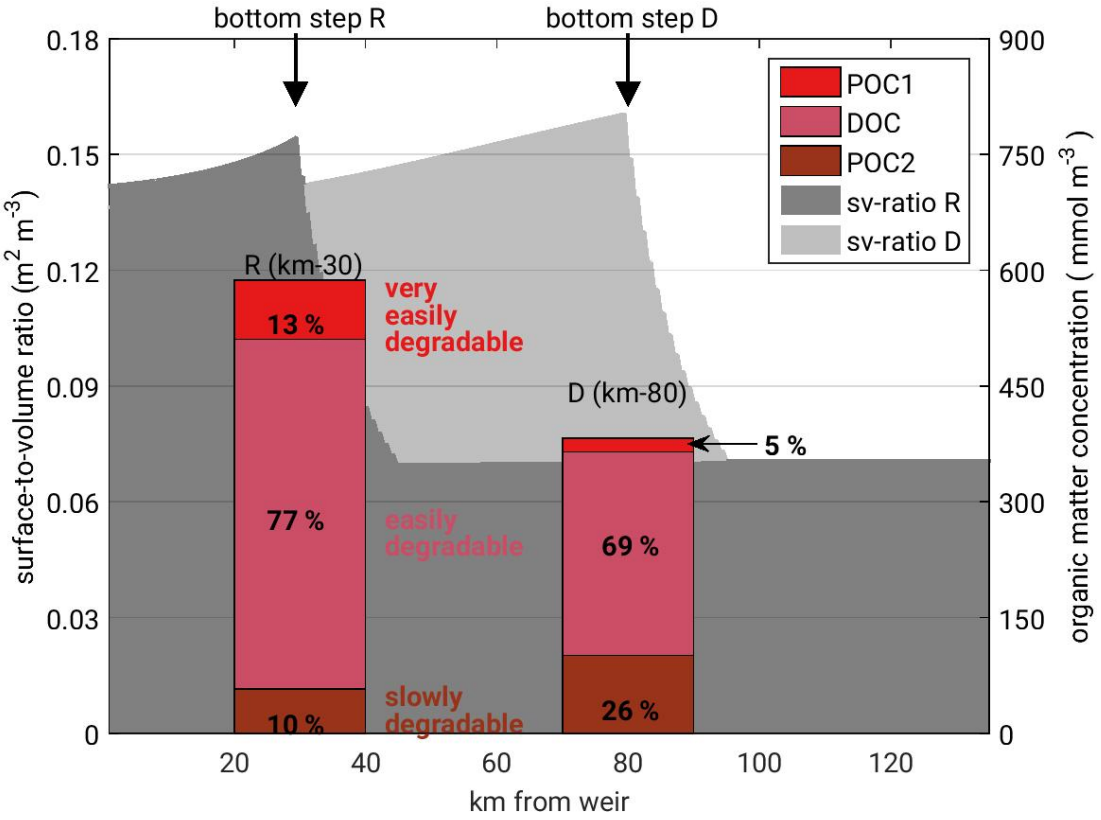

Figure 11: Surface-to-volume ratio of the water body for reference scenario R (dark grey area) and changed depth scenario D (light grey area) along the idealized estuarine domain. Bar plots show the concentrations of the carbon fractions POC1 (very easily degradable), DOC (easily degradable), POC2 (slowly degradable) and their relative contributions to the total amount of degradable organic matter, for scenario R at the position of the bottom step at km-30 and for scenario D at the position of the bottom step at km-80. Data plotted for the summer situation on 4-July-2011.

2.4. Discussion

2.4.1. Key processes of oxygen dynamics

Our sensitivity analysis shows highest dependency of estuarine oxygen levels on organic matter mineralization and phytoplankton mortality. This finding is confirmed by the rate analysis (section 2.3.4), which also underlines the relevance of organic matter degradation and mineralization. In addition to this expected outcome, our setup explains the pronounced oxygen minimum zone downstream of the bottom step in geometric terms. The strong increase in DO depletion downstream of the drop in bottom bathymetry results from the concurrence of two effects: first, the additional volume increase at the bottom step results in a sudden increase in degradable material and prolonged residence times, and thus accumulated consumption, per longitudinal segment; second, the available surface area for atmospheric oxygen input remains unchanged. The depth-integrated reaeration rates downstream of the bottom step corresponds to oxygen transfer coefficients of 0.7 - 2.8 m d^{-1}, which are higher than the values measured by *Kremer et al.* [2003] (0.36 - 1.68 m d^{-1}), but in the range of 0.6 - 3.0 m d^{-1} as given values for oxygen trans-

fer coefficients in *Thomann and Mueller* [1987], derived by the formulations of *O'Connor and Dobbins* [1958] and *Banks and Herrera* [1977].

Compared to mineralization by aerobic respiration, nitrification has a globally lower impact on the DO depletion - with the exception of further downstream areas during summer. Considering the overestimated NH4 concentration simulated during summer downstream of the bottom step, nitrification rate in our study may be too high so that one can expect an even lower influence of nitrification on DO than indicated by our results. This finding contrasts previous studies such as for the Pearl, Seine or the Forth estuary, where a larger relevance of nitrification has been suggested, possibly due to a lacking nitrification step in urban wastewater treatment [*Balls et al.,* 1996; *Garnier et al.,* 2001].

DO production by primary production in our model estuary with its reference bathymetry plays a minor role on DO dynamics and is merely performed by phytoplankton introduced from the continental river section. Our model predicts severe light limitation of phytoplankton growth, especially in the deeper sections of the estuary, very much in the range reported by *Soetaert et al.* [1994] for the Westerschelde. Light limitation might be even stronger in many estuaries because the SPMI concentration used in our study (47 g m^{-3}) is a low estimate, not only for the Elbe [*Weilbeer,* 2015], but also for many estuaries worldwide: it rarely falls below 50 g m^{-3} in the Columbia River estuary [*Gelfenbaum,* 1983], and may reaches up to more than 1000 g m^{-3} in highly turbid estuaries like the Ems [*Weilbeer,* 2008] and the Guadalquivir [*Diez-Minguito et al.,* 2014]. Altogether, oxygen yield by primary production only slightly counteracts the DO depletion in the most critical zone. Opposing evidences on the predominance of heterotrophy in estuaries [*Caffrey,* 2004; *Bianchi,* 2007; *Cloern et al.,* 2014; *Volta et al.,* 2016b] may, to some extent, merely reflect the diversity of estuarine systems. Our results reinforce the heterotrophic view, particularly for anthropogenically impacted estuaries.

2.4.2. Processes response to anthropogenic changes

Riverine nutrient and organic matter load and geometric/bathymetric modifications are two major human impact pathways on the estuarine biogeochemical system, which for the first time have been investigated in a coherent model study.

The study results show an almost linear response to the reduction in boundary input load on the process-based depth-integrated oxygen change rates and, thereby, DO depletion. Resulting summer minimum DO concentrations are less critical than in the reference scenario with unreduced riverine load. However, a quantitative conclusion on the reduction effect remains uncertain given that a range of potentially relevant processes were not included in our model, such as influences of benthic communities [*Herman et al.,* 1999], or storage mechanisms in bottom sediments and different ecological structures [*Howarth et al.,* 2011]. In addition, recovery pathways may differ from the eutrophication pathway, including hysteresis-like behavior [*Diaz and Rosen-*

berg, 2008]. Simulations aiming at a quantification of nutrient reduction effects will therefore have to cover several years to model the nutrient recovery response pathway. Though our results suffer from these shortcomings to make quantitative statements, our findings emphasize the role of riverine nutrient load reduction to combat anthropogenically induced estuarine DO depletion.

However, more complex feed-backs emerge in the scenario describing a bathymetric change, which constitutes a special case of a geometric change. Basically, a geometric change induces changes in hydrodynamic characteristics. Interdependencies between various hydrodynamic characteristics and biogeochemical processes have already been studied by e.g. *Regnier et al.* [2013] and *Arndt et al.* [2007]. In our study we focus on the biogeochemical system response of a bathymetric (i.e. depth related) change as the most pervasive human intervention in estuarine geometry nowadays. We show that a bathymetric change particularly entails an alteration in the surface-to-volume ratio. Thereby, the exchange possibility of gases with the atmosphere is altered. Our results illustrate that this effect strongly influences DO dynamics in such a way that high DO depletion occurs if a decrease in surface-to- volume ratio coincides with high concentrations of easily degradable material. So, we generally find the interplay between surface-to-volume ratio and the degradability state and amount of organic material to be most important in determining the specific ability of the system to recover high DO-mineralization losses by atmospheric input. This interrelation presumably plays a key role in other eutrophic well-mixed estuaries with heavy man-made bathymetric modifications and we suggest comparable analyses as done above in such systems. In the Loire (France), for example, the overall setting in terms of hydrodynamics, river discharge, riverine nutrient and phytoplankton load is comparable to the one used in this study, but the main bottom step is located much further downstream [*Abril et al.,* 2003; *Etcheber et al.,* 2007; *Walther et al.,* 2015]. A characteristic double peak in DO deficit corresponds to longitudinal variations in suspended sediment concentration [*Abril et al.,* 2003]. Based on our findings, it might be worth analyzing if the DO deficit is possibly also related to the maintained depths, and thus anthropogenically changed surface-to-volume ratios, for port access to St. Nazaire and Nantes.

In addition to DO, we furthermore expect a bathymetric impact, via the surface-to-volume ratio, on other biogeochemical elements having a gaseous phase and an air-water exchange. We especially suggest exploring the relevance of anthropogenically modified bathymetries to estuarine carbon outgassing.

When simultaneously realizing the two changes of nutrient reduction and bathymetry, an overlap of effects leads to a clear reduction of DO depletion. However, no synergetic effect in terms of DO recovery occurs. This may partly be ascribed to the simplicity of the model configuration, as discussed above, but the overlapping behavior more likely reflects the heterotrophic state: respiratory control of DO depletion as well as the bathymetric constraint on atmospheric DO supply

do not interact, but act additively. This holds as long as the bathymetric changes are not so substantial as to alleviate the light limitation and to enable a build-up of phytoplankton biomass in the estuary.

2.5. Conclusions

We present an integrated hydrodynamic-biogeochemical model which enables the investigation of anthropogenic impacts on estuarine biogeochemical processes and prove its skill in an idealized one-dimensional domain. Here, it discloses the quantitative interplay of different factors that shape the DO distribution in anthropogenically impacted systems. Moreover, our findings support the view of heterotrophic degradation prevailing over all other biogeochemical influences on DO, and nitrification playing only a minor role, at least in contemporary vertically well-mixed estuaries.

Our findings also underpin the effectiveness of nutrient reduction in the riverine catchment as a measure to reduce estuarine DO depletion. However, subsequent studies aiming at the quantification of nutrient reduction effects will have to explore the necessity of model enhancements in terms of benthic processes and delayed release from sediment storages.

We gain new scientific understanding of the role of bathymetric changes to biogeochemical cycling and especially to DO dynamics. A bathymetric change, as a subcase of geometric variations, alters the ratio of water surface to underlying water volume. Consequently, the relative ability of gas exchange with the atmosphere is changed. This effect may similarly apply to all biogeochemical substances having a relevant gaseous form. This study reveals the importance to DO depletion, particularly the joint effect of low surface-to-volume ratio in combination with high concentrations of easily degradable material. We therefore encourage consideration of the surface to volume ratio, in addition to the widely used residence time scales, when investigating anthropogenic changes of the estuarine geometry and their influence on DO depletion.

Altogether, our results contribute to a more integral assessment of the biogeochemical system response to man-made pressures on estuaries.

Acknowledgements

We would like to thank Werner Blohm for providing observational data for the Elbe estuary, and Günther Lang and Holger Weilbeer for helping to set up the hydrodynamic simulations. The work of Ingrid Holzwarth was funded as part of the Federal Waterways Engineering and Research Institute (BAW) departmental research and development program. The work of Kai W. Wirtz was supported by the German Federal Ministry of Education and Research (BMBF) through the MOSSCO project (grant number 03F0667A) and by the Helmholtz Society through the PACES program.

3. The effect of bathymetric modification on water age in the Elbe Estuary

This chapter is based on the paper "The effect of bathymetric modification on water age in the Elbe Estuary", which is submitted for publication to the journal Estuarine, Coastal and Shelf Science

Citation: Holzwarth I.; Weilbeer H. and Wirtz K.. The effect of bathymetric modification on water age in the Elbe Estuary. Submitted.

Abstract The transport time of substances is a physical factor that influences the completeness of biogeochemical reactions in the estuary or certain estuarine sections. Since hydrodynamic changes induce changes in transport time, river discharge and its seasonal variability strongly determine the transport time of riverine water and its fluctuations. A factor that leads to a permanent change in hydrodynamics is man-made bathymetric modification. However, the impact of such modification on transport time has never been quantified. Here we show for the Elbe Estuary (Germany) that the impact of typical, decadal man-made bathymetric modification on the transport time of riverine water is much smaller than the effect of the natural variability in river discharge. We used riverine water age to determine transport time and found the age difference due to river discharge variation to be in the order of days to weeks, depending on the location within the estuary. A simple approximation of the observed dependency between riverine water age and the inverse of the discharge is presented and discussed. In contrast to the strong influence of discharge, we found the age difference between scenarios which differ by the effect of 40 years of man-made bathymetric modification to be in the order of hours up to one day, depending on location and discharge. Overall, riverine water age increases by approximately 7 % in the higher impacted bathymetry, suggesting that transport time is only slightly affected by the considerable depth differences of several meters in large parts of the estuary. Nevertheless, the increase in transport time potentially poses an additional stressor to the estuarine oxygen minimum zone in the higher anthropogenically impacted bathymetry, especially in combination with the reduced reaeration ability due to the decreased water surface-to-volume ratio. A precise quantification in terms of oxygen, though, will have to consider a possible shift of the oxygen minimum location and requires investigation with a process-based biogeochemical model.

Keywords: well-mixed estuary; 3D numerical model; transport time; riverine water age; estuarine oxygen minimum zone

3.1. Introduction

The transport time of substances in estuaries is an important characteristic because it is the physical factor that influences the completeness of biogeochemical reactions in the estuary or certain estuarine sections. In the context of nutrient transport, phytoplankton dynamics, low oxygen situations, fate of pollutants and spill events, such transport times have been assessed in many estuarine systems worldwide [Chan et al., 2002; Fujiwara et al., 2002; Shen and Haas, 2004; Brye et al., 2012; Rayson et al., 2016; Ahmed et al., 2017]. Usually, a strong dependence of transport time on river discharge is either inherently given by the applied method, e.g. in Sheldon and Alber [2006], or observed in the results, e.g. in Kärnä and Baptista, [2016b].

Generally, changes in transport time are induced by changes in hydrodynamics. Thus, several other influence mechanisms than river discharge on transport time scales exist; of particular interest are man-made influences with regard to the interaction of the diverse human impacts on the biogeochemical system of estuaries. One of the worldwide dominating man-made intervention nowadays is the deepening of the estuarine bathymetry for navigational purpose [Avoine et al., 1981; Abood et al., 1999; Vriend et al., 2011; Meyers et al., 2014b; van Maren et al., 2015a]. While bathymetric changes involve changes in estuarine hydrodynamics [Liu et al., 2001; Prandle, 2003; Lane, 2004; Picado et al., 2010; Ensing et al., 2015], they potentially also induce a change in transport time. Despite the commonness of bathymetric deepening, the influence of man-made bathymetric modification on transport time has not been quantitatively investigated to date.

In this study, we examine the effect of a realistic, 40-year bathymetric change due to human interference on transport time scale in the Elbe Estuary (Germany), see Figure 12. The Elbe Estuary is a well-mixed alluvial estuary which is strongly exposed to anthropogenic influences, particularly by heavy man-made modifications of its geometry with considerable deepening of the bathymetry during the last centuries, and by riverine substance loads which lead to strong biogeochemical processes in the estuarine freshwater section [Schroeder, 1997; Dähnke et al., 2008; Amann et al., 2012, 2014].

Several methods exit to estimate or calculate time scales for the transport of substances. Some methods provide an integral time scale for the entire system, others give local results for the different positions in the estuary [Zimmerman, 1988]. The former kind of methods are so-called box model estimates [Zimmerman, 1988; Kärnä and Baptista, 2016b] which usually either base on the flushing time approach [Zimmerman, 1988; Monsen et al., 2002] or rely on tidal prism models [Luketina, 1998 and references therein]. The latter, local time scales are either section-wise applications of the box model estimates, or continuous methods that make use of numerical models. Of those local and continuous methods, the concept of water age is the most widely used [Shen and Haas, 2004; Brye et al., 2012; Kärnä and Baptista, 2016b]; it is mathematically well-

described [Delhez et al., 1999; Deleersnijder et al., 2001; Delhez and Deleersnijder, 2002; Delhez et al., 2004] and demarcated from related time scales [Delhez et al., 2014].

Here, we use water age to describe the local development of transport time scales along the Elbe Estuary and in comparison to a bathymetry with a different degree of human intervention. Finally, we assess the results with respect to biogeochemical processes, especially with regard to the regularly occurring seasonal estuarine oxygen minimum.

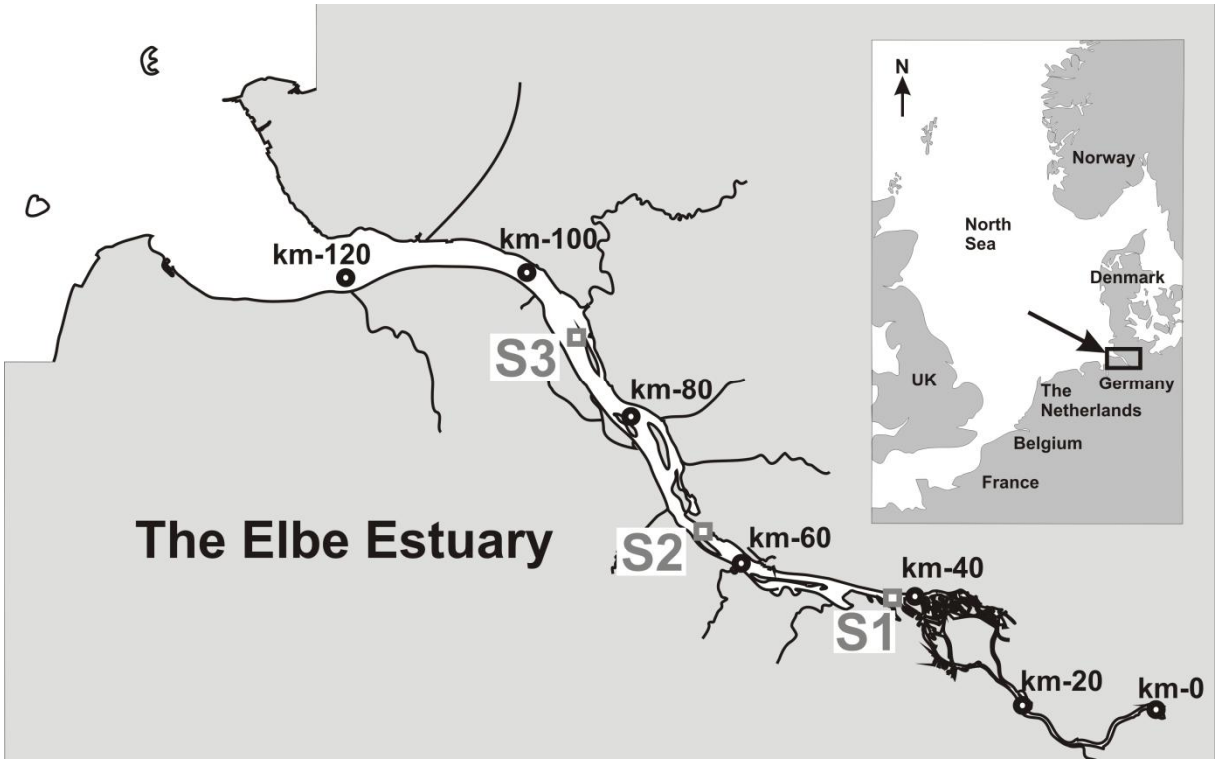

Figure 12: Location of the Elbe Estuary at the North Sea (small map). Thick black circles mark the distance in kilometers downstream of the tidal barrier at km-0, the three grey squares mark the positions of the observation stations S1 (Seemannshöft), S2 (Juelsand D2) and S3 (Rhinplate D4).

3.2. Method

3.2.1. Hydrodynamic model

We simulated hydrodynamics in the Elbe Estuary with the mathematical method Untrim [Casulli, 2009; Casulli and Stelling, 2010]. The Elbe Estuary model setup is adapted from the coarsest model described in [Sehili et al., 2014]. In comparison to the model used there, the largest difference in the model applied here is the position of the river boundary at the weir as tidal barrier (and not some location further upstream) and the use of a detailed distribution of bottom friction coefficients. The bathymetry resolution on subgrid level [Casulli and Stelling, 2010] enables a precise representation of water volume. The unstructured, orthogonal computational grid consists of roughly 11000 horizontal elements with 25 subgrid divisions per edge and a maximum of 31 vertical z-layers with a thickness of 1m.

The model domain extends along the 170 km estuarine shipping channel, starting at the tidal boundary (km-0, see Figure 12) down to the end of the maintained shipping channel in the inner German Bight, see Figure 13a. The domain contains the entire volume between the main dikes and includes the largest eight tributaries of the estuary.

The model is steered with realistic boundary values for the years 2010 and 2011: at the riverine boundary, we use daily measurements of river discharge at the last riverine gauging station Neu Darchau (50 km upstream of the weir at km-0; data from Water and Shipping Authority Lauenburg, accessed at www.fgg-elbe.de). Riverine water temperature values originate from observations at the station Cumlosen (115 km upstream of the weir at km-0; data from Landesamt für Umwelt Brandenburg, accessed at www.fgg-elbe.de) and salinity is kept constant at 0.4 psu. In the tributaries we employ long-term mean discharge estimates [IKSE, 2005] due to a lack of discharge measurements. Wind and air temperature fields for the entire domain are provided from daily forecasts (Deutscher Wetterdienst DWD). At the seaward open boundary, water level values stem from a numerical circulation model of the German Bight, salinity is kept constant at 32 psu and we use water temperature from the offshore observation station FINO1 (data from http://fino.bsh.de) which is located outside the model domain in the North Sea.

3.2.2. Scenario definitions

Two different bathymetric scenarios represent two states with different degrees of man-made modification: scenario “Hi” represents an actual, heavily impacted bathymetry. Scenario “Lo” represents a lesser impacted bathymetry, though far from being pristine. The modifications from Lo to Hi particularly include deepening and maintenance of the navigation channel, and silting of flood plains and side branches as related morphological reactions. Figure 13b and Figure 13c show that water depth in Hi is several meters higher compared to Lo in most sections of the navigation channel.

In Hi we use the bathymetry of the year 2010 as the most recent and consistent one available. In Lo, we replace the bathymetry in the section between the tidal barrier and km-120 by the 40 years older bathymetry of 1970. In the section of the replacement, bathymetry differences can be mainly attributed to anthropogenic modifications. We left the estuarine mouth area further downstream unchanged since there, bathymetric differences also result from natural morphologic changes. Note, that the peculiar depth peak in scenario Lo at km-40 (Figure 13c) is due to the open construction of an immersed tube tunnel below the Elbe at that time.

We combine the two bathymetric scenarios Hi and Lo with four different discharge regimes, resulting in eight simulated scenarios, see Table 4: Hi-M and Lo-M include the variable, observed riverine freshwater discharge in the years 2010 and 2011. Hi-3 and Lo-3 run with a constant discharge of 300 $m^3 s^{-1}$, corresponding to mean low summer discharge of 301 $m^3 s^{-1}$ [FHH and

HPA, 2014]. Hi-7 and Lo-7 (Hi-13 and Lo-13) run with 700 $m^3 s^{-1}$ (1300 $m^3 s^{-1}$), corresponding to mean discharge of 713 $m^3 s^{-1}$, and mean high summer discharge of 1280 $m^3 s^{-1}$, respectively.

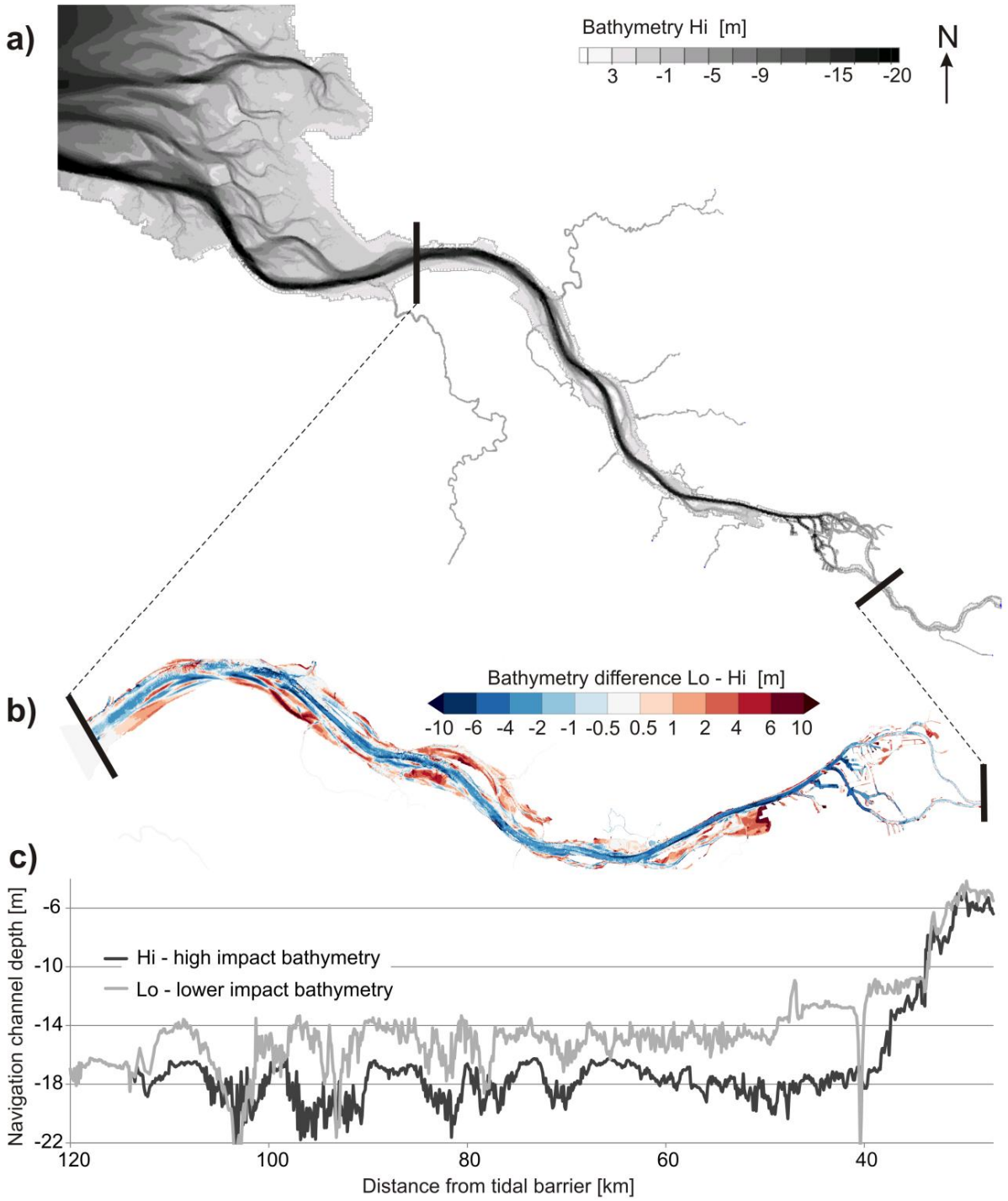

Figure 13: a) Model domain with bathymetry Hi, shown in the resolution as used in the subgrid bathymetry model. Thick black lines mark the section of largest bathymetry differences between Hi and Lo. b) Bathymetry difference Lo – Hi. Blue areas indicate that these parts are deeper whereas red areas are lower in the bathymetry Hi. c) Depth of the navigation channel along the estuary for the bathymetries Hi in black and Lo in grey.

Table 4: Overview on scenarios; scenarios differ in bathymetry (Hi, Lo) and riverine freshwater inflow. The reference simulation Hi-M is bases on the bathymetry Hi and measured riverine discharge; Hi-M thus represents the situation in the years 2010 and 2011.

Freshwater discharge	Measured 2010 – 2011	Constant 300 $m^3 s^{-1}$	Constant 700 $m^3 s^{-1}$	Constant 1300 $m^3 s^{-1}$
Hi	Hi-M (reference)	Hi3	Hi7	Hi13
Lo	Lo-M	Lo3	Lo7	Lo13

3.2.3. Water age calculation

Delhez et al. [1999] defines the age of a water parcel as the time that elapsed since the water parcel entered a domain of interest outside of which the age is prescribed to be zero. Thereby, age is a pointwise, time-dependent result in the domain and its calculation is derived in an Eulerian framework to run with the algorithms of a numerical model.

We use the calculation of water age implemented in D-Water Quality [Postma et al., 2003; Smits and van Beek, 2013], which is based on the tracking of two tracers that are transported by fluid motion. One tracer (Tcon) is conservative whereas the other tracer (Tdec) is subjected to exponential growth or decay and related to the concentration of Tcon according to: $C_{Tdec}(t) = C_{Tcon} \cdot e^{\gamma t}$.

The transport equations for the two tracers are

$$\frac{\partial C_{Tcon}}{\partial t} = -\nabla \cdot (\boldsymbol{u}\, C_{Tcon} - \boldsymbol{K}\, \nabla C_{Tcon}) \quad (1)$$

$$\frac{\partial C_{Tdec}}{\partial t} = -\gamma C_{Tdec} - \nabla \cdot (\boldsymbol{u}\, C_{Tdec} - \boldsymbol{K}\, \nabla C_{Tdec}) \quad (2)$$

The water age a is then calculated by

$$a = \frac{\ln(C_{Tdec}/C_{Tcon})}{\gamma} \quad (3)$$

We focus on the age of riverine water because the riverine substance load governs the strong biogeochemical processes in the Elbe Estuary [Schroeder, 1997; Dähnke et al., 2008; Amann et al., 2012, 2014]. To estimate the time that elapsed since a riverine water signal entered the estuary, we charge water discharge at the tidal barrier with constant concentrations of the conservative as well as the decayable tracer. During the simulation, riverine water age ariv is then calculated for each computational element, based on Equation 3.

3.3. Results

3.3.1. Hydrodynamic model validity

Reference simulation (Hi-M) results demonstrate that the hydrodynamic model is capable of simulating the estuarine water movement with a good overall agreement between simulated cell values and point measurements of water level, current velocity, and water temperature, see the

skill statistics in Table 5 and Figure 14. The deviation in salinity (Table 5) mainly results from using constant boundary conditions. Our results complement Sehili et al. [2014] who already showed good agreement between model results and observations for water level during selected periods in the years 2006 and 2011.

Time series comparison generally shows a good agreement between simulated and observed water level and current velocity, including magnitude and timing, see an example in Figure 15 at a station that is located close to S1 (Figure 12). The deviation in water temperature predominantly occurs during summer and originates from neglecting the effect of power plant cooling waters. Altogether, the model provides a reliable hydrodynamic base.

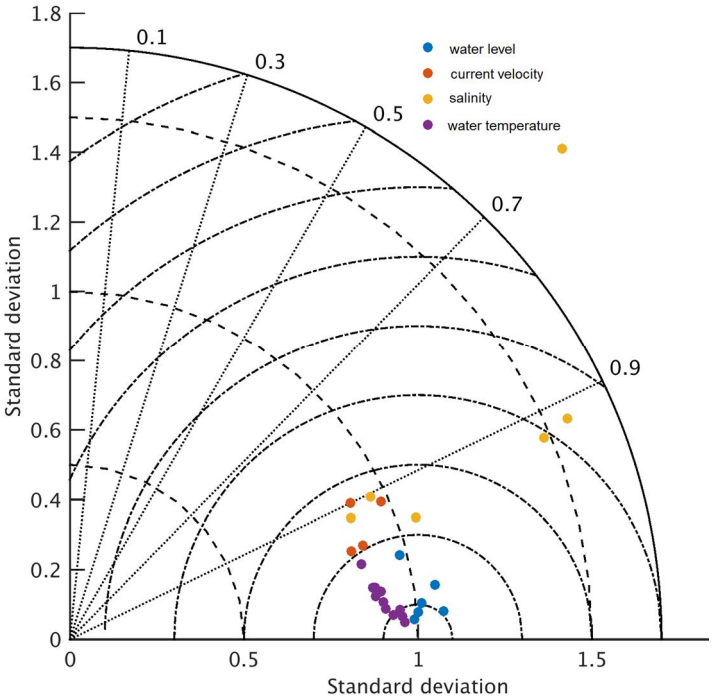

Figure 14: Taylor diagram on the statistical comparison of model results for the reference scenario HI-M with observations. Blue dots show values for model skill at the position of water level measurements, red dots for current velocities, yellow dots for salinity, and violet dots for water temperature. Observation stations and period of comparison are identical to the ones assessed in Table 5.

Table 5: Model skill in comparison to observations. n gives the number of observation stations. The statistical figures were calculated using all available measurements at each station for the entire simulation period from 01.01.2010 to 31.12.2011.

Variable with n = number of stations	Mean correlation	Mean difference	Mean deviation of means
Water level (n=6)	0.991	0.090 (m)	0.005 (m)
Current velocity (n=4)	0.930	0.114 (m/s)	-0.080 (m/s)
Salinity (n=10)	0.867	2.1 (1e-3)	2.0 (1e-3)
Water temperature (n=12)	0.991	0.97 (°C)	-0.77 (°C)

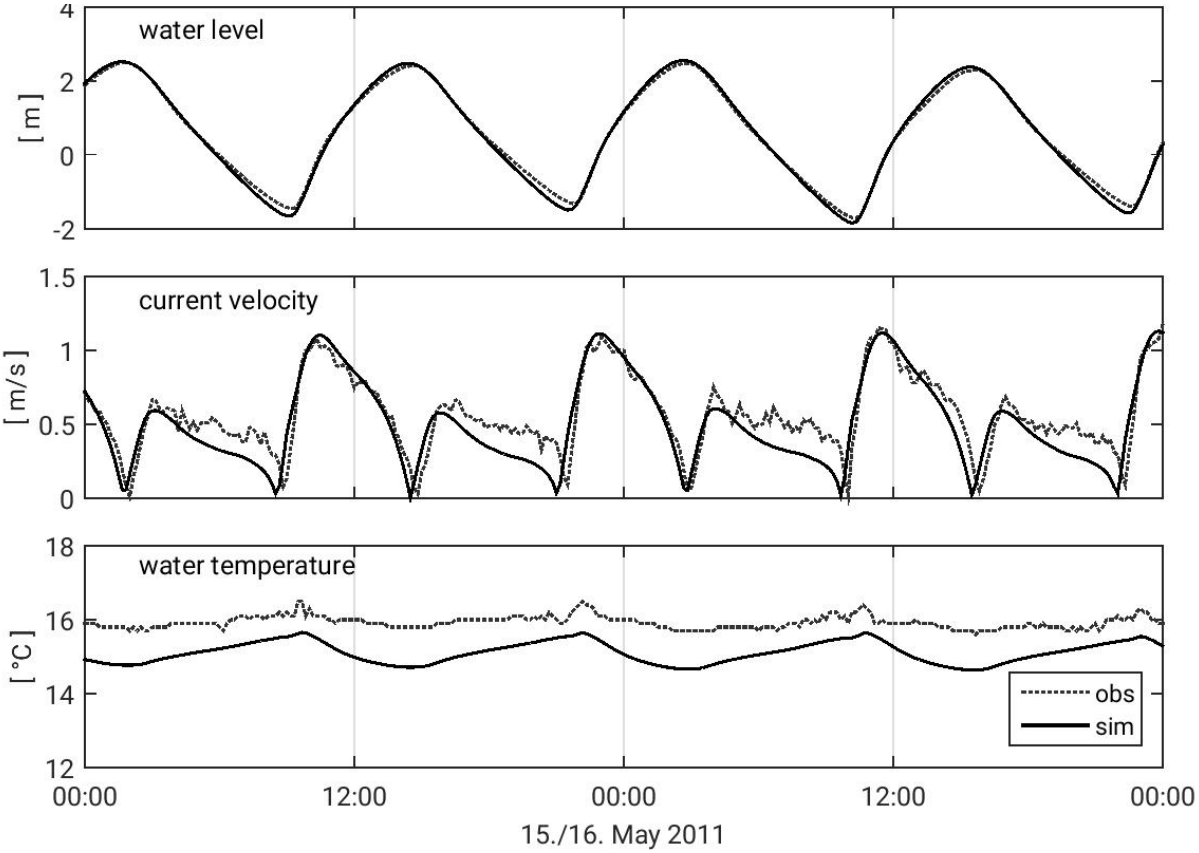

Figure 15: Time series comparison of observed and simulated water level, current velocity and water temperature of the reference scenario Hi-M for a period of two days in May 2011. Time series record is close to S1: water level data are compared at the gauging station Hamburg/St. Pauli (km-37). The absolute value of current velocity and water temperature are compared at the continuous measuring station D1-Hanskalbsand (km-57). Measurements from Water and Shipping Agency Hamburg, available on www.portaltideelbe.de. Salinity is not shown because the position is located in the freshwater section.

3.3.2. Reference water age

In the reference scenario Hi-M riverine water age a_{riv} for the reference scenario generally increases from upstream to downstream: Figure 16a shows a_{riv} during the year 2011 at three stations S1, S2, S3 along the estuarine shipping channel (positions marked in Figure 12) with S1 being the most upstream station and having smaller a_{riv} values than S2 than S3. The areal overview confirms that a_{riv} increases downstream, see Figure 17a, which shows spring-neap averaged a_{riv} values during low river discharge condition.

Riverine water age a_{riv} exhibits a strong dependency on river discharge (blue line in Figure 16a): after the high discharge event at the end of January, a_{riv} values are smallest for all stations (e.g. 0.9 days at S1, 3.8 days at S3) while values are largest in July after several weeks of low discharge (e.g. 9.1 days at S1, 25.2 days at S3). The more downstream the station, the bigger is the difference between smallest a_{riv} after high discharge and largest a_{riv} during low discharge: while this difference is about 8 days at S1, it is more than 20 days at S3. The a_{riv} difference between the

stations also depends on discharge, e.g. the a_{riv} difference between S1 and S3 after the peak discharge in January is about 3 days whereas it is more than 15 days during the low flow period in June/July.

When looking at a_{riv} values in dependence on river discharge without chronological allocation (dots in Figure 16b), the behavior described above appears even more consistent: at similar discharge, a_{riv} values are larger the more downstream the station; at the same station, a_{riv} values are larger the smaller the discharge; the more downstream the station, the larger the a_{riv} difference at high discharge compared to low discharge; and, finally, the lower the discharge, the higher the a_{riv} differences between upstream and downstream stations.

At each station, a_{riv} seems to be inversely proportional to river discharge Q; Figure 16b displays a fitted line at each station S1 to S3 of a_{riv} in dependence of Q^{-1}.

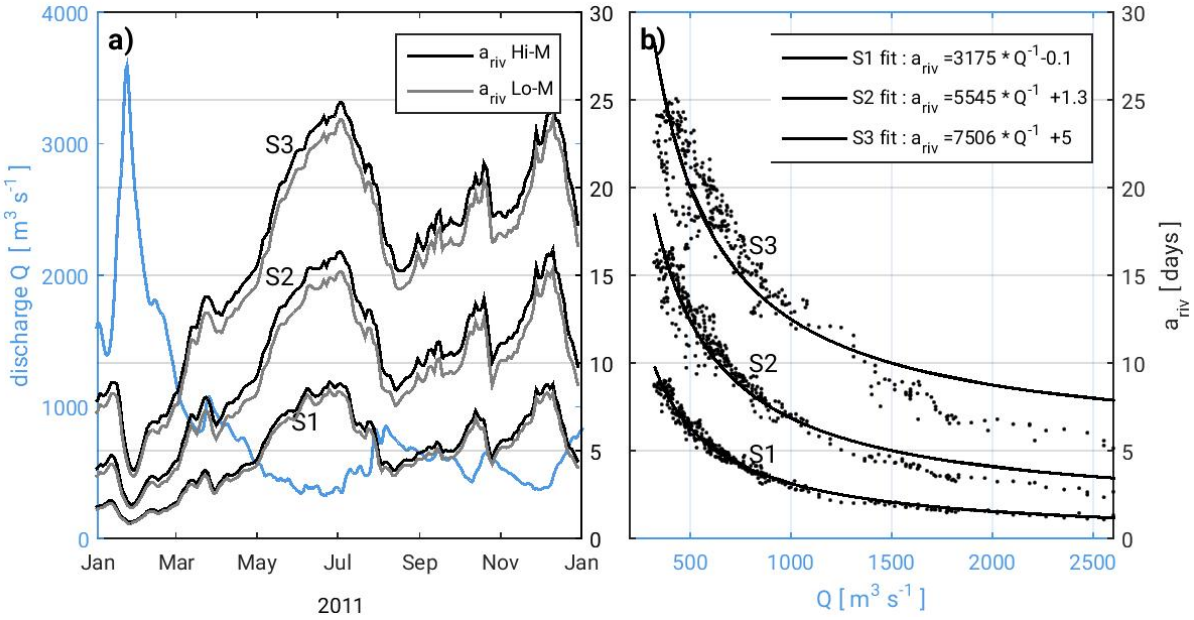

Figure 16: a) Time series of measured river discharge Q (blue line) and calculated riverine water age a_{riv} for the year 2011. Values for a_{riv} are shown at the stations S1 (km-43, position Seemannshöft) and S2 (km-65, D2 Julesand) in the estuarine freshwater part, and S3 (km-90, position D4 Rhinplate) in the salinity mixing zone for the scenarios Hi-M (black) and Lo-M (grey), respectively. b) Black dots show daily a_{riv} values plotted versus freshwater discharge Q for the stations S1, S2 and S3; the lines show a fit for each station with the equation given in the box.

3.3.3. Water age for bathymetric and constant discharge scenarios

In scenario Lo-M, a_{riv} is usually smaller compared to Hi-M, see in Figure 16a grey lines compared to black lines. The differences are in the range of hours at S1, S2, and S3, and thus lower than the differences caused by the natural variability of river discharge. At S1, the difference in a_{riv} between the two scenarios Hi-M and Lo-M is smallest following the flood event (~1 hour difference) and highest during the low-flow period (~14 hours difference). At S3, differences are larg-

er but behave in the same way: differences are smallest after the flood in January (~ 8 hours difference) and they are highest during low river discharge (~38 hours).

The areal differences between Hi-M and Lo-M (Figure 17b) confirm that a_{riv} is larger in Hi-M, apart from some harbor basins and bank areas that silted up or had been backfilled. Figure 17b also indicates that a_{riv} differences increase downstream.

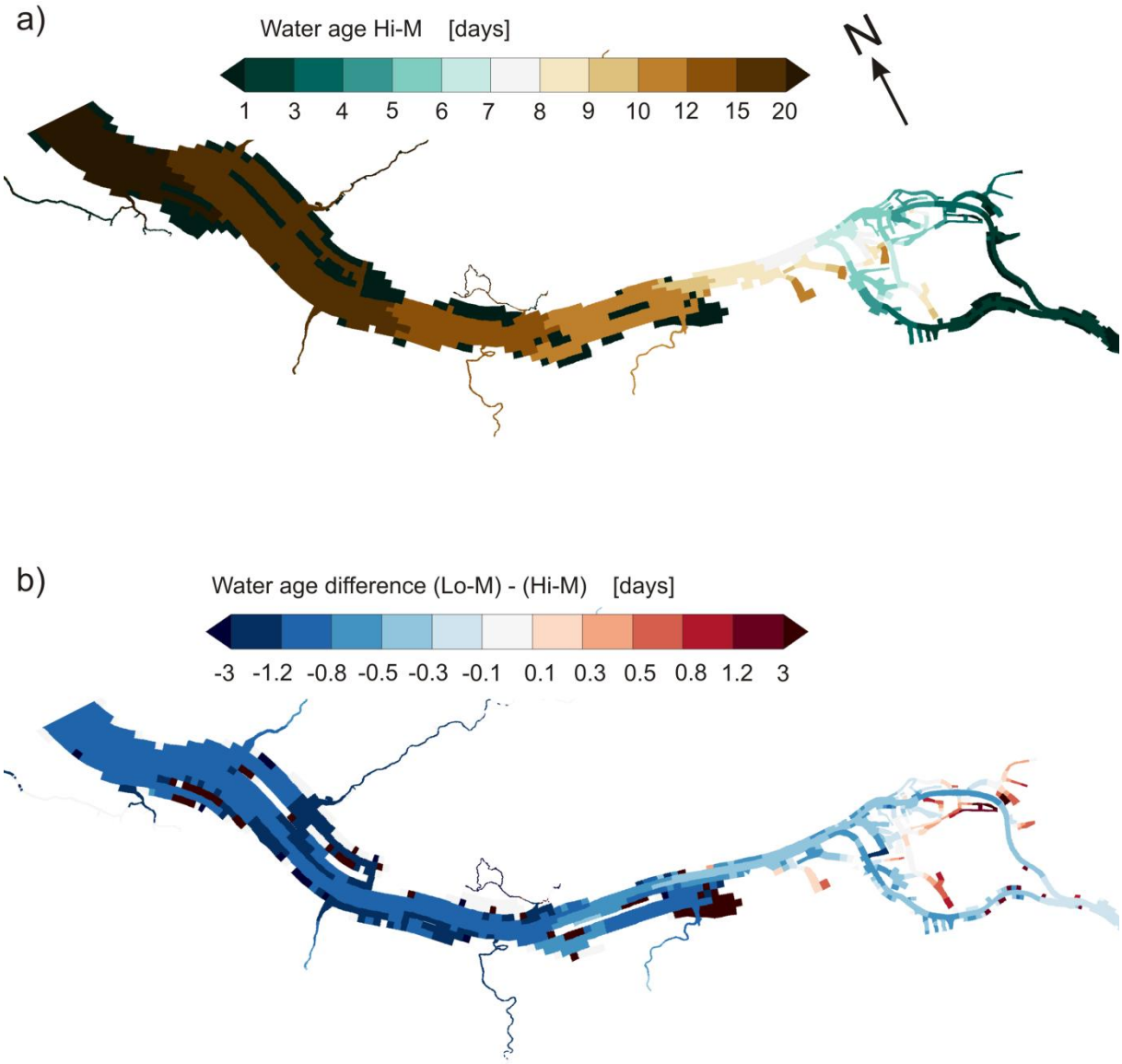

Figure 17: a) Spring-neap tidally averaged water age a_{riv} in June 2011 for scenario Hi-M. There are some conspicuous patches in the middle of the estuary (sand banks and islands) and at the banks that appear to have a water age below 1 day: these are elevated areas that have fallen dry and have a water age of zero. b) Water age difference (Lo-M) – (Hi-M) of spring-neap tidally averaged water age for boundary conditions of June 2011. Similar to a), there are patches where water age difference above 3 days is displayed: these areas fell dry in Hi-M but not in Lo-M, leading to the apparently high difference.

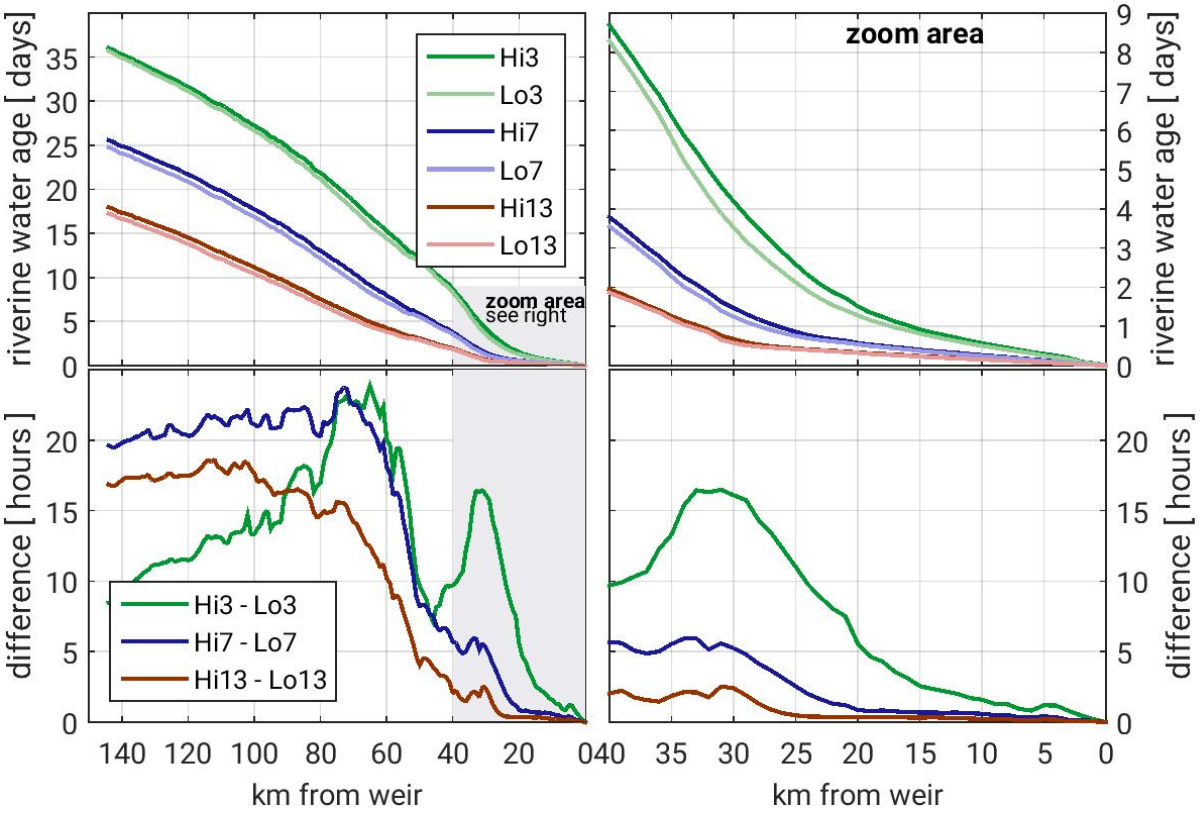

Figure 18: Upper panels: Riverine water age along the estuary for scenarios with constant discharge. Lower panels: Difference in riverine water age between scenarios with the same discharge but different bathymetries. Left panels show values along the entire shipping channel, right panels show a zoom in the upstream 40 km of the shipping channel.

In the constant freshwater discharge scenarios (Hi3, Hi7, Hi13), riverine water age a_{riv} behaves similarly to the scenarios with variable, measured discharge: a_{riv} increases with distance from the tidal barrier and with decreasing discharge (Figure 18 upper left panel). In addition to the variable discharge scenarios, the quasi-stationary results for the constant discharge scenarios better allow an evaluation on the longitudinal profile. Most prominent is the accelerated increase in a_{riv} between km-20 and km-35 (Figure 18 zoom area on upper right panel). During the 15 km long distance, a_{riv} increases from 1.5 days to 6.4 days in the low-flow scenario Hi3, from 14 hours to 2.5 days in Hi7 and from 8 hours to 1.3 days in Hi13. Downstream of km-35, the increase in a_{riv} continues steadily but more gradually. 55 km further downstream, at position S3, a_{riv} reaches values of 24.8 days in Hi3, of 15.6 days in Hi7 and of 9.5 days in Hi13.

Water age in the corresponding Lo constant discharge scenarios is always smaller (Figure 18 upper panels, flat-colored lines for Lo-scenarios in comparison to intensely-colored lines for Hi-scenarios). However, differences are in the order of a few hours up to 1 day maximum (see Figure 18 lower panels). While a_{riv} differences between Hi7 and Lo7, and Hi13 and Lo13, grow almost continuously from upstream to downstream until km-70 in Lo7 and until km-100 in Lo13, the differences between Hi3 and Lo3 peak twice along the estuary: at around km-30 where a_{riv} is 16 hours smaller, and second between km-60 and km-80 where it is almost 1 day smaller in the

shallower bathymetry Lo. Downstream of km-80, a_{riv} values in Hi3 and Lo3 converge whereas differences in Hi7/Lo7, Hi13/Lo13 respectively, appear to remain almost constant until km-140.

3.4. Discussion

3.4.1. Proportionality between water age and river discharge

The local dependency between riverine water age a_{riv} and river discharge Q seems to relate a_{riv} to the inverse of Q with some exponent. While *Kärnä and Baptista* [2016b], for example, found a slightly different dependence, $Q^{-0.66}$, for one specific section in the Columbia River estuary, we found Q^{-1} to fit our data well, especially in the lower discharge range and for upstream stations. The equations which we fitted to the results of the reference scenario Hi-M at the three stations S1, S2, S3, and which are indicated in Figure 16b, also approximates the age values in the constant discharge scenarios (Figure 18, upper panels) at each of the three locations. We provide a simple derivation of this dependency below.

Let Q be a specified river discharge; the estuarine width depends on distance x from the tidal limit (x = 0) with $B(x) = B_0 \cdot e^{k \cdot x}$ [*Prandle,* 1986], and depth H is assumed to be constant for simplicity. The exponent k is a constant shape factor for the estuarine funnel curvature and a system constant. Then, the cross-sectional area can be approximated by $A(x) = A_0 \cdot e^{k \cdot x}$, with $A_0 = B_0 \cdot H$. The residual, cross-sectional downstream velocity can be approximated by

$$v(x) = \frac{Q}{A_0} \cdot e^{-k \cdot x} \quad . \qquad [1]$$

The average residual velocity $\overline{v}$ for the section between x = 0 (tidal limit, point of release of river discharge Q) and some distance x downstream is

$$\overline{v} = \frac{\int_0^x v(x)\, dx}{x} = \frac{Q}{A_0 \cdot k} \cdot \frac{1}{x} \cdot [1 - e^{-k \cdot x}] \quad . \qquad [2]$$

So, the average time a water parcel needs to flow from the point of release to some position x downstream is

$$T(x) = \frac{x}{\overline{v}} = \frac{A_0 \cdot k \cdot x^2}{Q \cdot [1 - e^{-k \cdot x}]} \quad . \qquad [3]$$

While A_0 and k are constants for a specific estuary, $T(x)$ in Equation 3 solely depends on the inverse of river discharge, Q^{-1}.

The derivation above provides a generic approximation for a dependency of riverine water age a_{riv} on the inverse of river discharge Q. However, several constrains to this approximation explain the differences of the ideal fit from calculated values in Figure 16b: most importantly, the effect of a change in Q needs some time to propagate through the system and the assumption of fast/instantaneous adaptation of a_{riv} becomes less precise the more downstream the location of interest. Furthermore, the underlying estuarine geometry describes an ideal, convergent shape

but real estuarine shapes deviate from it and include, e.g., non-monotonic growth in cross-section.

Nevertheless, the generic dependency in Equation 3 lets us expect a similar relation in other estuaries and we encourage riverine water age assessments similar to ours.

3.4.2. Effect of man-made bathymetric modification on water age

Large depth differences exist between the bathymetric scenarios Hi and Lo (Figure 13b and Figure 13c). In scenario Hi, the navigation channel is several meters deeper whereas lateral areas at the banks of the estuary are up to several meters shallower. In total, the estuarine volume is about 6.7% larger in Hi compared to Lo. The larger water volume explains the general increase in riverine water age under the higher human impact in Hi-M.

During the time period that we considered in this study, discharge values were not constant long enough for a_{riv} to reach steady state values. We therefore also studied scenarios with different constant discharges and found the a_{riv} differences between the bathymetric scenarios (Hi3 and Lo3, Hi7 and Lo7, Hi13 and Lo13, respectively) to be in the same order of magnitude as the difference between Hi-M and Lo-M. This consistency in results for different discharge regimes lets us reliably determine the difference in a_{riv} due to the bathymetric modifications to be in the order of several hours in most sections of the estuary, corresponding to 6-8% of the absolute value.

Overall, the variation in water age a_{riv} due to varying discharge within each of the scenarios Hi-M and Lo-M is much larger than the difference in a_{riv} due to a different bathymetry at any equal discharge regime.

3.4.3. Relation to estuarine oxygen dynamics

Transport time scales are usually explored in the context of biogeochemical or water quality issues [*Chan et al.,* 2002; *Fujiwara et al.,* 2002; *Shen and Haas,* 2004; *Brye et al.,* 2012; *Rayson et al.,* 2016; *Ahmed et al.,* 2017]. Here, we focus on estuarine oxygen dynamics because in the Elbe Estuary [Schroeder, 1997; Amann et al., 2012] and in many other contemporary estuaries worldwide, estuarine oxygen minimum zones (eOMZs) are frequently observed [*Billen et al.,* 2001; *Abril et al.,* 2003; *Hagy et al.,* 2004; *Zhang and Li,* 2010; *Ruiz et al.,* 2015; *Tomaso and Najjar,* 2015]. The eOMZs are mainly linked to anthropogenic impacts, of which eutrophication is the most frequently reported cause [*Cloern,* 2001; *Diaz,* 2001; *Breitburg et al.,* 2003; *Paerl,* 2006; *Kemp et al.,* 2009; *Conley et al.,* 2009; *Paerl,* 2009; *Rabalais et al.,* 2010; *Howarth et al.,* 2011; *Díaz and Rosenberg,* 2011]: the increase in land-borne nutrients due to the wash out of agricultural fertilizers increases primary production in the limnic river sections which transforms into labile detritus when reaching the deeper and more turbid estuarine sections. Bacterial respiration of

such easily degradable detritus consumes oxygen and results in an eOMZ if the oxygen depletion cannot be counterbalanced by atmospheric reaeration or primary production.

Generally, physical and biogeochemical processes interact in the formation and control of eOMZs [*Kemp and Boynton,* 1980; *Du and Shen,* 2015]. Previous studies have attempted to estimate the effect of physical processes on eOMZs, mainly for stratified and partially stratified estuaries [*Fujiwara et al.,* 2002; *Scully,* 2013; *Bruce et al.,* 2014; *Du and Shen,* 2015], where wind conditions and freshwater discharge govern the strength of the stratification and thus are the dominating physical influence mechanisms. In well-mixed estuaries, comparable studies are missing, maybe because the intrinsic hydrodynamic conditions are favorable to counteract low dissolved oxygen concentrations by the generally greater possibility to supply oxygenated water from the surface. Nevertheless, eOMZs regularly occur in many well-mixed estuaries [*Schroeder,* 1997; *Verity et al.,* 2006; *Lanoux et al.,* 2013; *Diez-Minguito et al.,* 2014].

Bathymetric deepening in well-mixed estuaries influences physical factors of eOMZ formation, mainly the transport of degradable organic matter via changes in hydrodynamics and the relative atmospheric interface for reaeration due to the reduction in water surface-to-volume ratio (sv-ratio). Despite these possible influences of bathymetric deepening on an eOMZ, there is no quantification of physical effects known to us, though, similar to the Elbe Estuary, many well-mixed estuaries worldwide experience the phenomena of a strongly deepened navigation channel and severe eOMZs, like the upper Delaware Estuary [*DiLorenzo et al.,* 1994; *Sharp,* 2010; *Tomaso and Najjar,* 2015], the Scheldt [*Meire et al.,* 2005; *van Damme et al.,* 2005], the Loire [*Abril et al.,* 2003; *Etcheber et al.,* 2007; *Walther et al.,* 2015] or the Guadalquivir [*Diez-Minguito et al.,* 2014; *Ruiz et al.,* 2015].

The time it takes for degradable organic matter to be transported to a specific location determines the completeness of its heterotrophic degradation. *Middelburg and Herman* [2007], for example, showed that organic matter is extensively modified due to heterotrophic processing in estuaries with long residence times compared to estuaries with shorter residence times. An analysis in *Lanoux et al.* [2013] for the Gironde estuary hints at lower oxygen concentration during a period of longer residence times compared to a period of shorter residence time under otherwise similar environmental conditions. It is thus a plausible concept that a longer transport time induces higher accumulated oxygen consumption between the origin of degradable organic matter and some specific location. If the higher oxygen consumption will also lead to a more severe eOMZ, strongly depends on the possibility for reaeration [*Holzwarth and Wirtz,* 2018].

3.4.4. Indicator-based approach

Is it possible to assess whether a bathymetric modification will cause notable impacts on estuarine oxygen dynamics, solely based on hydrodynamic information? We propose that at least the influence of physical changes can be estimated by the use of suitable indicators. In case the indi-

cation hints at potentially small impacts, further evaluation with a sophisticated biogeochemical model can be saved.

Since an oxygen deficit results from oxygen consumption exceeding oxygen supply [*Streeter and Phelps,* 1925; *Chapra,* 2008], hydrodynamic influence on an eOMZ may be exerted in both ways, by oxygen consumption and/or supply. We thus investigate two indicators, one for changes in oxygen demand due to bathymetric modification and one for changes in oxygen supply.

Based on the considerations in the previous section, we take organic matter transport time as an indicator for accumulated oxygen demand and assume that riverine water age a_{riv} represents organic matter transport time. Given the detected increase in a_{riv} of approximately 7 %, our results hint at an increase in accumulated oxygen demand caused by a realistic, 40-year bathymetric change due to human interference.

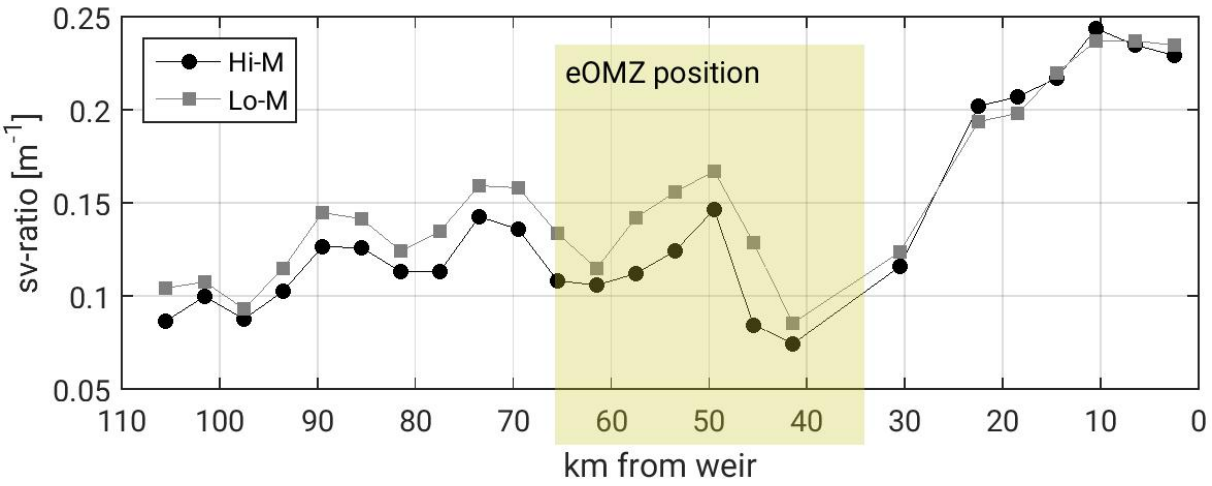

Figure 19: Surface-to-volume ratio (sv-ratio) for the scenarios Hi-M (black) and Lo-M (grey) along the Elbe Estuary. The shaded area marks the section with typical position of the eOMZ.

Likewise, we use sv-ratio as an indicator for oxygen supply because it describes how much water volume is oxygenated through a unit of water surface area. Especially in shallow and well-mixed systems, with easy supply of oxygen-enriched water from the surface to the underlying water body, the amount of oxygen that is exchanged with the atmosphere is critically restricted by the relative surface area. The sv-ratio varies with location and water level, and thus with tidal phase, freshwater discharge and meteorological condition. Here, we determine the sv-ratio by averaging the simulation results of water volume and water surface area in Hi-M and Lo-M for the entire simulation period. The resulting values are presented in Figure 19; on average the sv-ratio is 10% lower in Hi-M compared to Lo-M, and 15% lower if we only consider the estuary downstream of km-30, which corresponds to the section with maintained marine navigation channel. The lower sv-ratio in Hi-M is mainly created by the greater water depth. A variation in river discharge slightly influences the sv-ratio in the most upstream estuarine part but does not affect the overall values mentioned above. The decrease in sv-ratio caused by the realistic bathymetric

modification implies that more water volume has to be reaerated through the same surface area and thus indicates a lower oxygen supply to the eOMZ.

In Figure 20 the indicator-based approach is summarized. Overall, both indicators show a change due to more intense man-made bathymetric modification, each in a direction to create adverse effects on the eOMZ. However, the magnitude of 7 % and 10 – 15 %, respectively, is neither negligible nor notably high, and a clear categorization of the severity of the man-made hydrodynamic impact on the eOMZ is not possible.

Generally, a precise quantitative estimation of the influence of man-made bathymetric modifications on an eOMZ in terms of oxygen necessitates a model that dynamically simulates the important interactions between physical and biogeochemical factors and that also includes the interactions between several biogeochemical quantities. Some biogeochemical effects due to the change in depth, like the influence on primary production [*Kemp and Boynton,* 1980; *Soetaert et al.,* 1994] or suspended sediment concentration [*Talke et al.,* 2009; *de Jonge, Victor N. et al.,* 2014] possibly prevail in some estuaries. In addition, the validity of the hydrodynamic indicators is arguable. Most importantly, our indicator for oxygen demand, riverine water age, relies on the assumption that transport time of organic matter is proportional to the transport time of water. We imply that the a_{riv} difference between the two bathymetric scenarios is unaffected by particle processes and thereby neglect that bathymetric deepening may affect the transport of particulate matter in several ways [*van Maren et al.,* 2015a].

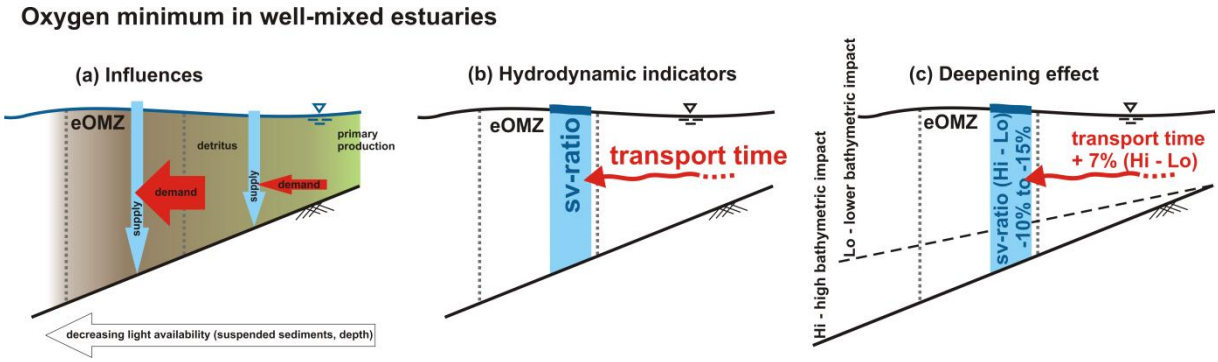

Figure 20: a) Influences that form an estuarine oxygen minimum zone (eOMZ) in well-mixed estuaries; b) derived hydrodynamic indicators for changes in those influences. c) Impact of bathymetric change with numbers giving the quantitative effect from scenario Lo-M (anthropogenically lower impacted bathymetry) to scenario Hi-M (high man-made bathymetric modifications).

3.4.5. Possible quantitative influence on the eOMZ in the Elbe Estuary

Does the magnitude of the differences that we found in our scenario comparison for the hydrodynamic indicators imply possible changes on the eOMZ? We tentatively estimate the effect of such changes to the observed eOMZ during summer 2011 between km-35 and km-60. Dissolved oxygen concentrations in this area dropped to 3 g O_2 m^{-3} at water temperatures around 20 °C,

meaning an oxygen deficit of about 6 g O_2 m^{-3} generated by high respiration of detritus from riverine phytoplankton.

The sv-ratio difference between Hi-M and Lo-M takes effect through the reaeration surface. At an oxygen deficit of 6 g O_2 m^{-3} and with typical oxygen gas transfer coefficients (piston velocities) between 0.6 m d^{-1} to 3 m d^{-1} [*O'Connor and Dobbins,* 1958; *Banks and Herrera,* 1977; *Thomann and Mueller,* 1987], reaeration can produce an oxygen enrichment of 3.6 – 18 g O_2 m^{-2} d^{-1}. In the region with lowest sv-ratio (around km-40), 1m^2 of surface area has to supply 13.5 m^3 of water in Hi and 11.8 m^3 in Lo, leading to a lower possible enrichment in Hi-M of 0.04 - 0.2 g O_2 m^{-3} d^{-1}. Directly downstream, in the region with the largest sv-ratio difference (around km-45), the possible enrichment is 0.16 – 0.8 g O_2 m^{-3} d^{-1} lower in the deeper bathymetry Hi.

To roughly estimate the effect of different water ages, we assume that respiration commences directly downstream of the weir. From there, water needs about 8.5 days in Hi-M and 8 days in Lo-M to reach km-40 (S1, see Figure 16). Applying an exponential law of organic matter decay and an overall decay rate of 0.1 to 0.2 day^{-1} (applied in models for the Elbe [*Schroeder,* 1997; *Holzwarth and Wirtz,* 2018]), 5 to 10 % more material will have decayed and depleted oxygen in Hi-M compared to Lo-M when arriving at km-40. If we further assume about 2.4 to 4.8 mg C m^{-3} of initially available degradable organic carbon at the weir, 0.33 – 0.74 g O_2 m^{-3} more oxygen is consumed between the weir and station S1 in Hi-M compared to Lo-M. Though, a part of this additional consumed oxygen will be resupplied atmospherically.

In Hi-M, riverine water stays longer in the estuary and sv-ratio is lower compared to Lo-M. Both effects lead to lower oxygen concentrations, the first one by higher oxygen depletion in the more upstream sections of the estuary and the second one by impaired atmospheric compensation. In the example above, the effects of both impact pathways are in the same order of magnitude, each up to 10 % of the absolute deficit at the current position. However, also the eOMZ position can be influenced by bathymetric deepening: the higher oxygen demand upstream may also shift the eOMZ further upstream, or lead to higher reaeration compensation of the deficit, so that a pure additive effect of increased demand and decreased supply is unlikely.

3.5. Conclusion

Riverine water age in the Elbe Estuary is governed by river discharge; the age is small after time intervals with high discharges and increases, proportional to the inverse of discharge, during periods of low discharge. Thereby, the age difference between highest and lowest discharge is in the order of days for upstream stations and grows to weeks for stations in the salinity gradient zone. The generic approximation that we derived for the dependency between riverine water age and river discharge is presumably applicable for many funnel-shaped estuaries.

The effect of a bathymetric difference, which reflects a realistic 40-year impact of typical man-made modification, on riverine water age is much smaller than the effect of the natural, seasonal variability in river discharge. The age difference between the bathymetric scenarios lies in the order of hours up to one day maximum, depending on location and discharge.

With regard to the anthropogenically driven problem of estuarine oxygen minimum zones, we propose to use riverine water age as a hydrodynamic figure that indicates possible changes in accumulated oxygen consumption. Such an indicator-based approach provides some advantages: first, it helps disentangling the effects of hydrodynamic and biogeochemical processes which is important to track the clear and quantitative cause and effect relations. Second, in case of potentially small indicated impacts, an evaluation with a sophisticated biogeochemical model can be saved. In this study, the impact of the investigated man-made modification on riverine water age is 10 - 15 % and process-based biogeochemical modeling appears necessary to more precisely quantify oxygen related impacts, including a possible shift of the oxygen minimum location.

Notwithstanding the apparently small impact, the effect of the larger water age in the higher impacted bathymetry potentially leads to higher accumulated oxygen consumption. In combination with reduced oxygen reaeration due to the decreased water surface-to-volume ratio, the higher impacted bathymetry generates additional stressors to the estuarine oxygen minimum zone, acting into the direction of lower oxygen levels. We thus expect hydrodynamic effects by deepening to intensify the eutrophication impact, which certainly constitutes the main stressor to estuarine oxygen levels.

Acknowledgements

We thank Frank Böker (BAW) for preparing the different model bathymetries and Günther Lang (BAW) for his valuable input on deriving the generic approximation on the dependency between water age and discharge.

The work of Ingrid Holzwarth and Holger Weilbeer was funded as part of the Federal Waterways Engineering and Research Institute (BAW) departmental research and development program. The work of Kai W. Wirtz was supported by the German Federal Ministry of Education and Research (BMBF) through the MOSSCO project and by the Helmholtz Society through the PACES program.

4. A 3D estuarine biogeochemical model to evaluate the impact of man-made bathymetric modification and nutrient reduction on dissolved oxygen

This chapter is a manuscript in preparation by Holzwarth I. and Wirtz K. "A 3D estuarine biogeochemical model to evaluate the impact of man-made bathymetric modification and nutrient reduction on dissolved oxygen".

Abstract Several anthropogenic impacts influence estuarine oxygen concentrations. Of those possible impacts, eutrophication and bathymetric modifications, such as deepening, are direct human interventions which affect the entire estuarine system. However, the influence of realistic bathymetric modification in relation to a change in nutrient load on dissolved oxygen levels has never been quantified.

Here, we introduce a 3D hydrodynamic-biogeochemical model with precise representation of the bathymetry for the vertically well-mixed Elbe Estuary. Results explain the formation of the estuarine oxygen minimum by a sequence of related oxygen-consuming processes. We illustrate that a 50 % reduction in riverine load has a much larger effect on relieving an estuarine oxygen deficit compared to restoring the bathymetry to an anthropogenically less impacted state of 40 years ago.

Nevertheless, bathymetric modifications pose an additional stressor to the oxygen system and the cumulative effect of many bathymetric modifications over centuries may be particularly relevant. Overall, our results emphasize the key priority of nutrient reduction when tackling oxygen deficits, and relegate bathymetric improvements to a position behind.

Keywords: Realistic bathymetric modification; 3D hydrodynamic-biogeochemical model; estuarine oxygen minimum zone; nutrient reduction; well-mixed estuary

4.1. Introduction

Increasing evidence for severe dissolved oxygen (DO) deficits in vertically well-mixed estuaries due to anthropogenic nutrient enrichment is observed [*Schroeder,* 1997; *Abril et al.,* 2003; *van Damme et al.,* 2005; *Verity et al.,* 2006; *Mallin et al.,* 2006; *Ruiz et al.,* 2015]. Thereby, the development in well-mixed systems follows a global trend that is predominantly observed in vertically stratified water bodies [*Kemp et al.,* 2009; *Rabalais et al.,* 2009; *Conley et al.,* 2011; *Breitburg et al.,* 2018].

The fact that DO deficits develop in well-mixed systems, despite their physically favorable conditions, may solely be the consequence of the large amount of riverine organic matter and/or ammonium load. However, many of the well-mixed estuaries also serve as major shipping routes to large ports, that are located far upstream the mouth of the estuary like the Humber Ports (Humber, UK), Antwerpen (Schelde, Belgium), Hamburg (Elbe, Germany), or Seville (Guadalquivir, Spain). To ensure port access also for ocean cargo vessels, these estuaries contain a substantially deepened shipping channel which can be more than twice as deep as the estuary's natural state. The bathymetric modifications to meet navigational needs induce changes that are potentially relevant to oxygen dynamics: such as hydrodynamics and morphologic responses [*Nichols,* 1988; *Pan et al.,* 2012; *Meyers et al.,* 2014a; *Wan et al.,* 2014; *van Maren et al.,* 2015a; *Zarzuelo et al.,* 2015], that also alter transport characteristics. In addition, geometric relations change by deepening.

An important geometric relation for the dynamics of estuarine oxygen minimum zones (eOMZs) in vertically well-mixed systems is the ratio of water surface to underlying water volume: it describes the relevant interface on which the reaeration rate is active and thereby constrains the amount of atmospheric oxygen that can be supplied to the underlying water column. In *Holzwarth and Wirtz* [2018] we demonstrated that the interplay between water surface-to-volume ratio and the degradability state of the organic material is a key for the severity of DO deficits in consumption-dominated estuaries. Subsequently, we compared two realistic bathymetric states that differed in the degree of man-made modification and derived indicators from hydrodynamic results to estimate if the bathymetric differences might also influence DO dynamics to a notable extend (Chapter 3). Results hinted at small effects in an order of magnitude of about 10 %. Here, we combine the biogeochemical configuration and the anthropogenic impact scenarios from the first study [*Holzwarth and Wirtz,* 2018] with the detailed and realistic three-dimensional model domain from the second study (Chapter 3). This approach seeks to obtain detailed insights into biogeochemical process dynamics, their dependencies and the contribution of individual processes to the eOMZ. A comprehensive analysis of the complex interplay especially between physical and biogeochemical processes defines a persistent challenge in estuarine research. Furthermore, owing to a great relevance in estuarine management, we aim at a

quantitative assessment of the realistic man-made bathymetric modifications in comparison to changes in anthropogenic nutrient enrichment on estuarine DO dynamics.

4.2. Method

4.2.1. Mathematical models

We couple a state-of-the-art biogeochemical model with a 3D hydrodynamic model. Estuarine hydrodynamics, including salt and water temperature transport, are simulated with Untrim [*Casulli,* 2009; *Casulli and Stelling,* 2010], which includes a detailed model bathymetry on subgrid level [*Casulli and Stelling,* 2010; *Sehili et al.,* 2014]. The method allows a precise representation of water volume up to measurement accuracy. Another advantage of this method relevant to our study is the possibility to trace the water surface area on subgrid scale and thus in great detail: while in classical approaches to wetting and drying, a grid cell can be only handled as either wet or dry, in the method for subgrid bathymetry of *Casulli* [2009] grid cells can also be partially wet in the intertidal area. Furthermore, no drying threshold is required.

The biogeochemical equations are solved with D-Water Quality [*Postma et al.,* 2003; *Smits and van Beek,* 2013]. The two, individually mass-conserving, mathematical models Untrim and D-Water Quality communicate through a coupling module that enables mass-conserving transfer [*Lang,* 2012] of the hydrodynamic characteristics from Untrim to D-Water Quality, including water temperature, salinity and turbulent diffusivities.

We simulated the oxygen-relevant biogeochemical processes of organic matter cycling including phytoplankton growth, mortality and detritus degradation, and nitrification with the configuration developed in *Holzwarth and Wirtz* [2018]. There, the configuration has been successfully tested to provide a realistic account of major processes driving estuarine oxygen dynamics. One outcome was that primary production in the estuary is strongly light limited and its importance to DO dynamics is low. In this study we thus reduced the biogeochemical configuration by the phosphorous and silicate state variables because no influence on DO dynamics is given.

4.2.2. Data integration

At the river boundary, we force the hydrodynamic model with measured daily mean freshwater discharge at the gauging station Neu Darchau (50 km upstream of the weir at km-0; data from Water and Shipping Authority Lauenburg, accessed at www.fgg-elbe.de) and water temperature from the gauging station Cumlosen, about 115 km upstream of the weir (provided by Landesumweltamt Brandenburg, available on www.fgg-elbe.de), and salinity is kept constant at 0.4 psu. In the tributaries we employ long-term mean discharge estimates [IKSE, 2005] due to a lack of discharge measurements. Wind and air temperature fields for the entire domain are provided from daily forecasts (Deutscher Wetterdienst DWD). At the seaward open boundary, water level

values stem from a numerical circulation model of the German Bight, salinity is kept constant at 32 psu and we use water temperature from the offshore observation station FINO1 (data from http://fino.bsh.de) which is located outside the model domain in the North Sea.

Observational biogeochemical data at the model boundaries are scarce. Most importantly for this study are riverine boundary values; here, we used observations from helicopter sampling directly upstream of the weir, and from continuous/biweekly observational data at the stations Cumlosen and Schnackenburg (all data from FGG Elbe, www.fgg-elbe.de). We compiled these measurements to boundary values under certain assumptions: chlorophyll-a to carbon conversion factor is 0.05 g Chl-a g^{-1} C, algal stoichiometry agrees to the Redfield Ratio, slowly degradable particulate organic matter is half as rich in nutrients compared to easily degradable particulate organic matter, and 1% of the measured, total amount of DOC is labile. At the seaward boundary, we applied linearly interpolated rare measurements from helicopter sampling. For a detailed description of biogeochemical boundary values see *Holzwarth and Wirtz* [2018].

For comparison, DO values from several observation stations inside the model domain were available (from upstream to downstream): Obs1 at km-23 (Bunthaus), Obs2 at km-42 (Seemannshoeft), Obs3 at km-49 (Blankenese), Obs4 at km-57 (D1 Hanskalbsand), Obs5 at km-65 (D2 Juelsand), Obs6 at km-75 (Grauerort), Obs7 at km-79 (D3 Pagensand), and Obs8 at km-90 (D4 Rhinplate). Data from Obs1 to Obs3 are provided by Institut fuer Hygiene und Umwelt Hamburg, licence dl-de/by-2-0, www.wgmn.hamburg.de. Data from Obs4, Obs 5, Obs7 and Obs8 are provided by water and shipping agency Hamburg, available on www.portaltideelbe.de. Data from Obs6 are provided by NLWKN Stade, accessed on www.elbe-datenportal.de/FisFggElbe.

4.2.3. Simulated scenarios

The reference scenario in this study represents an anthropogenically heavily impacted state of the Elbe Estuary and is labeled “HIGH” (derived from *high* water depth in the shipping channel due to *high* human impact). The underlying hydrodynamic reference scenario is identical to the reference scenario in Chapter 3: we simulated the years 2010 and 2011 with observed boundary values on a bathymetry from the year 2010. We labeled this reference bathymetry “Hi”, due to the high water depths in the navigation channel.

We subjected the reference scenario “HIGH” to a small sensitivity test regarding the uncertainties in boundary values, especially the labile share of riverine DOC. The documented range in literature is large [Moran et al., 1999; Raymond and Bauer, 2000; Butman et al., 2007; Guillemette and del Giorgio, 2011] but rarely mentions values above 10 % labile DOC of the total amount of DOC. We tested the sensitivity of DO results for shares of 1 %, 10 % and 100 % labile DOC, with model runs tagged HIGH, HIGHx10 and HIGHx100, respectively.

Furthermore, we simulated scenarios of a different human impact with regard to bathymetric modification and riverine substance load: in addition to the reference bathymetry “Hi”, we con-

structed a model bathymetry "Lo" with a less heavy impact of human modification; the "Lo"-bathymetry has lower water depths in the navigation channel because on the first 120 km downstream of the tidal limit the "Hi"-bathymetry has been replaced by a 40 years older, less anthropogenically impacted bathymetry from 1970, see section 3.2.2 for more detailed information .

Regarding riverine substance load, we also defined an alternative scenario to the situation in the reference simulation, similar to the study in *Holzwarth and Wirtz* [2018]: while in HIGH, we used realistic riverine boundary values for nutrient, phytoplankton, and particulate and dissolved organic matter, we halved this riverine load in another scenario. Unlike an observed historic situation, the value of 50 % approximately corresponds to the mean percentage between estimated pristine river concentrations [*Topcu et al.,* 2011] and actually measured concentrations [*FGG Elbe,* 2017] for total nitrogen and total phosphorous. Combining the scenarios of varying DOC lability, bathymetry and riverine boundary load, gave in total six different scenarios, which are summarized in Table 6. In all cases, the simulation period was the year 2011 due to its representative discharge conditions [*Holzwarth and Wirtz,* 2018].

Table 6: Modeled human impact and boundary DOC lability scenarios.

	Reference load 1% labile DOC	50% riverine load	10% labile DOC	100% labile DOC
Bathymetry Hi (year 2010)	HIGH (reference)	LOWnutrients	HIGHx10	HIGHx100
Bathymetry Lo (year 1970)	LOWbathymetry	LOW	- / -	- / -

4.3. Results

4.3.1. Reference scenario HIGH

DO results in HIGH show qualitative agreement with observed DO values along the Elbe Estuary for six selected observation stations, see Figure 21. Quantitatively, we observe some deviations: simulated DO values are often slightly higher than observed values, expect for the most upstream station Obs1. At Obs1, the seasonal variation in DO values is less pronounced compared to the other stations, while short-term variations in DO levels at Obs1 are strong, especially in summer, e.g. at the beginning of July with a DO increase of more than 100 mmol m^{-3} within a few days. At Obs1, but also at other stations, simulated DO peaks during summer are generally lower than observed.

The characteristic drop in summer DO values, which indicates the presence of an eOMZ, is most distinct at the stations Obs2 and Obs3 followed by a gradual DO increase downstream at Obs4,

Obs6 and Obs8. The drop and the subsequent gradual increase, in space and in time, are well represented by model results (Figure 21).

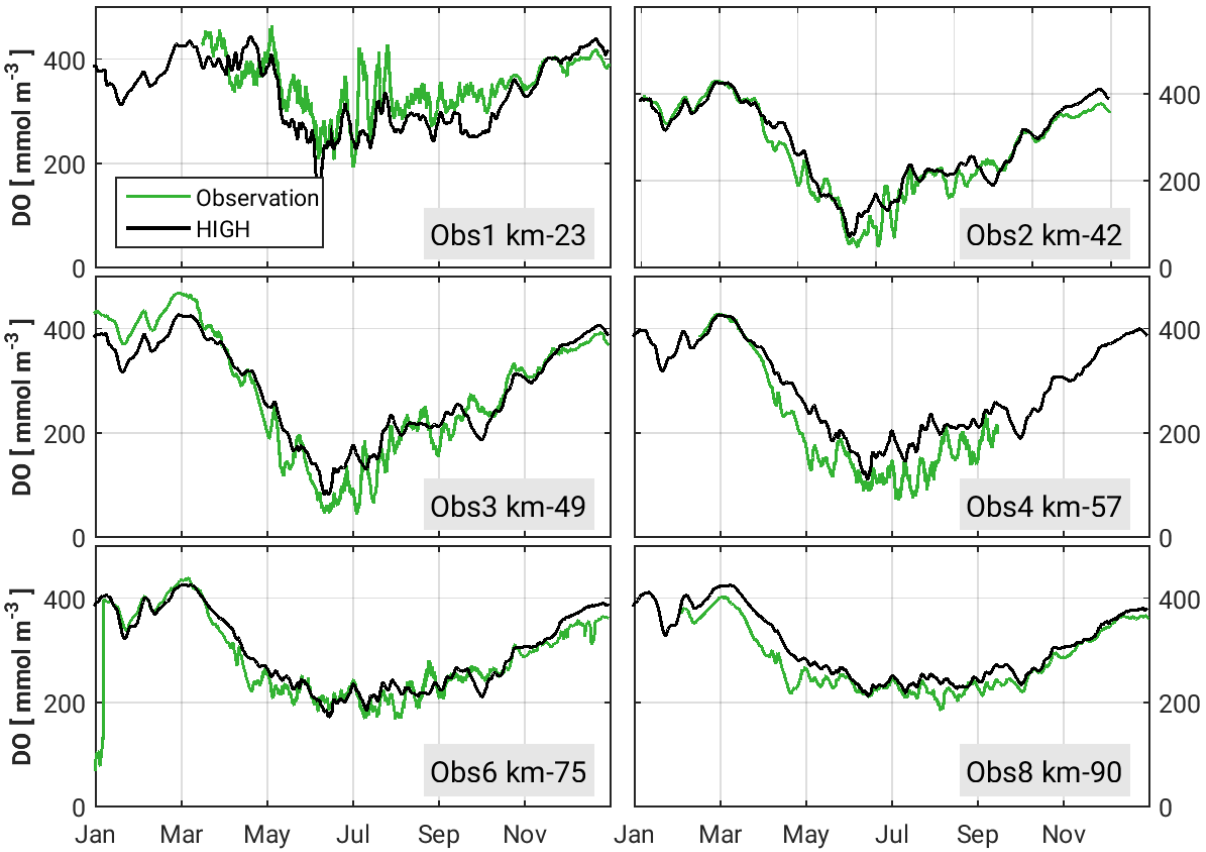

Figure 21: Simulated dissolved oxygen concentrations of the reference scenario HIGH (black lines) and observed concentrations (green lines) at several measuring stations along the Elbe Estuary during the year 2011. Obs1 is the most upstream station, Obs8 the most downstream station, see also Figure 25. Simulation results are taken from the uppermost model layer that never fell dry at the position of the observation stations during the simulation period (-2 m to –1 m above mean sea level).

Table 7: Mean absolute deviation of simulated DO concentration from observations at the measuring stations along the Elbe Estuary, except for Obs7 (km-79), where large data gaps exist in 2011.

Station ID	Obs1	Obs2	Obs3	Obs4	Obs5	Obs6	Obs8	⌀
position	km-23	km-42	km-49	km-57	km-65	km-75	km-90	all
Mean absolute deviation [mmol m^{-3}]	39.8	23.4	31.6	45.6	41.4	18.2	22.7	31.8

Overall, simulated DO concentrations in the reference scenario “HIGH” represent observed DO values along the Elbe Estuary with a mean absolute deviation of 31.8 mmol m^{-3}, see Table 7. For calculating the deviation, we closed data gaps in the observational data, which were shorter than 6 h, by spline interpolation. For time spans of longer data gaps we proceeded as follows: in case,

the gaps were at the beginning or end of the time series, we shortened the respective time series. In case the gaps were in between valid measurements but during periods of overall stable DO concentrations, we filled these gaps by linear interpolation. In case, data gaps longer than 6h existed during periods of rapidly changing DO concentrations (> 62.5 mmol m^{-3} between last measurement before and first measurement after the data gap), we dismissed the entire observation station. Using these criteria, we did not take the data at Obs7 (km-79) into account.

Vertical DO and salinity profiles show that the water column is well-mixed during all tidal phases in the freshwater part (Figure 22 left). In the area of increasing salinity, short periods of stratification may occur, as in the example on Figure 22 (right): the flood current (third panel from above, 2011-06-12 01:00) pushes water with higher salinity above less saline water, leading to temporary stratification. Apart from the vertical salinity distribution, the non-parabolic shape of the vertical turbulent viscosity also indicates stratification during these periods. However, the vertical distribution of DO in the water column is almost constant, apart from the value in the uppermost cell and sometimes slightly bended profiles, as in Figure 22, left, 2011-06-12 01:00.

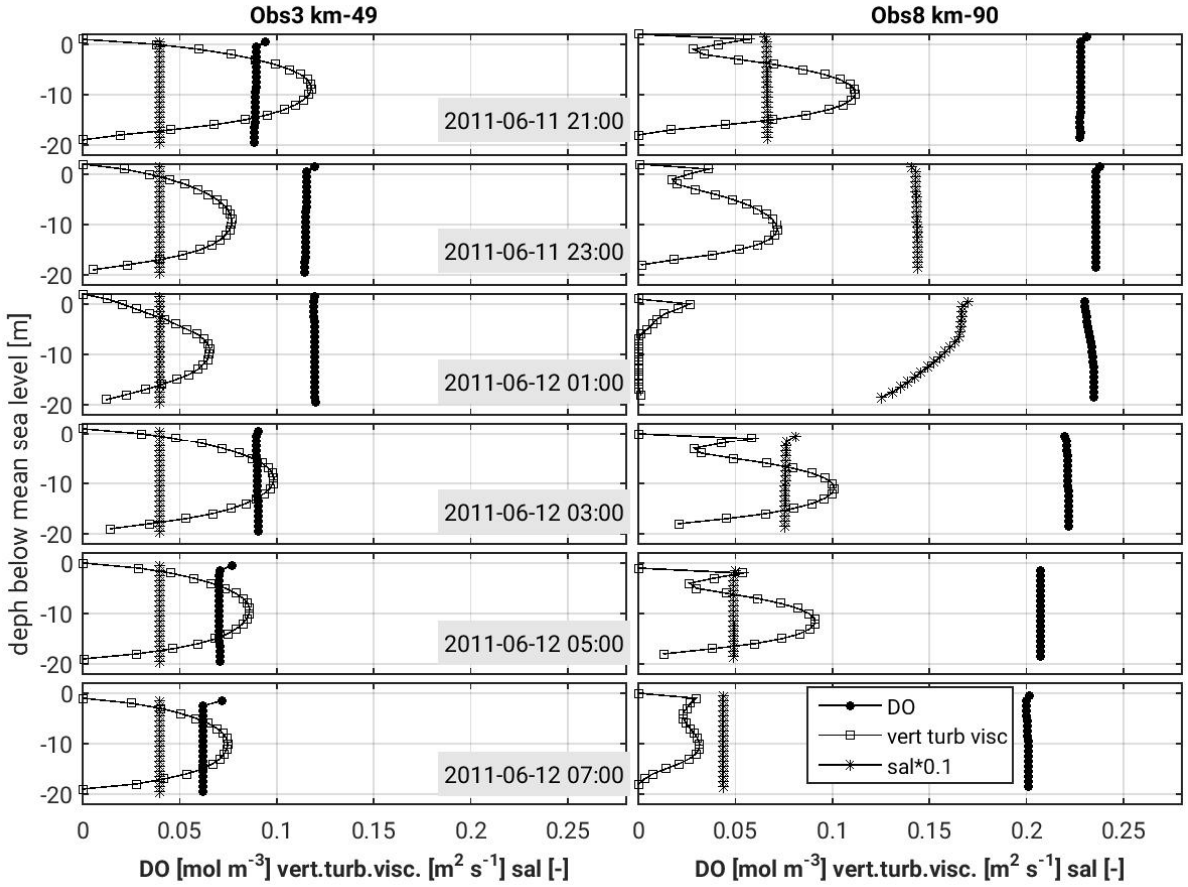

Figure 22: Simulated vertical profiles of dissolved oxygen concentration, salinity (scaled with 1/10), and vertical turbulent diffusivity at the computational element representing station Obs3 (Blankenese) and Obs8 (D4 Rhinplatte) for the reference scenario HIGH and over one tidal cycle in June 2011. Vertical turbulent viscosities are calculated with a k-ε turbulence model in the GLS approach [*Umlauf and Burchard,* 2003].

4.3.2. Sensitivity to boundary value DOC lability

The spactio-temporal distribution of DO turned out highly sensitive to the varied lability shares in DOC boundary values, see Figure 23. Simulated DO concentrations are consistently lower in scenario HIGHx100 with all DOC being labile (light grey line in Figure 23), compared to the cases in HIGHx10 or HIGH (dark grey and black line, respectively). Sometimes, DO concentration differences between scenario HIGHx100 and the other two lability scenarios are larger than 100 mmol m^{-3} at certain stations during certain periods, like at Obs3 during August. In relation to this, differences in simulated DO between HIGHx10 and HIGH is small, commonly less than 5 mmol m^{-3}, with a maximum of about 15 mmol m^{-3} during August. When compared to observed DO concentration (green line in Figure 23), the values in HIGHx100 are too low for all stations during most of the year. In contrast, the deviations of the simulated DO values in HIGHx10 and HIGH from observed values are clearly smaller and very similar. However, during March and April simulated DO in HIGHx100 meets the observation better than the results from HIGHx10 or HIGH.

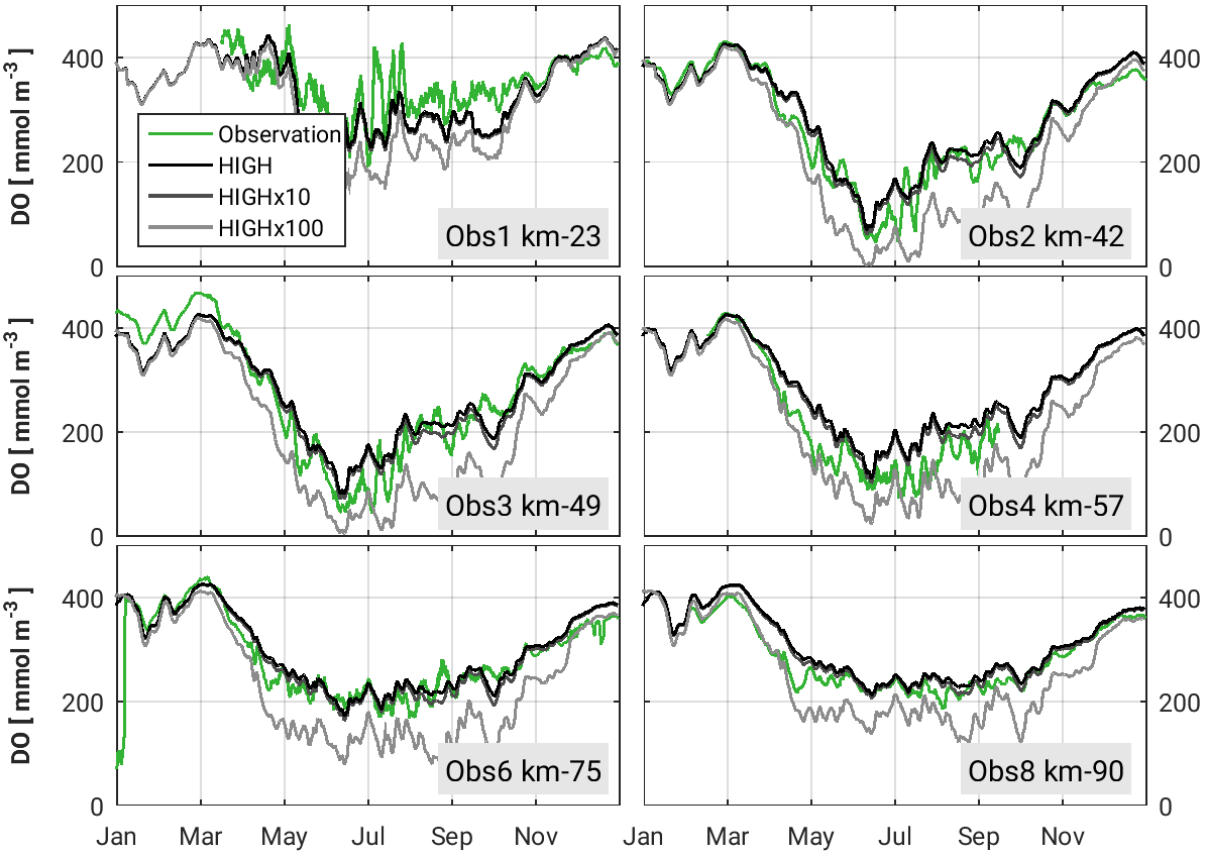

Figure 23: Dissolved oxygen concentrations at six observation stations along the Elbe Estuary for the year 2011(see Figure 25 for the position of the observation stations). The green line shows measured DO concentrations; the grey-shaded lines show simulated DO concentrations of the boundary value lability scenarios: black line corresponds to 1% labile DOC (scenario HIGH), dark grey line corresponds to 10% labile DOC (scenario HIGHx10), and light grey line corresponds to 100% labile DOC (scenario HIGHx100).

4.3.3. Sensitivity to bathymetry and river load

DO results for the scenarios HIGH and LOWbathymetry show that DO concentrations are commonly higher in LOWbathymetry, see Figure 24 (grey line, compared to black line) and Figure 25B (red areas show higher values for LOWbathymetry). Differences are usually below 15 mmol m^{-3}. However, in specific areas (downstream of Hamburg harbor around Obs2 and Obs3, see Figure 25B) or certain periods (August 2011, see Figure 24) differences can exceed 20 mmol m^{-3}. A few, confined areas show higher DO concentrations in HIGH, like on Figure 25B some harbor basins or a section south of Obs3; these areas usually experienced strong sedimentation and are substantially shallower in HIGH compared to LOWbathymetry.

DO concentrations for LOWnutrients are overall larger than those for HIGH. The largest differences occur in areas and during periods of low DO levels, see Figure 24 (red line compared to black line) and Figure 25C (red areas indicate that DO is higher in LOWnutrients); they can become as large as 100 mmol m^{-3} during May to July at Obs2 and Obs 3 (Figure 24). Compared to LOWnutrients, DO concentrations for LOW are usually marginally larger but never deviate more than 5 mmol m^{-3} from the results of scenario LOWnutrients.

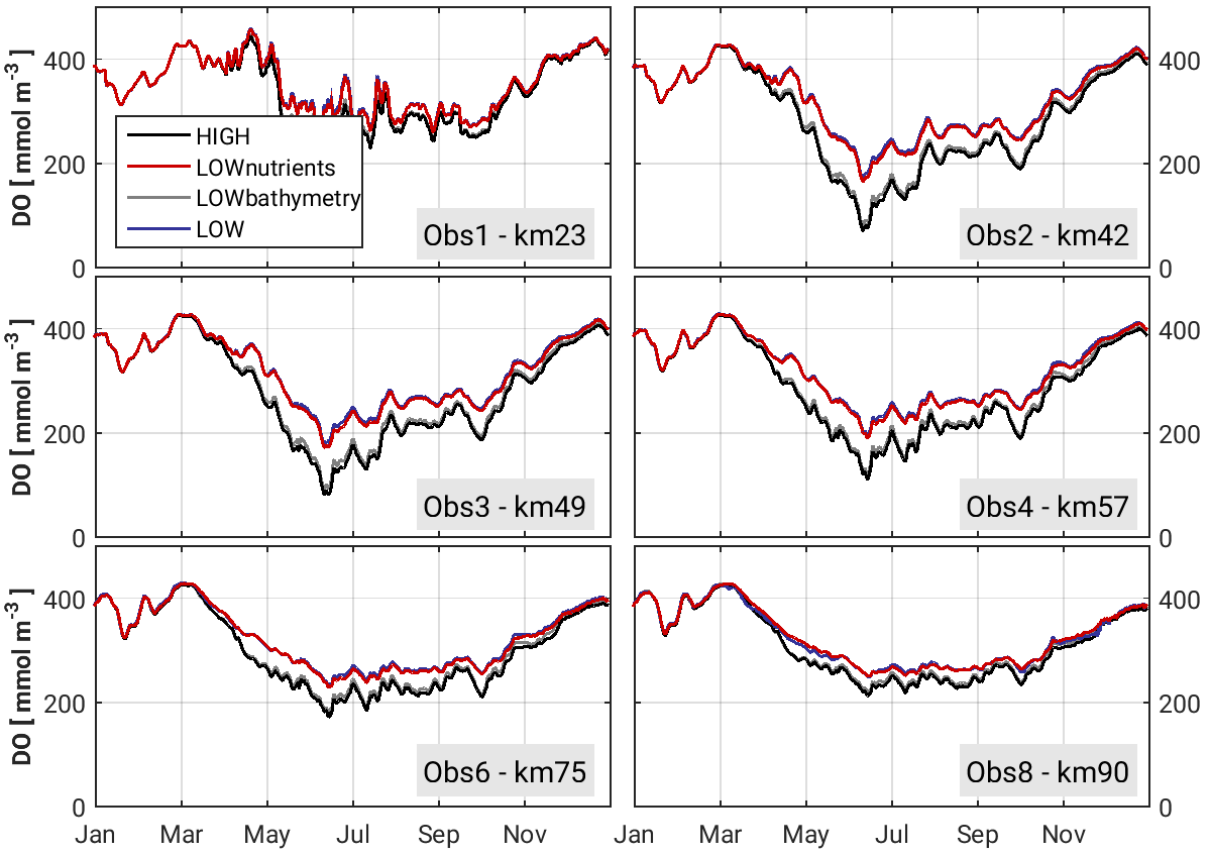

Figure 24: Seasonality of DO concentration for 2011 in different scenarios: HIGH (black line; reference scenario with high impact bathymetry and realistic boundary load), LOWbathymetry (grey line; lower impact bathymetry and realistic boundary load), LOWnutrients (red line; high impact bathymetry and 50% boundary load), LOW(blue line; lower impact bathymetry and 50% boundary load).

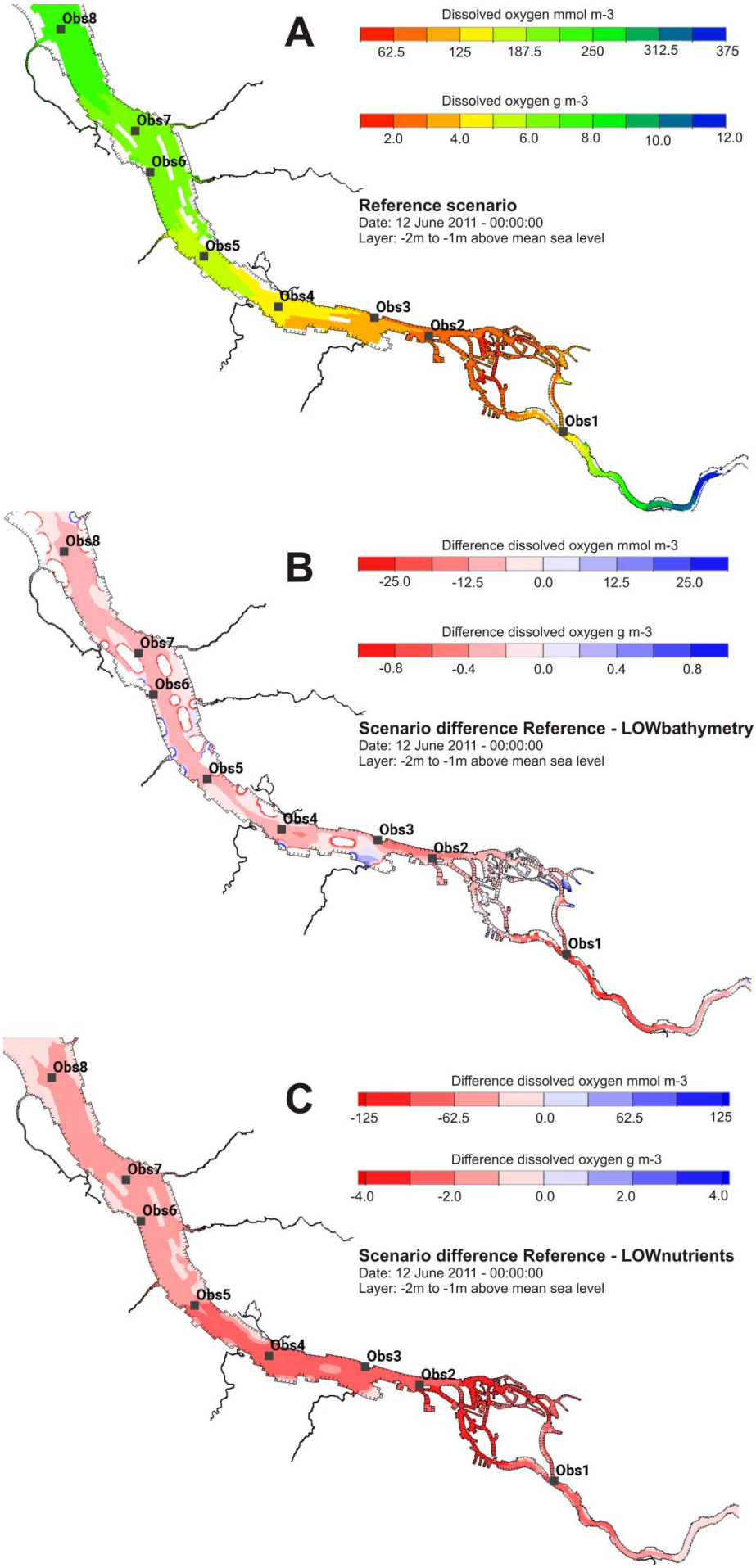

Figure 25:
A: Simulated DO for the reference scenario HIGH on June, 12th, 2011 in a layer close to the water surface. B: simulated DO difference of HIGH - LOWbathymetry. Red areas indicate higher DO concentrations in LOWbathymetry. C: simulated DO difference of HIGH – LOWnutrients. Note the different color scale in B and C.

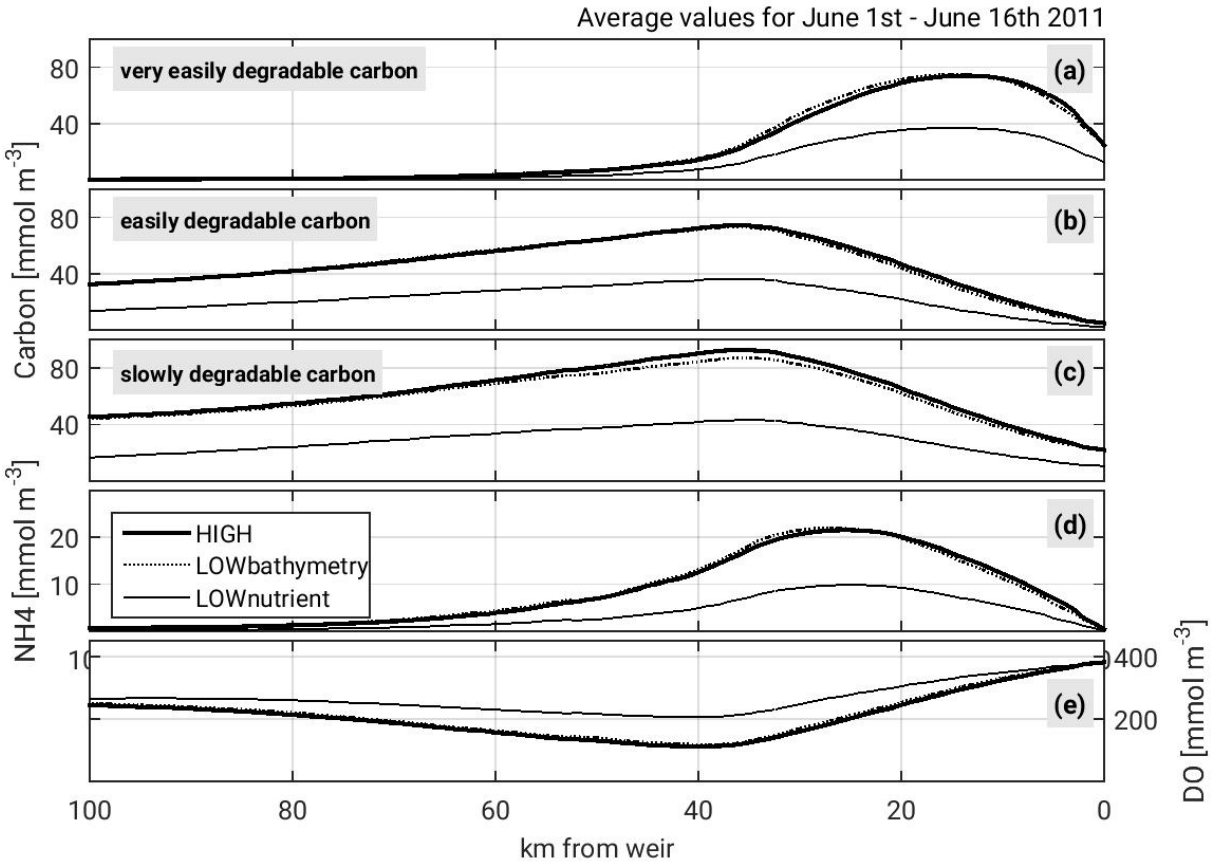

Figure 26: Simulated concentrations for the three degradable carbon fractions, ammonium and DO on a longitudinal profile along the navigation channel. Thick black lines show the results for the scenario HIGH, dashed lines for LOWbathymetry, and thin lines for LOWnutrients. Values are averages over one spring-neap cycle at the beginning of June 2011. Differences between the results for LOW and LOWnutrients are not noticable on the plot scale; therefore, only LOWnutrients results are displayed in the figure.

During the period of lowest overall DO concentration (June, see Figure 23 and Figure 24) the area with lowest DO is around km-40 (upstream of Obs2 in Figure 25A, and Figure 26e). This position lies directly downstream of maximum concentrations of the most easily degradable carbon fraction (Figure 26a) and ammonium (Figure 26d), and coincides with maximum concentrations of the two less degradable carbon fraction (Figure 26b and c). Concentration differences between the scenarios HIGH and LOWbathymetry are below 10 mmol m^{-3} for DO, below 1 mmol m^{-3} for ammonium , and below 5 mmol m^{-3} for the most easily degradable carbon fraction (3 mmol m^{-3} and 6 mmol m^{-3} for medium easily and slowly degradable, respectively). In comparison, DO concentration in LOWnutrients are up to100 mmol DO m^{-3} larger than in HIGH, and other substance concentrations are about half of their values in HIGH, with not more than 12 mmol N m^{-3} for NH4, and at most 35 – 45 mmol C m^{-3} for the different carbon fractions (45 for POC2, 37 for POC1, 38 for DOC). By contrast, the differences between LOWnutrients and LOW are smaller, hardly to distinguish, and values of LOW are therefore not shown in Figure 26.

4.4. Discussion

4.4.1. Key processes of dissolved oxygen dynamics

In all scenarios, estuarine DO concentrations are determined by the two major consumption processes of organic matter mineralization and nitrification (Figure 27, Figure 28). This is particularly evident in the oxygen minimum zone. Eventually, the resulting DO concentrations arise from a balance between consumption and reaeration, the latter being a response to the forming DO deficit (Figure 26e). Primary production, as potential oxygen source, is too weak for notable oxygen production; net primary production even acts as an, albeit minor, oxygen sink due to respiratory consumption.

The strong dominance of oxygen consuming processes with low relevance of primary production differs from the situation described for stratified systems: there, primary production usually dominates in the surface layer while consumption prevails in the deeper sections of the water column [*Welsh and Eller,* 1991; *Melrose et al.,* 2007; *Kemp et al.,* 2009; *Zhang and Li,* 2010; *Zhang et al.,* 2010; *Zhu et al.,* 2011; *Scully,* 2013].

Nevertheless, it is equally interesting in the vertically well-mixed case which is examined in this study to analyze the spatial dynamics of the DO relevant processes because they determine the severity and the position of the eOMZ. Most importantly, we identified two mineralization hot spots, which govern DO dynamics of the entire estuary in all scenarios: an upstream section (between km-0 and km-30), and a section further downstream (between km-35 and km-45). The reasons for the existence of these two sections are different and can be derived from a combined analysis of the values using both a volume-based and a surface-area-based perspective. When oxygen process rates are displayed as depth-integrated values they show the oxygen changes per unit water surface area (Figure 27); when oxygen process rates are displayed as water column averages they show the oxygen changes per unit water volume (Figure 28). The volume-based way of presentation includes an averaged reaeration rate, which might appear uncommon or even false as reaeration only acts at the water surface. In the well-mixed water column, though, the depth-averaged reaeration rate stands for the portion that effectively enriches a unit of water volume.

The upstream hot spot section can be clearly identified in Figure 27 by the high values for depth-integrated oxygen change due to mineralization, and in Figure 28 by the high values for depth-averaged, oxygen-based mineralization rate, respectively. The high values originate from the almost complete mineralization of the very easily degradable material, which is maximal in this section (Figure 26a).

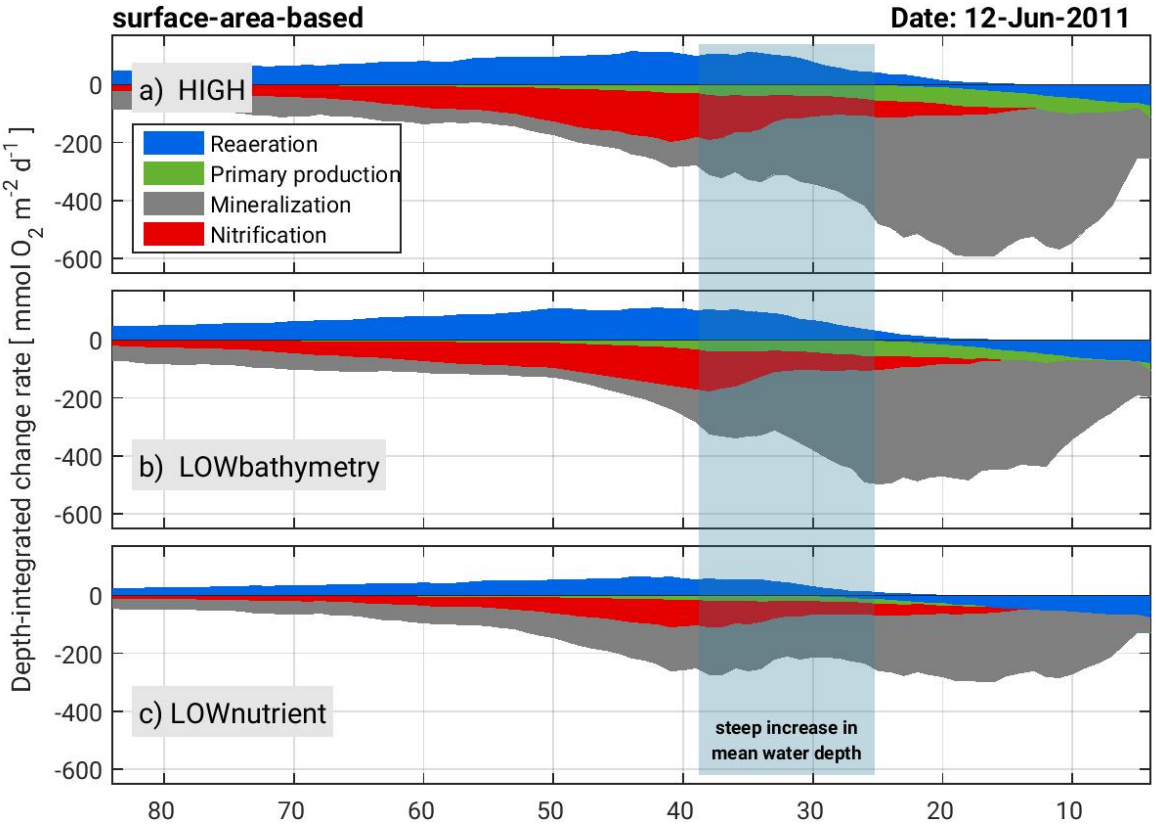

Figure 27: Simulated, depth-integrated DO bulk changes along the shipping channel at June, 12th 2011; a) for scenario HIGH, b) LOWbathymetry, and c) LOWnutrient.

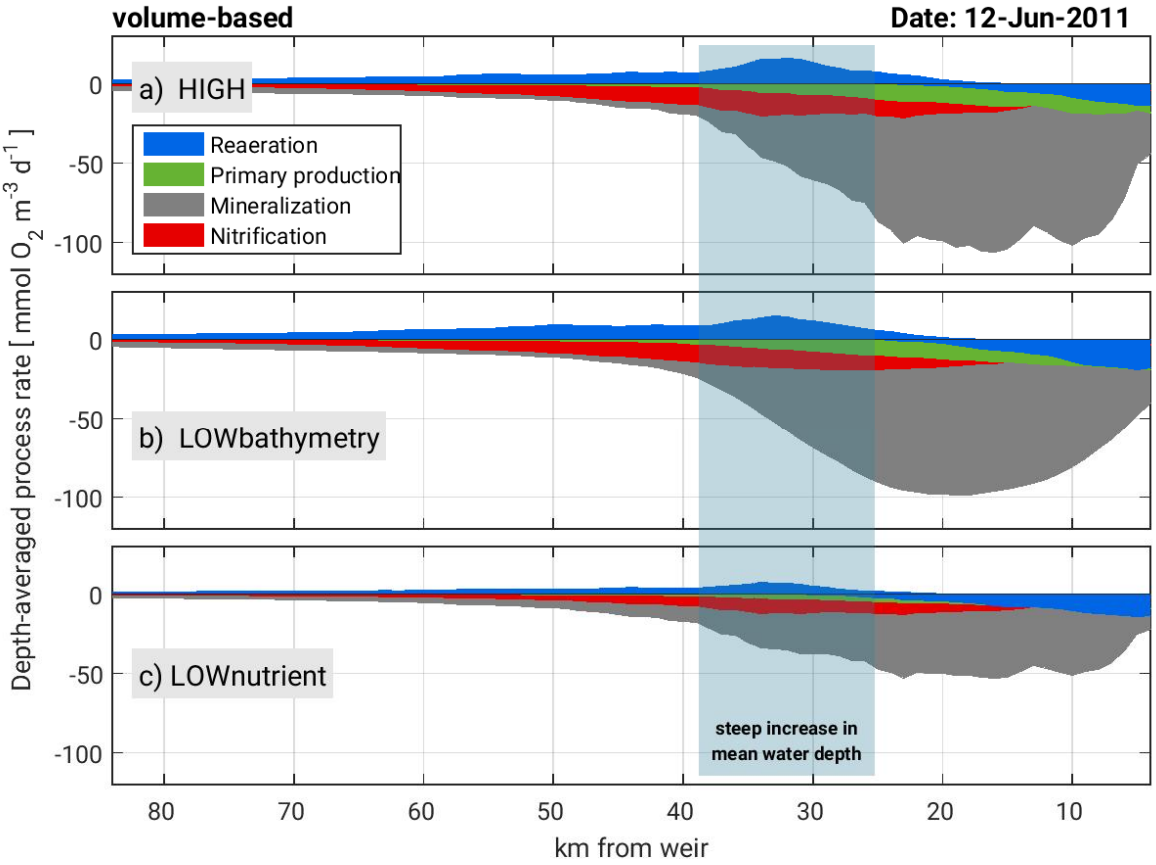

Figure 28: Simulated, depth-averaged DO process rates along the shipping channel at June, 12th 2011; a) for scenario HIGH, b) LOWbathymetry, and c) LOWnutrient.

The second hot spot section is caused by the depth increase at the beginning of the shipping channel. At that position, a second peak for depth-integrated oxygen change due to mineralization forms (most clearly for scenario LOWnutrient, Figure 27c). However, the peak of the depth-integrated values is neither accompanied by a peak of the depth averaged values (Figure 28), nor by a considerable change in organic matter concentration (Figure 26a-c). The second hot spot section thus develops by accumulation of mineralization activity due to the larger volume of the water column.

Mineralization promotes subsequent nitrification, and maximum DO changes due to nitrification, depth integrated and depth-averaged (though less pronounced there), occur in the second hot spot. There, the two effects described above for mineralization obviously coincide for nitrification: a strong respiratory activity (Figure 28) because of high ammonium concentration (Figure 26d) overlaps with the surface-related accumulation due to depth increase.

In stratified systems, oxygen enrichment critically depends on the strength of stratification and related downward mixing of oxygen-rich waters; *Scully* [2010], for example, describes the wind-induced modulation of hypoxia in Chesapeake Bay. In vertically well-mixed systems as the one studied here, enrichment is not limited by the downward transport of oxygen within the water column, as can be seen from the constant distribution of DO over depth (Figure 22). Instead, DO enrichment is restricted by the amount of oxygen that is able to enter the water column at the atmospheric surface. In our model, this oxygen amount is determined by (i) the oxygen transfer rate, which in turn depends on the magnitude of the DO deficit, wind and current velocity [*Banks and Herrera,* 1977; *O'Connor and Dobbins,* 1958], neglecting microscale processes at the water surface like bubbles, sea spray, rain and surface films [*Garbe et al.,* 2014], and (ii) the available surface area for exchange. In case neither the transfer rate nor the surface area changes substantially, the impact of reaeration on DO concentration may still change due to volumetric relations. This is the main reason why also oxygen reaeration is affected by the depth increase at the beginning of the shipping channel: the depth-integrated DO reaeration (which corresponds to the total amount of oxygen exchange at the water surface) and the depth-averaged DO reaeration increase almost linearly up to km-35. Downstream, in the second hot spot section, the depth-integrated values (Figure 27) remain at a constant, high level due to the minimum DO concentrations (Figure 26e). In contrast, the depth-averaged DO reaeration values (Figure 28) peak at km-35 and decrease downstream, which means that the DO-enrichening impact of reaeration on the volumetric DO concentration declines with the beginning of the shipping channel. Thereby, the relevance of the sv-ratio (ratio of water surface area to underlying water volume) on DO dynamics, as already described in *Holzwarth and Wirtz* [2018] for idealized cases, is also verified in a realistic system.

4.4.2. The role of organic matter quality

DO is predominantly consumed in areas where most substrate for oxidation is generated, and directly downstream of such areas due to the combination of residual flow direction of the water body and reaction kinetics. The mineralization of the most easily degradable carbon fraction, and nitrification, have the highest reaction rate constants (1 day^{-1} and 0.4 day^{-1}, respectively, [*Holzwarth and Wirtz,* 2018]), leading to a fast depletion in substrate as well as oxygen along the estuary (Figure 26a and e). In case of the most easily degradable carbon, almost all substrate is depleted at the point of lowest DO concentration, either by remineralization or by conversion to the less degradable carbon fractions (with reaction rate constants of 0.15 day^{-1} and 0.05 day^{-1}), which peak at this position. Their remineralization also produces NH4 which is therefore not as fast depleted as the most easily degradable carbon. Instead, it leads, together with the remineralization of the two remaining carbon fractions, to DO consumption downstream of the DO minimum and therefore counteracts fast oxygen enrichment by oxygen reaeration.

The processes inside the estuary notably depend on the quality (not only the quantity) of the material that the estuary receives from upstream. The relevance of the quality is demonstrated by the sensitivity of model results to the fraction of labile boundary DOC (remember Figure 23); in the reference scenario, 1 % of the total DOC at the model boundary was labile with the effect that the predominant part of carbonaceous substrate for oxidation is produced in the estuarine section covered by the model; it stems from the high limnic phytoplankton concentration in spring and summer which is transported downstream from the river into the estuary [*Schroeder,* 1997; *Amann et al.,* 2012]. In our model the phytoplankton is included as landward boundary value; its mortality and the degradation of its detritus induce a sequence of carbon mineralization processes that includes three organic matter pools. If the labile organic matter fraction in the landward DOC boundary value was higher (as in HIGHx10 and HIGHx100), the ratio of internally produced substrate for oxidation to external substrate decreases; the ratio eventually gets dominated by external substrate in case the lability DOC-fraction approaches 100 % in scenario HIGHx100, see Figure 29a. This situation appears in estuaries with substantially higher DOC lability, e.g. the Pearl River Estuary where consumption seems to mainly driven by DOC from sewage inflow [*Zhang and Li,* 2010; *He et al.,* 2010].

Nitrification, as the directly DO-relevant process during nitrogen cycling, is mainly fueled by ammonium from organic matter mineralization, and thus by substrate originating from processes acting in the estuary. This relation can be derived from Figure 26a and Figure 26d, showing maximum ammonium concentration directly downstream of maximum organic carbon concentration, and in combination with Figure 27a giving spacial indication of mineralization and nitrification as related processes. Higher DOC-lability at the model boundary in HIGHx10 and HIGHx100 also yields substantially more ammonium (see Figure 29b), which, in turn, has strong

impacts on the DO concentrations (Figure 29c). A major quantitative uncertainty thereby lies in the phytoplankton N-ratio, which can vary considerably in freshwater biomass (e.g. *Montagnes and Franklin* [2001], *Sterne*,[2011] and references therein).

These effects underline the importance of knowledge on the quality of organic material (including its nitrogen ratio) that is transported into an estuary; the total amount of organic matter merely represents an upper limit of the possibly oxygen-relevant amount.

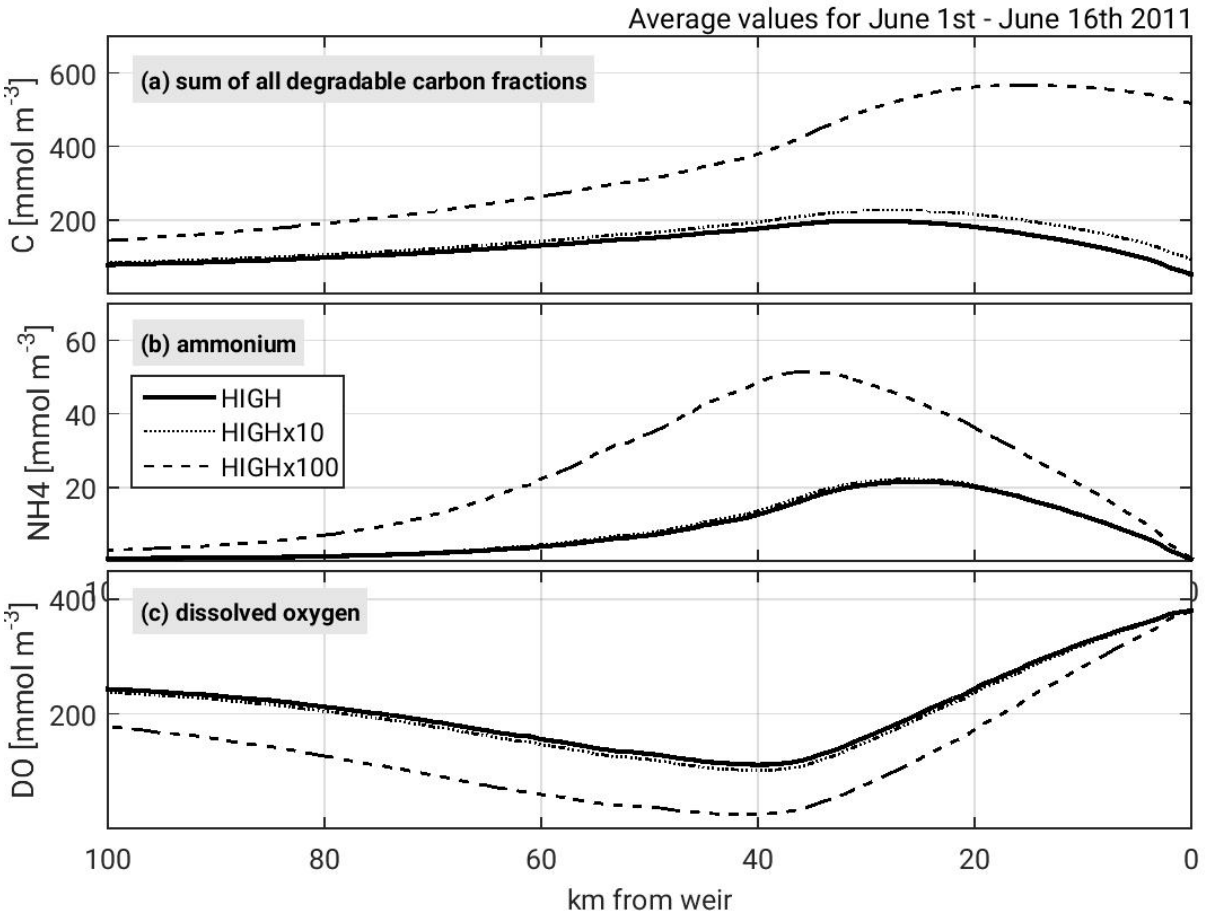

Figure 29: Simulation results for the sensitivity runs with different lability fractions (1, 1/10, 1/100) in DOC boundary value along the longitudinal profile; (a) sum of all degradable carbon fractions, (b) ammonium, (c) dissolved oxygen.

4.4.3. Bathymetric modification versus riverine load reduction

Compared to the reference situation, the riverine load reduction has a much larger impact on DO levels than the bathymetry with substantially lower man-made modifications. In case of load reduction, the lower input of phytoplankton from upstream leads to lower concentrations of degradable/nitrifiable material which reduces the severity of the eOMZ (Figure 26). This effect, and a similar relation of about 100 mmol m^{-3} more DO in the eOMZ due to a 50 % reduction in riverine nutrient and organic matter load, is consistent with the results from Chapter 2.

In case of a less heavily modified bathymetry, DO concentrations are commonly, though modestly, higher than in the reference scenario HIGH (Figure 22B, Figure 24, Figure 26e). This result

complements findings from Chapter 3: there, hydrodynamic indicators, water age and surface-to-volume ratio, were used to evaluate the same bathymetric change as analyzed in the present study. Results in Chapter 3 hint at small to moderate effects on the DO dynamics. We can now confirm the expected magnitude with process-based results from the actual study, though impacts on DO concentrations are even lower than expected from Chapter 3. An example in Figure 30 shows that during the period of observed DO concentration below 200 mmol m^{-3}, riverine water age is about 4-7 % lower and DO undersaturation is about 3-5 % less in LOWbathymetry compared to HIGH (Figure 30c). In addition, the sv-ratio is about 15 % larger in the area around the shown position (km-42, Figure 19). The relatively low impact that this variation has on DO compared to physical characteristics such as water age, illustrates that the biogeochemical system reacts in a non-linear way and the impact of changes to external conditions is thus difficult to predict without taking into account all relevant processes.

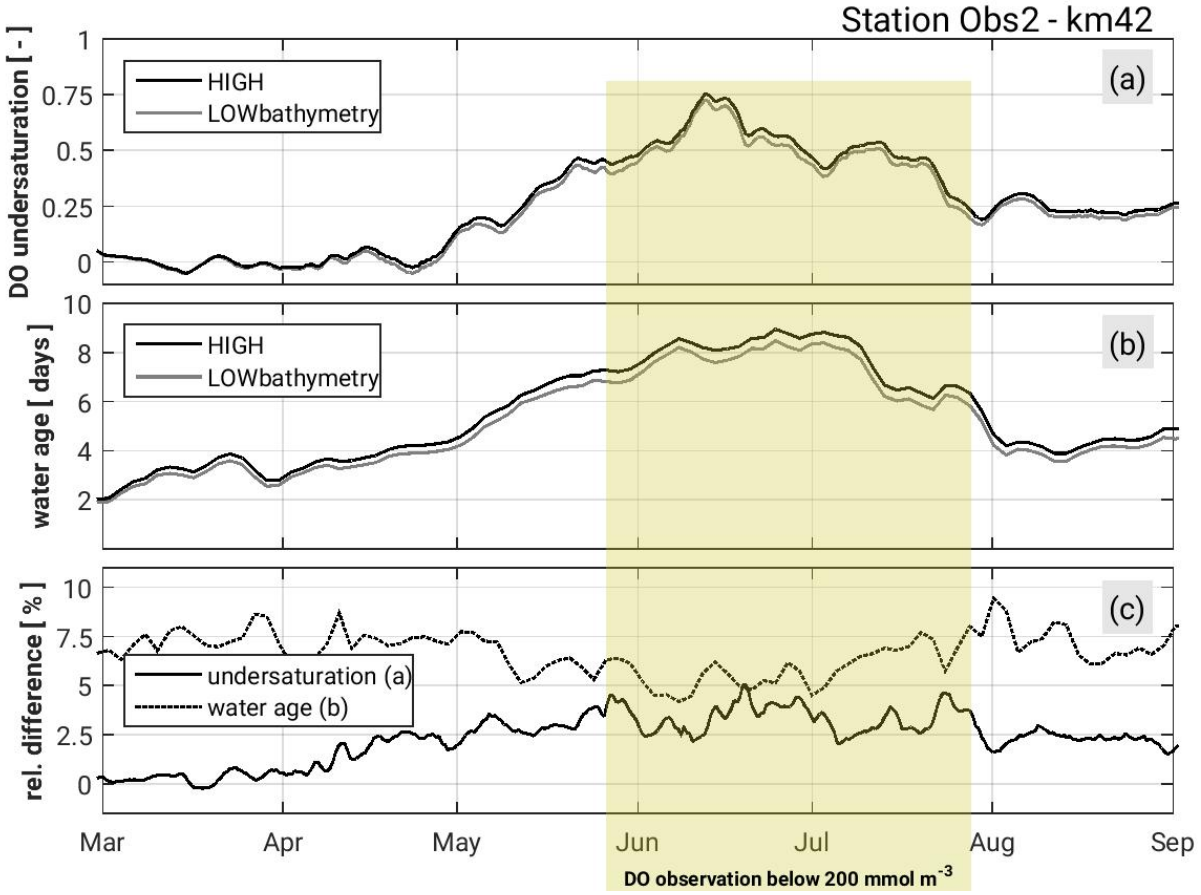

Figure 30: (a) Time series of simulated DO undersaturation for the scenarios HIGH and LOWbathymetry. (b) Time series of simulated riverine water age for the scenarios HIGH and LOWbathymetry, from Chapter 3. (c) Relative difference HIGH-LOWbathymetry for DO undersaturation (from a) and riverine water age (from b).

However, it is difficult to generalize the dominance of eutrophication effects on DO dynamics over those of realistic, decadal man-made bathymetric modifications. The relation found in the Elbe Estuary might not necessarily be the same for all estuaries, particularly not for shallow systems: generally, the impact of a specific deepening measure will increase with decreasing mean

depth because of the larger relative change; this especially applies to a volume increase with related increase in water residence time, and decrease in surface-to-volume ratio.

The deepening impact on light conditions was minor in the Elbe Estuary system under study, but will be more relevant in shallow estuaries. Shallow estuaries host active primary production including macro algae and benthic production [*Caffrey,* 2004; *Trancoso et al.,* 2005]; if at all, they suffer from dial oxygen minima [*Kemp et al.,* 2009]. The effect of deteriorated water column light availability by man-made bathymetry deepening may lead to notable changes in primary production, both benthic and pelagic, which may cause lower DO in some systems because of less biogenic DO input, but higher DO in other systems due to lower amounts of degradable algal detritus.

4.4.4. Limitations

The greater sensitivity of DO to load reduction is subjected to a number of uncertainties, mainly due to the scenario definition and model limitations:

The scenarios LOWbathymetry and LOWnutrients are not readily comparable as equivalent severe deviations from the reference situation: whereas LOWbathymetry represents a possible realistic state of a less severe human impact, such a state is often unknown for the riverine load. Decreasing the entire riverine boundary load by 50 % in the nutrient reduction scenario is a vague approximation of a realistic scenario and approximately represents a nutrient state for total nitrogen and total phosphorous that lies in between actual and pristine conditions [*Topcu et al.,* 2011; *FGG Elbe,* 2017]. It remains an uncertain assumption that the reduction in macro nutrients also leads to a 50% reduction in organic matter (namely phytoplankton as well as dissolved and particulate carbon and nitrogen). While *Quiel et al.* [2011] showed for the river Elbe that a reduction in phosphorous load does not necessarily lead to a reduction in riverine algae biomass, the prevailing opinion is that a reduction in both macronutrients N and P will control eutrophication [*Conley et al.,* 2009; *Testa et al.,* 2014] and therefore, phytoplankton biomass. Given the complex interrelations of eutrophication, and considering the large variety of cases with dual N and P reduction reported in *Paerl et al.* [2016] for freshwater lakes, our 50 % scenario does not appear less unlikely than others. Though, more reliable riverine input load scenarios would improve the assessment of nutrient load reduction effects in estuaries. This holds especially true due to the importance of riverine quantity and quality of degradable organic matter and its nitrogen content, as detected in Section 4.4.2.

First model limitations arise from possibly incomplete description of relevant biogeochemical processes and their uncertain because unconstrained parametrization. Our approach considers water column processes only, and hence neglects effects from sediment dynamics:

Most importantly our model does not yet resolve oxygen-related processes in and at the sediment bed, like described in detail by *Middelburg and Levin* [2009]. Our biogeochemical model

configuration only accounts for basic organic matter degradation in sediments by enhanced process rate constants of water column mineralization, nitrification and denitrification. Many studies note the importance of these sediment biogeochemical processes on the water body above in stratified or partially stratified estuaries [*Cowan and Boynton,* 1996; *Paerl,* 2006] and sediment oxygen demand (SOD) has been suggested to be important to, if not the major driver of, bottom water hypoxia, like in the Pearl River Estuary [*Wang et al.,* 2017], off the Changjiang Estuary [*Zhang et al.,* 2017], the Lower St. Lawrence Estuary [*Lehmann et al.,* 2009] or in the Northern Gulf of Mexico [*Fennel et al.,* 2013]. Nevertheless, some studies report the opposite like *Hetland and DiMarco* [2008] for the Atchafalaya River plume.

The importance of SOD in well-mixed estuaries is unknown. Given the high flow velocities, we can merely expect the exchange via the sediment-water interface to be constrained by the reaction rate of the bottom material, not by material supply limitation [*Nakamura and Stefan,* 1994]. The estimation of SOD in estuaries with high anthropogenic use is further complicated because human activities continuously disturb the upper sediment layer in certain sections by, e.g. dredging, dumping and ship movements. Thus, findings from systems with an anthropogenically undisturbed upper sediment layer, like shelf seas and bays, may not necessarily be transferable to strongly impacted systems. Our simplified approach of enhanced water column process rates thus remains a valid concept until more detailed knowledge is available; the approach is justified by the following two considerations: first, water column DO results do not depend on the origin (pelagic or benthic) of DO demand, due to the well-mixed character of the water column. Second, spatially varying SOD may originate from large amounts of degradable organic matter preferably deposited at specific locations, but our results did not show such notable sedimentation. This model result, however, is possibly constrained by disregarding flocculation processes in our model: particulate organic matter might be present in aggregates instead of single particles. The settling velocity of aggregates that consist of several organic particles and/or heavier mineral particles might differ from the settling velocity of a single organic particle, and with it sediment dynamics [*Abril et al.,* 1999; *Talke et al.,* 2009]. We neglected biomediated aggregation, or flocculation, of organic and inorganic particles because so far only conceptual models resolve these processes in shallow water systems [*Maerz and Wirtz,* 2009; *Lee et al.,* 2014], such that reliable formulations applicable in three-dimensional numerical models of estuarine scale are missing.

Another possible shortcoming of our approach is the treatment of mineral suspended sediments and their dynamics. Estuaries generally display high concentrations of mineral suspended sediments, which may even exceed 1000 $g\ m^{-3}$ in extreme cases like the estuaries of the Ems [*Weilbeer,* 2008] or the Guadalquivir [*Diez-Minguito et al.,* 2014] in the so-called estuarine turbidity maximum. Thus, primary production in estuaries is usually light-limited [*Pennock,* 1985; *Soetaert et al.,* 1994; *Irigoien and Castel,* 1997]. This holds particularly true for the Elbe Estuary: we dynamically simulated changes in light attenuation due to biochemical substances in the wa-

ter while keeping attenuation by lithogenic particles constant for reasons of model simplicity and traceability. Though the constant value we used was at the lower end of the expected range of values, primary production was already very low; in addition, a sensitivity study [*Holzwarth and Wirtz,* 2018] showed almost no sensitivity of the modeled DO minimum to a variation in the possible range of values (Figure 8 f). Nevertheless, in some estuarine systems, a close relationship between the increase in the concentration of mineral suspended sediments and a decrease in DO concentrations following navigation channel deepening has been suggested [*Kerner,* 2007; *Talke et al.,* 2009; *van Maren et al.,* 2015b]. However, the effects of sediment disposal strategies for continuous channel maintenance, which usually lead to recirculation of material within the estuary, have not quantitatively been distinguished from the effect of a deeper system alone; besides, some literature findings on decreasing DO due to bathymetric deepening might be limited to system specific features, like in the hyper-turbid Ems [*Winterwerp et al.,* 2017] which is dominated by the degradation of high amounts of refractory material that is attached to mineral suspended sediments [*Talke et al.,* 2009]. In case bathymetric modifications have a strong impact on suspended sediment concentrations, as e.g. stated by *Jonge et al.* [2014] and *van Maren et al.* [2015a], the impediment of gas exchange at the water surface due to turbulence damping by very high suspended sediment concentrations [*Abril et al.,* 2009] may influence the reaeration ability of the eOMZ.

All neglected processes, as described above, have in common that their account would further reduce DO concentrations. Consequently, our result represents a lower limit (best case) for the impact of a bathymetric change on DO minima.

4.4.5. Added value of the three-dimensional model

Modelling studies about geometric impacts on biogeochemical processes are rare, and previous works only distinguished between estuarine systems that varied in their natural geometry [*Volta et al.,* 2016a; *Volta et al.,* 2016b] or they introduced a hypothetical change [*Holzwarth and Wirtz,* 2018]. These studies used one-dimensional model set-ups and aimed at a general system understanding of geometric/bathymetric effects on the biogeochemical system of estuaries. In contrast, eutrophication and nutrient reduction scenarios have already been studied with higher resolution numerical models in a variety of estuarine systems and to different degrees of geometric detail [*Cerco and Cole,* 1993; *Neumann et al.,* 2002; *Wool et al.,* 2003; *Khangaonkar et al.,* 2012; *Testa et al.,* 2014; *Wild-Allen and Andrewartha,* 2016].

We here apply a three-dimensional model that resolves the estuarine bathymetry and its changes to a most realistic degree, which in parts has been faciliated by its its subgrid-scale technology for bathymetry [*Casulli and Stelling,* 2010; *Sehili et al.,* 2014; *Wang et al.,* 2014; *MacWilliams et al.,* 2016]. Using this subgrid-technology our model captures geometric features such as water volume and water surface-to-volume ratio, on the level of measurement accuracy in the real

system. Hence, this study is the first that gives a precise quantitative idea on the impact of a bathymetric change caused by direct human activities for navigational purpose. In addition this study quantitatively compares the bathymetric impact to eutrophication-related impacts on oxygen dynamics in a well-mixed estuary.

Additionally, we are able to compare the effects of the detailed 3D model to a geometrically less realistic approximation: in a preceding study, we used an equal biogeochemical configuration, a similar model set-up but a geometrically idealized model domain [*Holzwarth and Wirtz,* 2018]. With the more realistic 3D model used in this study, we can support some of our previous, general conclusions:

- Oxygen dynamics in the well-mixed estuary is driven by oxygen consuming processes. Thereby, remineralization is most dominant followed by nitrification.
- Reaeration is the major process counteracting DO depletion; the actual dimension of the DO minimum strongly depends on the conditions for atmospheric reaeration which is determined by the sv-ratio.
- Riverine load is the key cause for severe oxygen deficiency and load reduction appears to be the most effective mitigation measure.

Nevertheless, some of the former findings need to be revisited, particularly the interplay between organic matter transport and the location of strongest oxygen consumption. We observe a difference in the position of highest DO deficit, remineralization and nitrification rate: in the 1D set-up the DO minimum formed too far downstream when compared to measurements. This position is better met in the 3D set-up (Figure 23). We can explain the positional deviation between 1D- and 3D-results with the help of riverine water age (Chapter 3) as a measure for transport time scales. Figure 31 shows time series of riverine water age at two different positions: in the 1D model, water from the riverine boundary travels much faster through the estuary than in the 3D model (red lines compared to blue lines in Figure 31). This differing behavior certainly arises from the fact that, sections wise, the 1D model volume did not correspond to the real volume, though it did in total: the upstream parts contained too little volume, and water flowed through too fast. Consequently, the riverine load also passed the upstream section of the estuary faster in the 1D model, and the location of most massive remineralization with subsequent nitrification is situated further downstream, and coincides with the position of the steep increase in water depth. In the 3D model, the slower residual transport behavior leads to the two distinct mineralization hot spot regions (see Section 4.4.1).

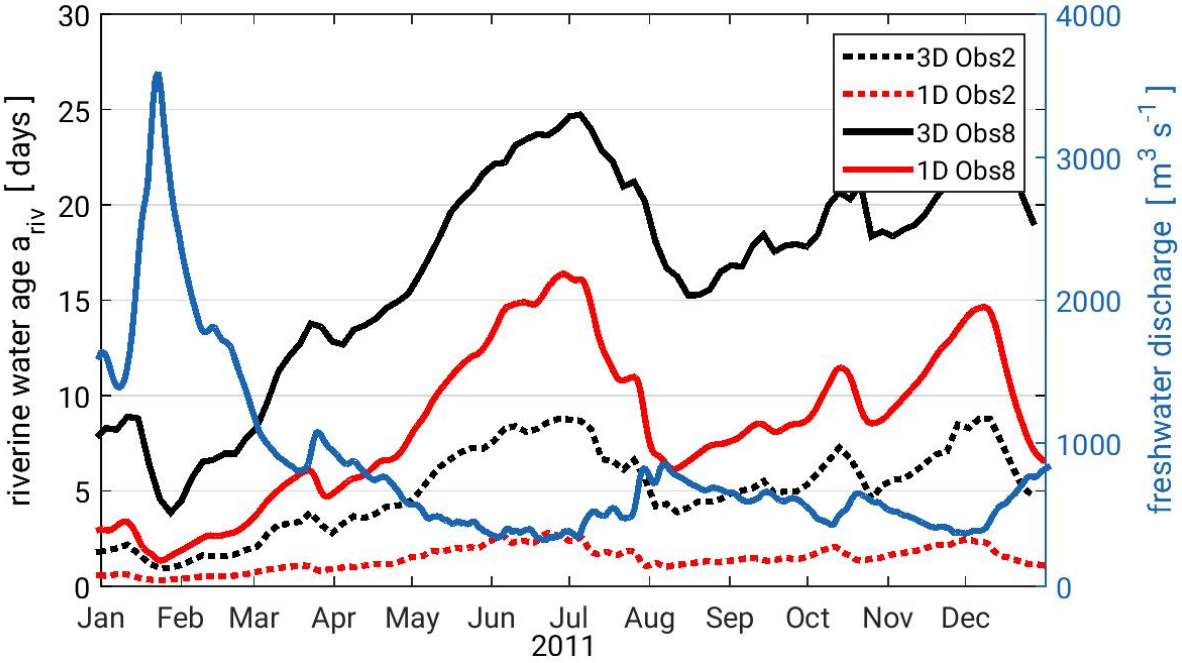

Figure 31: Freshwater discharge (blue continuous line) at the riverine model boundary, and simulated riverine water ages at the positions Obs2 (dotted lines) and Obs8 (continuous lines) for the year 2011. Black lines display results of the 3D model; red lines display results for the idealized 1D model.

4.5. Conclusion

Man-made bathymetric changes of estuaries pose an additional stressor to the oxygen situation in well-mixed systems; however the impact appears minor compared to eutrophication influences. This finding can be consolidated by future studies that include major factors neglected here suach as mineral suspended sediment dynamics and benthic processes. These could specifically better integrate the influence of dredging and dumping as continous activities to manage man-made impacts. Certainly, a mechanistic understanding and a profound data base for these processes has to be build up by in-situ observations; only then, reliable and meaningful simulations are possible.

Likewise, knowlegde on the organic matter quality, particularly lability and nitrogen content, as well as its variablity has to be improved. This is essential for severely light limited estuaries where oxygen consumption dominates over autotrophic oxygen production, and remineralization with subsequent nitrification make the key processes.

A hydrodynamic indicator, riverine water age in this case, appears suitable to assess the possible effect size of man-made bathymetric modifications on DO dynamics. In our case, riverine water age hinted at small changes; as indicators do not refelct the multiple interrelations between physical, geological and biogeochemical processes, the results of our process-based model can be taken as first confirmation. Generally, such indicators may help to decide wether an impact pathway is sufficiently relevant to demand for more complex impact assessments.

Finally, we demonstrated that the geometrically idealized set-ups are suitable for the study of system behavior, relevance of processes and process sensitivity. For quantitative information and realistic process understanding, the model should represent the real system as detailed as possible, especially regarding its underlying hydrodynamic characteristics including transport time scales.

5. Conclusions

Results of this thesis clearly reinforce that oxygen consumption by heterotrophic organic matter degradation dominates the DO dynamics in an anthropogenically influenced estuary with high nutrient and phytoplankton load from the river. Additionally, the detailed process-based analysis discloses, that nitrification plays an important role in the spacial extend of an eOMZ as it follows organic matter remineralization in time and thus downstream in space; there, the oxygen consumption by nitrification counteracts the reaeration compensation of the eOMZ and thus extends the eOMZ further downstream.

Man-made bathymetric modifications have an influence on DO dynamics in vertically well-mixed estuaries. However, in comparison to anthropogenic nutrient enrichment, the man-made bathymetric effect in the studied system is considerably lower. It is rather one of several stressors in addition to nutrient enrichment.

To see a strong effect, the bathymetric difference obviously has to be larger than the decadal man-made modification investigated in the Chapters 3 and 4, though effects are expected to be more relevant in more shallow estuaries (see Section 4.4.3). The results of the more conceptual investigation in Chapter 2 nevertheless show that a strong bathymetric difference substantially influences the severity of an eOMZ. The bathymetric difference that was studied in Chapter 2 rather depicts either a historically different, but still man-made, development over centuries, or two estuaries that fundamentally differ in their bathymetries. Transferred to the Elbe Estuary, the first case would correspond to a scenario in which the main sea port had developed in the city of Glückstadt instead of Hamburg. The second case exemplifies that the sensitivity of estuaries to eOMZ formation may be determined by their bathymetric characteristics.

Deepening as a bathymetric modification increases the vulnerability of estuaries to oxygen deficits by physical effects: deepening aggravates oxygen supply and potentially increases oxygen demand, and thereby the effects overlap with expected consequences from climate change. These mechanisms in well mixed waters can be seen in analogy to oOMZs (as an example for oxygen deficits stratified water bodies) responding to human-induced physical changes. In contrast to eOMZs, physical changes on the oOMZs can be expected to solely originate from anthropogenic global climate change, rather than from direct human interference. However, envisaged changes and causal pathways, though still uncertain [*Peña et al.,* 2010], share a number of similarities: First, again, human-induced global warming decreases oxygen concentrations due to a reduction in solubility [*Schmidtko et al.,* 2017]; secondly, also oOMZs will be subject to possible changes in circulation [*Shaffer et al.,* 2009]: perhaps most importantly, [*Keeling and Garcia,* 2002; *Keeling et al.,* 2010] emphasize the role of model-predicted enhanced stratification which

consequently impairs the downward transport of water that has been oxygenated in the surface, thereby limiting the oxygen supply pathway to an oOMZ. The warming effect on oxygen consumption in the oOMZs is less evident. Recent analysis of observational data indicates a possible increase in biological activity in the upper ocean linked to enhanced oxygen consumption in mid-depths up to 1000 m [*Schmidtko et al.,* 2017]. Though modelling studies hint at a slowdown of the downward organic matter transport from the surface layer, the described effects on oxygen concentrations in the oOMZ layer are differing and sometimes even opposing [*Matear and Hirst,* 2003; *Oschlies et al.,* 2008; *Keeling et al.,* 2010]. Taking together these physical influences, a resemblance of anthropogenic impacts on eOMZs and oOMZs can be recognized: most obvious is the reduction of solubility in a warmer climate. Apart from this, decreasing ratios of water surface to underlying water volume in estuaries and enhanced stratification in the ocean will aggravate oxygen minima via the hydrodynamic impact pathway on oxygen supply. Likewise but with less clear impact, deceleration of the transport of organic material seems to be a common feature to the eOMZ and the oOMZ.
Overall, oxygen minimum zones both in estuaries and in the ocean appear to intensify due to comparable physical impact mechanisms of anthropogenic origin, including impaired supply, increased consumption and decreased solubility of oxygen.

As bathymetric modifications induce hydrodynamic impacts, an approach was tested to used hydrodynamic indicators to assess whether a bathymetric modification will potentially cause notable impacts on estuarine DO dynamics. The idea behind this approach is that in case of potentially small impacts, an evaluation with a sophisticated biogeochemical model can be saved. In the tested case, the applied indicators – change in riverine water age for oxygen consumption, and change in surface-to-volume ratio for oxygen supply – both hinted at eOMZ intensification with a deeper bathymetry. However, their magnitude, 7 % and 10 – 15 % respectively, was neither clearly negligible nor particularly high, and the application of a more detailed, process based model seemed necessary for the quantification of the man-made impact. Overall, the indicator-based approach appears useful to determine the modeling effort during an impact assessment study; both in terms of required processes but also in constraining the spacial and temporal extend of a model application.

Some methodical conclusions can also be drawn from the application of a 3D model compared to an idealized 1D vertically and laterally averaged model in an otherwise similar model set-up: while it is possible to benefit from the illustrative ability of the 1D version, the 3D version is predictive. The 1D model proved to be suitable for the study of system behavior, the relevance of processes and the sensitivity of the eOMZ to certain parameter values; it also proved to be useful in illustrating basic relations and phenomena, like the eOMZ formation in dependence of bathy-

metric factors and the degradability state of the organic material. The findings from the 1D model are transferable to systems with similar characteristics (vertically well-mixed, high riverine organic matter load, anthropogenically deepened bathymetry), and the developed biogeochemical model configuration will be basically applicable to a wide range of eutrophicated aquatic systems. Likewise, the idealized 1D model domain can relatively easy been adapted to a geometrically different system (as done with bathymetry in Chapter 2, see Section 2.2.6) to study the basic behavior of a specific system.
In this thesis, by becoming geometrically more realistic, model results became predictive: first, the bathymetric scenarios could be included in a much more realistic way and, hence, their difference. Second, hydrodynamics are more precisely modeled in 3D, leading to different transport times (see Section 4.4.5) which are likely more realistic, though no observational data exist to verify this assumption. Third, the water surface-to-volume ratio in 3D corresponds to the ratio true to nature and thus, the amount of oxygen supply by reaeration is more realistic. Finally, vertical processes are resolved, which is particularly relevant in the saltwater mixing zone (see Figure 22). This last item will become more important when the interaction between organic and inorganic particulate material is simulated as the inorganic material usually exhibits a vertical gradient, even in vertically well-mixed systems.

The first evaluation of bathymetric deepening in relation to anthropogenic nutrient enrichment is provided with this thesis. The methods applied and developed here could be refined, especially by integrating more detailed interaction between organic and inorganic particulate matter, and by benthic processes (see Section 4.4.4). Therefore, process understanding for the derivation of mathematical formulations and the availability of observational data has to be improved, especially in anthropogenically impacted estuaries with continuous human interference in sediment dynamics by dredging, dumping and ship movements.
Furthermore, the effects of these continuous human activities themselves, for anthropogenic utilization and maintenance of estuaries, are also omnipresent interferences with implications on DO dynamics and thus an important and interesting topic for further research.

Appendix A. Biogeochemical model configuration

Table A1: Reaction-based changes in the concentration of the biogeochemical state variables, not related to transport.

State variable	Non-conservative change (see process rate formulations in Table A2 and parameter values in Table A3)
Carbon	
d/dt ALG1 (DIAT)	$nPP_1 - MORT_1 - SET_1$
d/dt ALG2 (NON-DIAT)	$nPP_2 - MORT_2 - SET_2$
d/dt POC1	$(1\text{-}fra) \times (MORT_1 + MORT_2) - DEC_{1,12} - DEC_{1,13} - MIN_{1,1} - SET_{1,1}$
d/dt POC2	$DEC_{1,12} - DEC_{1,23} - MIN_{1,2} - SET_{1,2}$
d/dt DOC	$DEC_{1,13} + DEC_{1,23} - MIN_{1,3}$
Nitrogen	
d/dt NH4	$RAM + \sum_{k=1}^{3} MIN_{2,k} - \sum_{i=1}^{2} UAM_i - NIT$
d/dt NO3	$NIT - \sum_{i=1}^{2} UNI_i - \sum_{k=1}^{3} MIN_{nit,k}$
d/dt PON1	$(1\text{-}fra) \times an \times (MORT_1 + MORT_2) - DEC_{2,12} - DEC_{2,13} - MIN_{2,1} - SET_{2,1}$
d/dt PON2	$DEC_{2,12} - DEC_{2,23} - MIN_{2,2} - SET_{2,2}$
d/dt DON	$DEC_{2,13} + DEC_{2,23} - MIN_{2,3}$
Phosphorous	
d/dt PO4	$RAP + \sum_{k=1}^{3} MIN_{3,k} - \sum_{i=1}^{2} UPH_i$
d/dt POP1	$(1\text{-}fra) \times ap \times (MORT_1 + MORT_2) - DEC_{3,12} - DEC_{3,13} - MIN_{3,1} - SET_{3,1}$
d/dt POP2	$DEC_{3,12} - DEC_{3,23} - MIN_{3,2} - SET_{3,2}$
d/dt DOP	$DEC_{3,13} + DEC_{3,23} - MIN_{3,3}$
Silicate	
d/dt Si	$RAS + DISS - USI$
d/dt OPAL	$(1 - fra) \times asi \times MORT_i - DISS$
Oxygen	
d/dt DO	$REAR + \sum_{i=1}^{2} nPP_i - \sum_{k=1}^{3} MIN_{oxy,k} - 2 \times NIT$

Table A2: Formulations of process rates and parameterizations. i is an index for algae class with 1 for DIAT (ALG1) and 2 for NON-DIAT (ALG2); j is an index for nutrient (1 for carbon, 2 for nitrogen, 3 for phosphorous, 4 for silicate); k an index for particulate matter class (1 fast particulate, 2 refractory particulate, 3 dissolved). H denotes water depth, v flow velocity, W wind speed; τ is bottom shear stress, and T temperature in °C as calculated by the hydrodynamic model. SOXY is oxygen saturation according to [*Weiss,* 1970].

Symbol	Process	Formulation (see parameter values in Table A3)	Unit
et	light extinction coefficient	etb + es × SPMI + $\sum_{i=1}^{2}$ (ea × ALG_i) + $\sum_{k=1}^{3}$ (ep × POC_k)	m^{-1}
$DEC_{j,kk}$	decomposition rate fast to slow	$fdec_{j,k}$ × $MIN_{j,k}$	mmol m^{-3} d^{-1}
DISS	OPAL dissolution rate	kdiss × OPAL (si_{eq} - Si)	mmol m^{-3} d^{-1}
fdl_i	daylength limitation	Min(DL,DLo_i) / DLo_i	-
fmn	contribution nitrate in mineral.	NO3 / (Ksni + NO3) × (1 - DO / (Ksoxi + DO)) × 1.12^{T-20}	-
fmo	contribution oxygen in mineral.	DO / (Ksoxc + DO) × 1.07^{T-20}	-
fn_i	nitrogen limitation function	(NH4 + NO3) / (NH4 + NO3 + Ksn)	-
$fnut_i$	nutrient limitation function	Min(fn_i, fp_i, fs_i)	-
fp_i	phosphorous limitation function	PO4 / (PO4 + Ksp)	-
$frad_i$	light limitation function	1.0	-
if	Is ≥ Io_i and Ib < Io_i	(1 + ln(Is/Io_i) - (Is/Io_i) × exp(-et × H))/(et × H)	
	Is < Io_i and Ib < Io_i	(Is/Io_i) × ((1-exp(-et × H))/(et × H))	
fram	fraction N consumed as NH4	1.0	-
if	NH4 < am_c	NH4 / (NH4 + NO3)	
frmn	rel. frac. nitrate in mineral.	fmn / (fmo + fmn)	-
frmo	rel. frac. oxygen in mineral.	fmo / (fmo + fmn)	-
fsi	Si limitation function	Si / (Si + Kssi)	-
Ib	light intensity at the bottom	Is × exp(-et × H)	W m^{-2}
Io_i	optimal light intensity	1.04^{T-20} × Io_i^{20}	W m^{-2}
klrear	oxygen transfer coefficient	$klrear^{20}$ × 0.92^{T-20}	m d^{-1}
$klrear^{20}$	transfer coefficient at 20 °C	3.863 × $(v/H)^{0.5}$ + 0.065 × $klrear^{20}$ W^2	m d^{-1}
kgp_i	gross pp rate of algae	fdl_i × $frad_i$ × $fnut_i$ × 1.4^{T-20} × kpp	d^{-1}
$krsp_i$	total respiration rate of algae	fgr × kgp_i + (1-fgr) × 1.07^{T-20} × kmr_i	d^{-1}
$MIN_{j,k}$	mineralization rate	$kmin_k$ × 1.2^{T-20} × POC/N/P_k	mmol m^{-3} d^{-1}
$MIN_{oxy,k}$	mineral. oxygen consumption	frmo × $\sum_{k=1}^{3}$ $MIN_{1,k}$	mmol m^{-3} d^{-1}
$MIN_{nit,k}$	mineral. denitrification	frmn × $\sum_{k=1}^{3}$ $MIN_{1,k}$	mmol m^{-3} d^{-1}
$MORT_i$	mortality rate phytoplankton	1.07^{T-20} × kmrt × ALG_i	mmol m^{-3} d^{-1}
NIT	nitrification rate	knit × 1.07^{T-20} × (NH4/(Ksam+NH4)) × (DO/(Ksox + DO))	mmol m^{-3} d^{-1}
nPP_i	net primary production rate	(kgp_i – $krsp_i$) ALG_i	mmol m^{-3} d^{-1}
RAM	Release of NH4 by autolysis	fra × an × ($MORT_1$ + $MORT_2$)	mmol m^{-3} d^{-1}
RAP	Release PO4 by autolysis	fra × ap × ($MORT_1$ + $MORT_2$)	mmol m^{-3} d^{-1}
RAS	Release Si by autolysis	fra × asi × $MORT_1$	mmol m^{-3} d^{-1}
REAR	reaeration rate	klrear × (SOXY - DO) / H	mmol m^{-3} d^{-1}
SET_i	settling rate phytoplankton	ftau × sv_{ALG}/H × ALG_i	mmol m^{-3} d^{-1}
$SET_{j,k}$	settling rate particulate matter	ftau × sv/H × POC/N/P_k	mmol m^{-3} d^{-1}
ftau	bottom shear stress function	max(0.0, (1-τ / τ_c))	-
UPH_i	phosphorous uptake rate	ap_i× nPP_i	mmol m^{-3} d^{-1}
UAM_i	NH4 uptake rate	fram (an_i× nPP_i)	mmol m^{-3} d^{-1}
UNI_i	NO3 uptake rate	(1-fram)× an × nPP_i	mmol m^{-3} d^{-1}
USI	Si uptake rate	asi × nPP_i	mmol m^{-3} d^{-1}

Table A3: Model parameters.

Symbol	Parameter	Value	Unit
an	stoichiometric ratio N:C phytoplankton	106 / 16	-
ap	stoichiometric ratio P:C phytoplankton	106 / 1	-
asi	stoichiometric ratio Si:C diatoms	106 / 15	-
am_c	critical concentration NH4 in uptake	0.71	mmol N m^{-3}
DL	length of daylight	calc. based on latitude and date	
DLo_1	opt. daylength for ALG1 growth	0.5	d
DLo_2	opt. daylength for ALG2 growth	0.58	d
ea	specific light extinction coeff. algae	0.0012	m^2 mmol C^{-1}
ep	specific light extinction coeff. POC	0.0012	m^2 mmol C^{-1}
es	spec. light extinction coeff. inorg. sus. matter	0.03	m^2 g^{-1}
etb	partial extinction coeff. background	0.08	m^{-1}
$fdec_{1,2}$	factor decomposition POC1 to POC2	0.5	-
$fdec_{1,3}$	factor decomposition POC1 to DOC	0.5	-
$fdec_{2,3}$	factor decomposition POC2 to DOC	1.0	-
fgr	growth respiration factor algae	0.065	-
fra	fraction released by autolysis	0.5	-
Is	light intensity at the water surface	model forcing	W m^{-2}
Io_1^{20}	optimal light intensity for ALG1	25.0	W m^{-2}
Io_2^{20}	optimal light intensity for ALG2	30.0	W m^{-2}
kdiss	OPAL dissolution reaction rate constant	3.1×10^{-6}	m^3 mmol Si^{-1} d^{-1}
$kmin_1$	mineralization rate constant POC1 at 20°C	0.4	d^{-1}
$kmin_2$	mineralization rate constant POC2 at 20°C	0.05	d^{-1}
$kmin_3$	mineralization rate constant DOC at 20°C	0.15	d^{-1}
kmr_1	ALG1 maintenance resp. rate constant at 20°C	0.036	d^{-1}
kmr_2	ALG2 maintenance resp. rate constant at 20°C	0.045	d^{-1}
kmrt	mortality rate constant phytoplankton at 20°C	0.5	d^{-1}
knit	nitrification rate constant at 20°C	28.6	mmol N m^{-3} d^{-1}
kpp	potential max. production rate constant ALG_i	1.2	d^{-1}
Ksam	half saturation NH4 limitation in nitrification	36	mmol N m^{-3}
Ksni	half saturation NO3 in denitrification	36	mmol N m^{-3}
Ksn	half saturation concentration nitrogen in nPP	0.36	mmol N m^{-3}
Ksox	half saturation DO in nitrification	31.3	mmol O_2 m^{-3}
Ksoxi	half saturation DO inhibition in denit.	94	mmol O_2 m^{-3}
Ksoxc	half saturation DO consumption in mineral.	63	mmol O_2 m^{-3}
Ksp	half saturation phosphorous in nPP	0.03	mmol P m^{-3}
Kssi	half saturation silicate in nPP	1	mmol Si m^{-3}
si_{eq}	equilibrium concentration Si	357	mmol Si m^{-3}
SPMI	inorg. sus. part. matter concentration	47.0	g m^{-3}
sv	settling velocity POC	0.5	m d^{-1}
sv_{ALG}	settling velocity phytoplankton	0.1	m d^{-1}
τ_c	critical bottom shear stress for settling	0.1	N m^{-2}

Appendix B. Riverine boundary values and flushing time

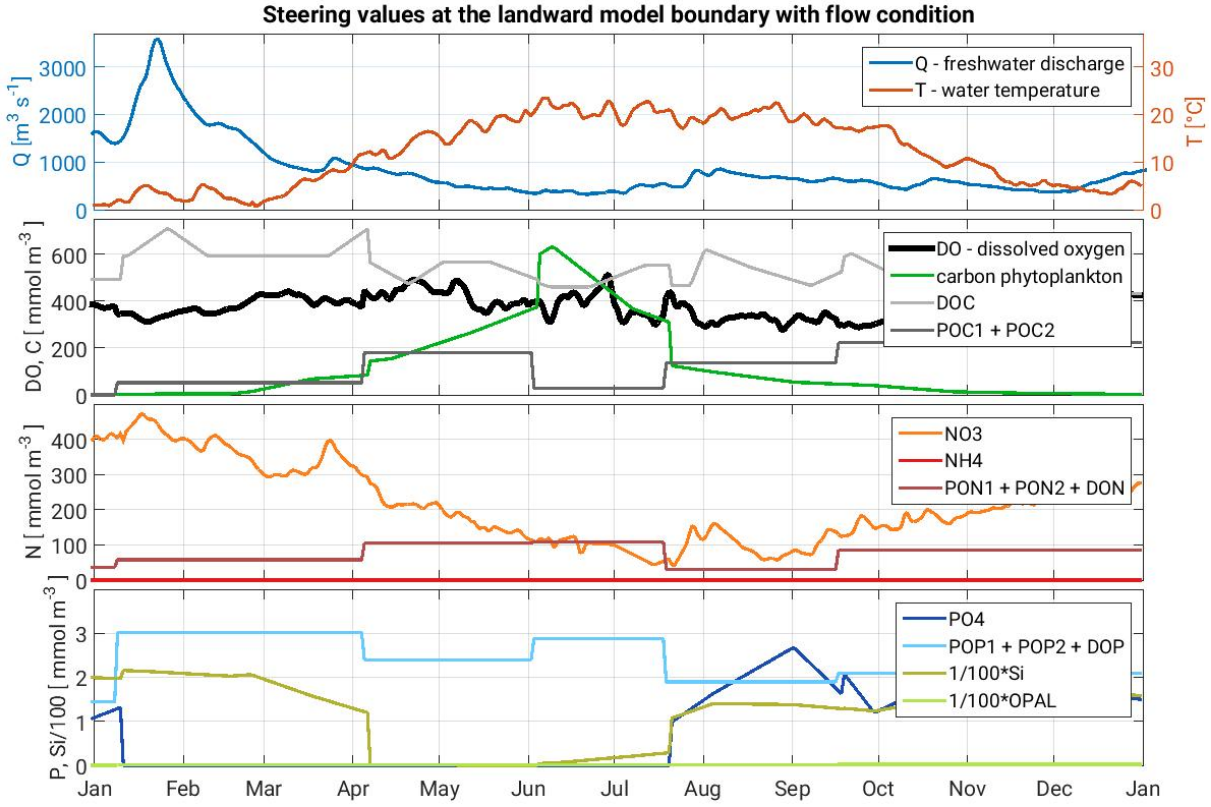

Figure B1: Boundary values for the year 2011 at the upstream/landward model boundary. Upper panel: Freshwater inflow, measured at Neu Darchau 50 km upstream of the weir, and water temperature, measured at Cumlosen 116 km upstream of the weir. The three panels below show concentrations of dissolved oxygen, phytoplankton carbon, DOC, the sum of POC1 and POC2; nitrogen in the inorganic forms NO3 and NH4, and in dissolved and particulate matter; phosphorous in PO4, and in dissolved and particulate matter. The values for Si and OPAL are shown as a hundredth. The values from the lower three panels are compiled from three observational data sources: the sparse data from the helicopter sampling directly upstream of the weir where complemented by continuous/biweekly observational data from the upstream stations Cumlosen and Schnackenburg.

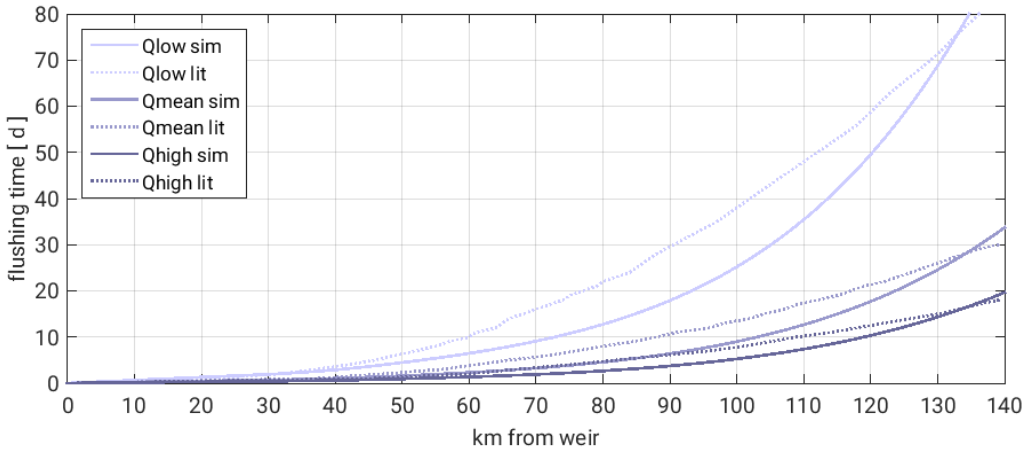

Figure B2: Flushing time for different constant discharge scenarios with Q_{low} = 250 $m^3 s^{-1}$, Q_{mean} = 700 $m^3 s^{-1}$, and Q_{high} = 1200 $m^3 s^{-1}$. Solid lines show values from the model based on simulated water volumes, dashed lines show values from *Bergemann et al.* [1996], based on volumes at half tide level from 1980

References

Abood, K. A., S. G. Metzger, and D. F. Distante (1999), Minimizing Dredging Disposal via Sediment Management in New York Harbor, *Estuaries, 22*(3), 763, doi:10.2307/1353109.

Abril, G., M.-V. Commarieu, A. Sottolichio, P. Bretel, and F. Guérin (2009), Turbidity limits gas exchange in a large macrotidal estuary, *Estuarine, Coastal and Shelf Science, 83*(3), 342–348, doi:10.1016/j.ecss.2009.03.006.

Abril, G., H. Etcheber, B. Delille, M. Frankignoulle, and A. V. Borges (2003), Carbonate dissolution in the turbid and eutrophic Loire estuary, *Mar. Ecol. Prog. Ser., 259,* 129–138, doi:10.3354/meps259129.

Abril, G., H. Etcheber, P. Le Hir, P. Bassoullet, B. Boutier, and M. Frankignoulle (1999), Oxic/anoxic oscillations and organic carbon mineralization in an estuarine maximum turbidity zone (The Gironde, France), *Limnol. Oceanogr., 44*(5), 1304–1315, doi:10.4319/lo.1999.44.5.1304.

Ahmed, A., G. Pelletier, and M. Roberts (2017), South Puget Sound flushing times and residual flows, *Estuarine, Coastal and Shelf Science, 187,* 9–21, doi:10.1016/j.ecss.2016.12.027.

Álvarez-Salgado, X. A., and A.E.J. Miller (1999), Dissolved organic carbon in a large macrotidal estuary (the Humber, UK): Behaviour during estuarine mixing, *Marine pollution bulletin, 37*(3-7), 216–224, doi:10.1016/S0025-326X(98)00156-8.

Amann, T., A. Weiss, and J. Hartmann (2012), Carbon dynamics in the freshwater part of the Elbe estuary, Germany: Implications of improving water quality, *Estuarine, Coastal and Shelf Science, 107,* 112–121, doi:10.1016/j.ecss.2012.05.012.

Amann, T., A. Weiss, and J. Hartmann (2014), Silica fluxes in the inner Elbe Estuary, Germany, *Biogeochemistry, 118*(1-3), 389–412, doi:10.1007/s10533-013-9940-3.

Arndt, S., J.-P. Vanderborght, and P. Regnier (2007), Diatom growth response to physical forcing in a macrotidal estuary: Coupling hydrodynamics, sediment transport, and biogeochemistry, *J. Geophys. Res., 112*(C5), doi:10.1029/2006JC003581.

Avoine, J., G. P. Allen, M. Nichols, J. C. Salomon, and C. Larsonneur (1981), Suspended-sediment transport in the Seine estuary, France: Effect of man-made modifications on estuary-shelf sedimentology, *Marine Geology, 40*(1-2), 119–137, doi:10.1016/0025-3227(81)90046-3.

Baird, D., R. R. Christian, C. H. Peterson, and G. A. Johnson (2004), Consequence of hypoxia on estuarine ecosystem function: Energy diversion from consumers to microbes, *Ecological Applications, 14*(3), 805–822, doi:10.1890/02-5094.

Balls, P. W., N. Brockie, J. Dobson, and W. Johnston (1996), Dissolved oxygen and nitrification in the Upper Forth Estuary during summer (1982–92): Patterns and trends, *Estuarine, Coastal and Shelf Science, 42*(1), 117–134, doi:10.1006/ecss.1996.0009.

Banks, R. B., and F. F. Herrera (1977), Effects of wind and rain on surface reaeration, *J. Environ. Eng. Div., Am. Soc. Civil Eng., 103*(EE3), pp. 489-504.

Benson, B. B., and D. Krause Jr. (1984), The concentration and isotopic fractionation of oxygen dissolved in freshwater and seawater in equilibrium with the atmosphere.

Bergemann, M., G. Blöcker, H. Harms, M. Kerner, R. Meyer-Niehls, W. Petersen, and F. Schroeder (1996), Der Sauerstoffhaushalt der Tideelbe, *Die Küste*(58), 199–261.

Bianchi, T. S. (2007), *Biogeochemistry of Estuaries,* Oxford University Press.

Billen, G., J. Garnier, A. Ficht, and C. Cun (2001), Modeling the response of water quality in the Seine River Estuary to human activity in its watershed over the last 50 years, *Estuaries, 24*(6), 977, doi:10.2307/1353011.

Blauw, A. N., H. F. J. Los, M. Bokhorst, and P. L. A. Erftemeijer (2009), GEM: a generic ecological model for estuaries and coastal waters, *Hydrobiologia, 618*(1), 175–198, doi:10.1007/s10750-008-9575-x.

Boehlich, M. J., and T. Strotmann (2008), The Elbe Estuary, *Die Küste, 74,* 288–306.

Breitburg, D. (2002), Effects of hypoxia, and the balance between hypoxia and enrichment, on coastal fishes and fisheries, *Estuaries, 25*(4), 767–781, doi:10.1007/BF02804904.

Breitburg, D., L. A. Levin, A. Oschlies, M. Grégoire, F. P. Chavez, D. J. Conley, V. Garçon, D. Gilbert, D. Gutiérrez, K. Isensee, G. S. Jacinto, K. E. Limburg, I. Montes, S. W. A. Naqvi, G. C. Pitcher, N. N. Rabalais, M. R. Roman, K. A. Rose, B. A. Seibel, M. Telszewski, M. Yasuhara, and J. Zhang (2018), Declining oxygen in the global ocean and coastal waters, *Science (New York, N.Y.), 359*(6371), doi:10.1126/science.aam7240.

Breitburg, D. L., A. Adamack, K. A. Rose, S. E. Kolesar, B. Decker, J. E. Purcell, J. E. Keister, and J. H. Cowan (2003), The pattern and influence of low dissolved oxygen in the Patuxent River, a seasonally hypoxic estuary, *Estuaries, 26*(2), 280–297, doi:10.1007/BF02695967.

Brossard, C., G. Lannuzel, J.-P. Helard, and B. Gallenne (1990), Technical improvements and maintenance economics for the maritime channels in the Loire Estuary, *Terra et Aqua*(43), 3–12.

Bruce, L. C., P. L. M. Cook, I. Teakle, and M. R. Hipsey (2014), Hydrodynamic controls on oxygen dynamics in a riverine salt wedge estuary, the Yarra River estuary, Australia, *Hydrol. Earth Syst. Sci., 18*(4), 1397–1411, doi:10.5194/hess-18-1397-2014.

Brye, B. de, A. de Brauwere, O. Gourgue, E. J.M. Delhez, and E. Deleersnijder (2012), Water renewal timescales in the Scheldt Estuary, *Journal of Marine Systems, 94,* 74–86, doi:10.1016/j.jmarsys.2011.10.013.

Caffrey, J. M. (2004), Factors controlling net ecosystem metabolism in U.S. estuaries, *Estuaries, 27*(1), 90–101, doi:10.1007/BF02803563.

Casulli, V. (2009), A high-resolution wetting and drying algorithm for free-surface hydrodynamics, *Int. J. Numer. Meth. Fluids, 60*(4), 391–408, doi:10.1002/fld.1896.

Casulli, V., and G. S. Stelling (2010), Semi-implicit subgrid modelling of three-dimensional free-surface flows, *Int. J. Numer. Meth. Fluids, 67*(4), 441–449.

Cerco, C. F., and T. Cole (1993), Three-dimensional eutrophication model of Chesapeake Bay, *Journal of Environmental Engineering, 119*(6), 1006–1025, doi:10.1061/(ASCE)0733-9372(1993)119:6(1006).

Cerco, C. F., and M. R. Noel (2004), The 2002 Chesapeake Bay eutrophication model, *EPA 903-R-04-004,* U.S. Environmental Protection Agency, Annapolis.

Chan, T. U., D. P. Hamilton, B. J. Robson, B. R. Hodges, and C. Dallimore (2002), Impacts of hydrological changes on phytoplankton succession in the Swan River, Western Australia, *Estuaries, 25*(6), 1406–1415, doi:10.1007/BF02692234.

Chapra, S. C. (2008), *Surface water-quality modeling,* xix, 844, Waveland Press, Long Grove, Ill.

Cloern, J. E. (2001), Our evolving conceptual model of the coastal eutrophication problem, *Mar. Ecol. Prog. Ser., 210,* 223–253, doi:10.3354/meps210223.

Cloern, J. E., P. C. Abreu, J. Carstensen, L. Chauvaud, R. Elmgren, J. Grall, H. Greening, J. O. R. Johansson, M. Kahru, E. T. Sherwood, J. Xu, and K. Yin (2016), Human activities and climate variability drive fast-paced change across the world's estuarine-coastal ecosystems, *Global change biology, 22*(2), 513–529, doi:10.1111/gcb.13059.

Cloern, J. E., S. Q. Foster, and A. E. Kleckner (2014), Phytoplankton primary production in the world's estuarine-coastal ecosystems, *Biogeosciences, 11*(9), 2477–2501, doi:10.5194/bg-11-2477-2014.

Conley, D. J., J. Carstensen, J. Aigars, P. Axe, E. Bonsdorff, T. Eremina, B.-M. Haahti, C. Humborg, P. Jonsson, J. Kotta, C. Lännegren, U. Larsson, A. Maximov, M. R. Medina, E. Lysiak-Pastuszak, N. Remeikaité-Nikiené, J. Walve, S. Wilhelms, and L. Zillén (2011), Hypoxia is increasing in the coastal zone of the Baltic Sea, *Environmental science & technology, 45*(16), 6777–6783, doi:10.1021/es201212r.

Conley, D. J., H. W. Paerl, R. W. Howarth, D. F. Boesch, S. P. Seitzinger, K. E. Havens, C. Lancelot, and G. E. Likens (2009), Ecology. Controlling eutrophication: Nitrogen and phosphorus, *Science (New York, N.Y.), 323*(5917), 1014–1015, doi:10.1126/science.1167755.

Cowan, J. L. W., and W. R. Boynton (1996), Sediment-water oxygen and nutrient exchanges along the longitudinal axis of Chesapeake Bay: Seasonal Patterns, Controlling Factors and Ecological Significance, *Estuaries, 19*(3), 562, doi:10.2307/1352518.

Dähnke, K., E. Bahlmann, and K. Emeis (2008), A nitrate sink in estuaries?: An assessment by means of stable nitrate isotopes in the Elbe estuary, *Limnol. Oceanogr., 53*(4), 1504–1511, doi:10.4319/lo.2008.53.4.1504.

Dallas, K. L., and P. L. Barnard (2011), Anthropogenic influences on shoreline and nearshore evolution in the San Francisco Bay coastal system, *Estuarine, Coastal and Shelf Science, 92*(1), 195–204, doi:10.1016/j.ecss.2010.12.031.

de Jonge, Victor N., H. M. Schuttelaars, van Beusekom, Justus E.E., S. A. Talke, and de Swart, Huib E. (2014), The influence of channel deepening on estuarine turbidity levels and dynamics, as exemplified by the Ems estuary, *Estuarine, Coastal and Shelf Science, 139,* 46–59.

Deleersnijder, E., J.-M. Campin, and E. J.M. Delhez (2001), The concept of age in marine modelling, *Journal of Marine Systems, 28*(3-4), 229–267, doi:10.1016/S0924-7963(01)00026-4.

Delhez, E. J.M., J.-M. Campin, A. C. Hirst, and E. Deleersnijder (1999), Toward a general theory of the age in ocean modelling, *Ocean Modelling, 1*(1), 17–27, doi:10.1016/S1463-5003(99)00003-7.

Delhez, É. J.M., B. de Brye, A. de Brauwere, and É. Deleersnijder (2014), Residence time vs influence time, *Journal of Marine Systems, 132,* 185–195, doi:10.1016/j.jmarsys.2013.12.005.

Delhez, É. J.M., and É. Deleersnijder (2002), The concept of age in marine modelling, *Journal of Marine Systems, 31*(4), 279–297, doi:10.1016/S0924-7963(01)00066-5.

Delhez, É. J.M., G. Lacroix, and É. Deleersnijder (2004), The age as a diagnostic of the dynamics of marine ecosystem models, *Ocean Dynamics, 54*(2), 221–231, doi:10.1007/s10236-003-0075-2.

Deltares (2014), D-Water Quality Processes Library Description: Technical Reference Manual, 459 pp., Delft.

Diaz, R. J. (2001), Overview of hypoxia around the world, *Journal of Environment Quality, 30*(2), 275, doi:10.2134/jeq2001.302275x.

Diaz, R. J., and D. L. Breitburg (2007), Chapter 1 The hypoxic environment, in *Fish physiology: Primitive fishes, Fish Physiology,* edited by W. S. Hoar et al., pp. 1–23, Elsevier.

Diaz, R. J., and R. Rosenberg (1995), Marine benthic hypoxia: a review of its ecological effects and the behavioural responses of benthic macrofauna, *Oceanography and Marine Biology, 33,* 245–303.

Diaz, R. J., and R. Rosenberg (2008), Spreading dead zones and consequences for marine ecosystems, *Science (New York, N.Y.), 321*(5891), 926–929, doi:10.1126/science.1156401.

Díaz, R. J., and R. Rosenberg (2011), Introduction to Environmental and Economic Consequences of Hypoxia, *International Journal of Water Resources Development, 27*(1), 71–82, doi:10.1080/07900627.2010.531379.

Diez-Minguito, M., A. Baquerizo, H. E. de Swart, and M. A. Losada (2014), Structure of the turbidity field in the Guadalquivir estuary: Analysis of observations and a box model approach, *J. Geophys. Res. Oceans, 119*(10), 7190–7204, doi:10.1002/2014JC010210.

DiLorenzo, J. L., P. Huang, M. L. Thatcher, and T. O. Najarian (1994), Dredging Impacts on Delaware Estuary Tides, in *Proceedings of the 3rd international conference / 3rd International Conference on Estuarine and Coastal Modeling: Oak Brook, Illinois, September 8 - 10, 1993, Estuarine and coastal modeling,* vol. 3, edited by M. L. Spaulding, American Soc. of Civil Engineers, New York, NY.

Du, J., and J. Shen (2015), Decoupling the influence of biological and physical processes on the dissolved oxygen in the Chesapeake Bay, *J. Geophys. Res. Oceans, 120*(1), 78–93, doi:10.1002/2014JC010422.

Duce, R. A., J. LaRoche, K. Altieri, K. R. Arrigo, A. R. Baker, D. G. Capone, S. Cornell, F. Dentener, J. Galloway, R. S. Ganeshram, R. J. Geider, T. Jickells, M. M. Kuypers, R. Langlois, P. S. Liss, S. M. Liu, J. J. Middelburg, C. M. Moore, S. Nickovic, A. Oschlies, T. Pedersen, J. Prospero, R. Schlitzer, S. Seitzinger, L. L. Sorensen, M. Uematsu, O. Ulloa, M. Voss, B. Ward, and L. Zamora (2008), Impacts of atmospheric anthropogenic nitrogen on the

open ocean, *Science (New York, N.Y.), 320*(5878), 893–897, doi:10.1126/science.1150369.

Eby, L. A., and L. B. Crowder (2002), Hypoxia-based habitat compression in the Neuse River Estuary: Context-dependent shifts in behavioral avoidance thresholds, *Can. J. Fish. Aquat. Sci., 59*(6), 952–965, doi:10.1139/f02-067.

Ekau, W., H. Auel, H.-O. Pörtner, and D. Gilbert (2010), Impacts of hypoxia on the structure and processes in pelagic communities (zooplankton, macro-invertebrates and fish), *Biogeosciences, 7*(5), 1669–1699, doi:10.5194/bg-7-1669-2010.

Ensing, E., H. E. de Swart, and H. M. Schuttelaars (2015), Sensitivity of tidal motion in well-mixed estuaries to cross-sectional shape, deepening, and sea level rise, *Ocean Dynamics, 65*(7), 933–950, doi:10.1007/s10236-015-0844-8.

Etcheber, H., A. Taillez, G. Abril, J. Garnier, P. Servais, F. Moatar, and M.-V. Commarieu (2007), Particulate organic carbon in the estuarine turbidity maxima of the Gironde, Loire and Seine estuaries: Origin and lability, *Hydrobiologia, 588*(1), 245–259, doi:10.1007/s10750-007-0667-9.

Evans, M. R., V. Grimm, K. Johst, T. Knuuttila, R. de Langhe, C. M. Lessells, M. Merz, M. A. O'Malley, S. H. Orzack, M. Weisberg, D. J. Wilkinson, O. Wolkenhauer, and T. G. Benton (2013), Do simple models lead to generality in ecology?, *Trends in ecology & evolution, 28*(10), 578–583, doi:10.1016/j.tree.2013.05.022.

Fennel, K., R. Hetland, Y. Feng, and S. DiMarco (2011), A coupled physical-biological model of the Northern Gulf of Mexico shelf: Model description, validation and analysis of phytoplankton variability, *Biogeosciences, 8*(7), 1881–1899, doi:10.5194/bg-8-1881-2011.

Fennel, K., J. Hu, A. Laurent, M. Marta-Almeida, and R. Hetland (2013), Sensitivity of hypoxia predictions for the northern Gulf of Mexico to sediment oxygen consumption and model nesting, *J. Geophys. Res. Oceans, 118*(2), 990–1002, doi:10.1002/jgrc.20077.

FGG Elbe (2017), Elbebericht: Entwicklung des ökologischen und chemischen Zustands der Elbe 2009 – 2012: Schwerpunktthema Nährstoffe, Elbe Water Quality Report Key issue: nutrients, River Basin Community Elbe, Magdeburg.

FHH, and HPA (2014), *Deutsches Gewässerkundliches Jahrbuch: Elbegebiet, Teil III Untere Elbe ab der Havelmündung,* in German, Hamburg.

Fujiwara, T., T. Takahashi, A. Kasai, Y. Sugiyama, and M. Kuno (2002), The role of circulation in the development of hypoxia in Ise Bay, Japan, *Estuarine, Coastal and Shelf Science, 54*(1), 19–31, doi:10.1006/ecss.2001.0824.

Fulweiler, R. W., N. N. Rabalais, and A. S. Heiskanen (2012), The eutrophication commandments, *Marine pollution bulletin, 64*(10), 1997–1999, doi:10.1016/j.marpolbul.2012.07.025.

Ganju, N. K., M. J. Brush, B. Rashleigh, A. L. Aretxabaleta, P. Del Barrio, J. S. Grear, L. A. Harris, S. J. Lake, G. McCardell, J. O'Donnell, D. K. Ralston, R. P. Signell, J. M. Testa, and J. M. P. Vaudrey (2016), Progress and challenges in coupled hydrodynamic-ecological

estuarine modeling, *Estuaries and Coasts, 39*(2), 311–332, doi:10.1007/s12237-015-0011-y.

Garbe, C. S., A. Rutgersson, J. Boutin, G. de Leeuw, B. Delille, C. W. Fairall, N. Gruber, J. Hare, D. T. Ho, M. T. Johnson, P. D. Nightingale, H. Pettersson, J. Piskozub, E. Sahlée, W.-t. Tsai, B. Ward, D. K. Woolf, and C. J. Zappa (2014), Transfer across the air-aea interface, in *Ocean-Atmosphere Interactions of Gases and Particles, Springer Earth System Sciences,* edited by P. S. Liss and M. T. Johnson, pp. 55–112, Springer Berlin Heidelberg; Imprint: Springer, Berlin, Heidelberg.

Garnier, J., P. Servais, G. Billen, M. Akopian, and N. Brion (2001), Lower Seine River and Estuary (France) carbon and oxygen budgets during low flow, *Estuaries, 24*(6), 964, doi:10.2307/1353010.

Gelfenbaum, G. (1983), Suspended-sediment response to semidiurnal and fortnightly tidal variations in a mesotidal estuary: Columbia River, U.S.A, *Marine Geology, 52*(1-2), 39–57, doi:10.1016/0025-3227(83)90020-8.

Gilbert, D., N. N. Rabalais, R. J. Díaz, and J. Zhang (2010), Evidence for greater oxygen decline rates in the coastal ocean than in the open ocean, *Biogeosciences, 7*(7), 2283–2296, doi:10.5194/bg-7-2283-2010.

Gross, E. S., M. L. MacWilliams, and W. J. Kimmerer (2010), Three-dimensional modeling of tidal hydrodynamics in the San Francisco Estuary, *San Francisco Estuary and Watershed Science, 7*(2).

Hagy, J. D., W. R. Boynton, C. W. Keefe, and K. V. Wood (2004), Hypoxia in Chesapeake Bay, 1950–2001: Long-term change in relation to nutrient loading and river flow, *Estuaries, 27*(4), 634–658, doi:10.1007/BF02907650.

Halpern, B. S., S. Walbridge, K. A. Selkoe, C. V. Kappel, F. Micheli, C. D'Agrosa, J. F. Bruno, K. S. Casey, C. Ebert, H. E. Fox, R. Fujita, D. Heinemann, H. S. Lenihan, E. M. P. Madin, M. T. Perry, E. R. Selig, M. Spalding, R. Steneck, and R. Watson (2008), A global map of human impact on marine ecosystems, *Science (New York, N.Y.), 319*(5865), 948–952, doi:10.1126/science.1149345.

Harremoës, P. (1982), Immediate and delayed oxygen depletion in rivers, *Water Research, 16*(7), 1093–1098, doi:10.1016/0043-1354(82)90124-5.

He, B., M. Dai, W. Zhai, L. Wang, K. Wang, J. Chen, J. Lin, A. Han, and Y. Xu (2010), Distribution, degradation and dynamics of dissolved organic carbon and its major compound classes in the Pearl River estuary, China, *Marine Chemistry, 119*(1-4), 52–64, doi:10.1016/j.marchem.2009.12.006.

Herman, P.M.J., J. J. Middelburg, J. van de Koppel, and C.H.R. Heip (1999), Ecology of estuarine macrobenthos, in *Advances in ecological research, Advances in ecological research,* vol. 29, edited by D. B. Nedwell et al., pp. 195–240, Academic Press, New York.

Hetland, R. D., and S. F. DiMarco (2008), How does the character of oxygen demand control the structure of hypoxia on the Texas–Louisiana continental shelf?, *Journal of Marine Systems, 70*(1-2), 49–62, doi:10.1016/j.jmarsys.2007.03.002.

Holzwarth, I., and K. Wirtz (2018), Anthropogenic impacts on estuarine oxygen dynamics: A model based evaluation, *Estuarine, Coastal and Shelf Science,* doi:10.1016/j.ecss.2018.01.020.

Howarth, R., F. Chan, D. J. Conley, J. Garnier, S. C. Doney, R. Marino, and G. Billen (2011), Coupled biogeochemical cycles: Eutrophication and hypoxia in temperate estuaries and coastal marine ecosystems, *Frontiers in Ecology and the Environment, 9*(1), 18–26, doi:10.1890/100008.

IKSE (2005), *Die Elbe und ihr Einzugsgebiet: Ein geographisch-hydrologischer und wasserwirtschaftlicher Überblick,* in German, International Commission for the Protection of the Elbe, Magdeburg.

IKSE (2016), Wasserrahmenrichtlinie im Einzugsgebiet der Elbe: Informationsblatt der IKSE Nr. 5, http://www.ikse-mkol.org/fileadmin/media/user_upload/D/06_Publikationen/01_Wasserrahmenrichtlinie/2016_IKSE_Infoblatt_Nr_5_WFD.pdf.

Irigoien, X., and J. Castel (1997), Light limitation and distribution of chlorophyll pigments in a highly turbid estuary: The Gironde (SW France), *Estuarine, Coastal and Shelf Science, 44*(4), 507–517, doi:10.1006/ecss.1996.0132.

Jenny, J.-P., P. Francus, A. Normandeau, F. Lapointe, M.-E. Perga, A. Ojala, A. Schimmelmann, and B. Zolitschka (2016), Global spread of hypoxia in freshwater ecosystems during the last three centuries is caused by rising local human pressure, *Global change biology, 22*(4), 1481–1489, doi:10.1111/gcb.13193.

Jickells, T.D., J.E. Andrews, D.J. Parkes, S. Suratman, A. A. Aziz, and Y. Y. Hee (2014), Nutrient transport through estuaries: The importance of the estuarine geography, *Estuarine, Coastal and Shelf Science,* doi:10.1016/j.ecss.2014.03.014.

Jonge, V. N. de, H. M. Schuttelaars, van Beusekom, Justus E.E., S. A. Talke, and H. E. de Swart (2014), The influence of channel deepening on estuarine turbidity levels and dynamics, as exemplified by the Ems estuary, *Estuarine, Coastal and Shelf Science, 139,* 46–59, doi:10.1016/j.ecss.2013.12.030.

Justić, D., N. N. Rabalais, R. Eugene Turner, and W. J. Wiseman (1993), Seasonal coupling between riverborne nutrients, net productivity and hypoxia, *Marine pollution bulletin, 26*(4), 184–189, doi:10.1016/0025-326X(93)90620-Y.

Justić, D., N. N. Rabalais, and R. E. Turner (2005), Coupling between climate variability and coastal eutrophication: Evidence and outlook for the northern Gulf of Mexico, *Journal of Sea Research, 54*(1), 25–35, doi:10.1016/j.seares.2005.02.008.

Kappenberg, J., and I. Grabemann (2001), Variability of the mixing zones and estuarine turbidity maxima in the Elbe and Weser Estuaries, *Estuaries, 24*(5), 699, doi:10.2307/1352878.

Kärnä, T., and A. M. Baptista (2016a), Evaluation of a long-term hindcast simulation for the Columbia River estuary, *Ocean Modelling, 99,* 1–14, doi:10.1016/j.ocemod.2015.12.007.

Kärnä, T., and A. M. Baptista (2016b), Water age in the Columbia River estuary, *Estuarine, Coastal and Shelf Science,* doi:10.1016/j.ecss.2016.09.001.

Keeling, R. E., A. Körtzinger, and N. Gruber (2010), Ocean deoxygenation in a warming world, *Annual review of marine science, 2,* 199–229, doi:10.1146/annurev.marine.010908.163855.

Keeling, R. F., and H. E. Garcia (2002), The change in oceanic O(2) inventory associated with recent global warming, *Proceedings of the National Academy of Sciences of the United States of America, 99*(12), 7848–7853, doi:10.1073/pnas.122154899.

Kemp, W. M., and W. R. Boynton (1980), Influence of biological and physical processes on dissolved oxygen dynamics in an estuarine system: Implications for measurement of community metabolism, *Estuarine and Coastal Marine Science, 11*(4), 407–431, doi:10.1016/S0302-3524(80)80065-X.

Kemp, W. M., J. M. Testa, D. J. Conley, D. Gilbert, and J. D. Hagy (2009), Temporal responses of coastal hypoxia to nutrient loading and physical controls, *Biogeosciences, 6*(12), 2985–3008, doi:10.5194/bg-6-2985-2009.

Kerimoglu, O., R. Hofmeister, J. Maerz, R. Riethmüller, and K. W. Wirtz (2017), The acclimative biogeochemical model of the southern North Sea, *Biogeosciences, 14*(19), 4499–4531, doi:10.5194/bg-14-4499-2017.

Kerner, M. (2007), Effects of deepening the Elbe Estuary on sediment regime and water quality, *Estuarine, Coastal and Shelf Science, 75*(4), 492–500, doi:10.1016/j.ecss.2007.05.033.

Khangaonkar, T., B. Sackmann, W. Long, T. Mohamedali, and M. Roberts (2012), Simulation of annual biogeochemical cycles of nutrient balance, phytoplankton bloom(s), and DO in Puget Sound using an unstructured grid model, *Ocean Dynamics, 62*(9), 1353–1379, doi:10.1007/s10236-012-0562-4.

Kremer, J. N., A. Reischauer, and C. D'Avanzo (2003), Estuary-specific variation in the air-water gas exchange coefficient for oxygen, *Estuaries, 26*(4), 829–836, doi:10.1007/BF02803341.

Kuo, A. Y., and B. J. Neilson (1987), Hypoxia and salinity in Virginia estuaries, *Estuaries, 10*(4), 277, doi:10.2307/1351884.

Lajaunie-Salla, K., K. Wild-Allen, A. Sottolichio, B. Thouvenin, X. Litrico, and G. Abril (2017), Impact of urban effluents on summer hypoxia in the highly turbid Gironde Estuary, applying a 3D model coupling hydrodynamics, sediment transport and biogeochemical processes, *Journal of Marine Systems, 174,* 89–105, doi:10.1016/j.jmarsys.2017.05.009.

Lane, A. (2004), Bathymetric evolution of the Mersey Estuary, UK, 1906–1997: Causes and effects, *Estuarine, Coastal and Shelf Science, 59*(2), 249–263, doi:10.1016/j.ecss.2003.09.003.

Lang, G. (2012), *Horizontal and vertical fluxes from Untrim2 results: Reconstruction of fluxes for use with a conservative water quality model,* paper presented at *Untrim User Meeting,* Trento, Italy.

Lanoux, A., H. Etcheber, S. Schmidt, A. Sottolichio, G. Chabaud, M. Richard, and G. Abril (2013), Factors contributing to hypoxia in a highly turbid, macrotidal estuary (the Gironde, France), *Environ. Sci.: Processes Impacts, 15*(3), 585, doi:10.1039/c2em30874f.

Lee, B. J., E. Toorman, and M. Fettweis (2014), Multimodal particle size distributions of fine-grained sediments: mathematical modeling and field investigation, *Ocean Dynamics, 64*(3), 429–441.

Legović, T., D. Petricioli, and V. Žutić (1991), Hypoxia in a pristine stratified estuary (Krka, Adriatic Sea), *Marine Chemistry, 32*(2-4), 347–359, doi:10.1016/0304-4203(91)90048-2.

Lehmann, M. F., B. Barnett, Y. Gélinas, D. Gilbert, R. J. Maranger, A. Mucci, B. Sundby, and B. Thibodeau (2009), Aerobic respiration and hypoxia in the Lower St. Lawrence Estuary: Stable isotope ratios of dissolved oxygen constrain oxygen sink partitioning, *Limnol. Oceanogr., 54*(6), 2157–2169, doi:10.4319/lo.2009.54.6.2157.

Liu, W.-C., M.-H. Hsu, A. Y. Kuo, and M.-H. Li (2001), Influence of bathymetric changes on hydrodynamics and salt intrusion in estuarine system, *J Am Water Resources Assoc, 37*(5), 1405–1416, doi:10.1111/j.1752-1688.2001.tb03648.x.

Luketina, D. (1998), Simple Tidal Prism Models Revisited, *Estuarine, Coastal and Shelf Science, 46*(1), 77–84, doi:10.1006/ecss.1997.0235.

MacWilliams, M., A. Bever, and E. Foresman (2016), 3-D simulations of the San Francisco Estuary with subgrid bathymetry to explore long-term trends in salinity distribution and fish abundance, *SFEWS, 14*(2), doi:10.15447/sfews.2016v14iss2art3.

Maerz, J., and K. Wirtz (2009), Resolving physically and biologically driven suspended particulate matter dynamics in a tidal basin with a distribution-based model, *Estuarine, Coastal and Shelf Science, 84*(1), 128–138, doi:10.1016/j.ecss.2009.05.015.

Mallin, M. A., V. L. Johnson, S. H. Ensign, and T. A. MacPherson (2006), Factors contributing to hypoxia in rivers, lakes, and streams, *Limnol. Oceanogr., 51*(1part2), 690–701, doi:10.4319/lo.2006.51.1_part_2.0690.

Marmin, S., J.-C. Dauvin, and P. Lesueur (2014), Collaborative approach for the management of harbour-dredged sediment in the Bay of Seine (France), *Ocean & Coastal Management, 102,* 328–339, doi:10.1016/j.ocecoaman.2014.10.012.

Matear, R. J., and A. C. Hirst (2003), Long-term changes in dissolved oxygen concentrations in the ocean caused by protracted global warming, *Global Biogeochem. Cycles, 17*(4), n/a-n/a, doi:10.1029/2002GB001997.

McCormick, L. R., and L. A. Levin (2017), Physiological and ecological implications of ocean deoxygenation for vision in marine organisms, *Philosophical transactions. Series A, Mathematical, physical, and engineering sciences, 375*(2102), doi:10.1098/rsta.2016.0322.

Meier, H. E. M., H. C. Andersson, K. Eilola, B. G. Gustafsson, I. Kuznetsov, B. Müller-Karulis, T. Neumann, and O. P. Savchuk (2011), Hypoxia in future climates: A model ensemble study for the Baltic Sea, *Geophys. Res. Lett., 38*(24), n/a-n/a, doi:10.1029/2011GL049929.

Meire, P., T. Ysebaert, S. van Damme, E. van den Bergh, T. Maris, and E. Struyf (2005), The Scheldt estuary: A description of a changing ecosystem, *Hydrobiologia, 540*(1-3), 1–11, doi:10.1007/s10750-005-0896-8.

Melrose, D. C., C. A. Oviatt, and M. S. Berman (2007), Hypoxic events in Narragansett Bay, Rhode Island, during the summer of 2001, *Estuaries and Coasts, 30*(1), 47–53, doi:10.1007/BF02782966.

Meyers, S. D., A. J. Linville, and M. E. Luther (2014a), Alteration of residual circulation due to large-scale infrastructure in a coastal plain estuary, *Estuaries and Coasts, 37*(2), 493–507, doi:10.1007/s12237-013-9691-3.

Meyers, S. D., A. J. Linville, and M. E. Luther (2014b), Alteration of Residual Circulation Due to Large-Scale Infrastructure in a Coastal Plain Estuary, *Estuaries and Coasts, 37*(2), 493–507, doi:10.1007/s12237-013-9691-3.

Middelburg, J. J., and P. M.J. Herman (2007), Organic matter processing in tidal estuaries, *Marine Chemistry, 106*(1-2), 127–147, doi:10.1016/j.marchem.2006.02.007.

Middelburg, J. J., and L. A. Levin (2009), Coastal hypoxia and sediment biogeochemistry, *Biogeosciences, 6*(7), 1273–1293, doi:10.5194/bg-6-1273-2009.

Monsen, N. E., J. E. Cloern, L. V. Lucas, and S. G. Monismith (2002), A comment on the use of flushing time, residence time, and age as transport time scales, *Limnol. Oceanogr., 47*(5), 1545–1553, doi:10.4319/lo.2002.47.5.1545.

Montagnes, D. J. S., and M. Franklin (2001), Effect of temperature on diatom volume, growth rate, and carbon and nitrogen content: Reconsidering some paradigms, *Limnol. Oceanogr., 46*(8), 2008–2018, doi:10.4319/lo.2001.46.8.2008.

Müller, B., L. D. Bryant, A. Matzinger, and A. Wüest (2012), Hypolimnetic oxygen depletion in eutrophic lakes, *Environmental science & technology, 46*(18), 9964–9971, doi:10.1021/es301422r.

Murphy, R. R., W. M. Kemp, and W. P. Ball (2011), Long-term trends in Chesapeake Bay seasonal hypoxia, stratification, and nutrient loading, *Estuaries and Coasts, 34*(6), 1293–1309, doi:10.1007/s12237-011-9413-7.

Najjar, R. G., C. R. Pyke, M. B. Adams, D. Breitburg, C. Hershner, M. Kemp, R. Howarth, M. R. Mulholland, M. Paolisso, D. Secor, K. Sellner, D. Wardrop, and R. Wood (2010), Potential climate-change impacts on the Chesapeake Bay, *Estuarine, Coastal and Shelf Science, 86*(1), 1–20, doi:10.1016/j.ecss.2009.09.026.

Najjar, R. G., H. A. Walker, P. J. Anderson, E. J. Barron, R. J. Bord, Gibson, JR, V. S. Kennedy, C. G. Knight, J. P. Megonigal, R. E. O'Connor, C. D. Polsky, N. P. Psuty, B. A. Richards, L. G. Sorenson, E. M. Steele, and R. S. Swanson (2000), The potential impacts of climate change on the mid-Atlantic coastal region, *Clim. Res., 14,* 219–233, doi:10.3354/cr014219.

Nakamura, Y., and H. G. Stefan (1994), Effect of flow velocity on sediment oxygen demand: Theory, *Journal of Environmental Engineering, 120*(5), 996–1016, doi:10.1061/(ASCE)0733-9372(1994)120:5(996).

Neumann, T., W. Fennel, and C. Kremp (2002), Experimental simulations with an ecosystem model of the Baltic Sea: A nutrient load reduction experiment, *Global Biogeochem. Cycles, 16*(3), 7-1-7-19, doi:10.1029/2001GB001450.

Neumann, T., and G. Schernewski (2008), Eutrophication in the Baltic Sea and shifts in nitrogen fixation analyzed with a 3D ecosystem model, *Journal of Marine Systems, 74*(1-2), 592–602, doi:10.1016/j.jmarsys.2008.05.003.

Nicholls, R. J., and A. Cazenave (2010), Sea-level rise and its impact on coastal zones, *Science (New York, N.Y.), 328*(5985), 1517–1520, doi:10.1126/science.1185782.

Nichols, M. M. (1988), The consequences of dredging, in *Hydrodynamics of estuaries,* edited by B. Kjerfve, CRC Press, Boca Raton.

Nixon, S. W. (1995), Coastal marine eutrophication: A definition, social causes, and future concerns, *Ophelia, 41*(1), 199–219, doi:10.1080/00785236.1995.10422044.

O'Connor, D., and W. Dobbins (1958), Mechanism of reaeration in natural streams, *Transactions of the American Society of Civil Engineers, 123,* 641–684.

Oreskes, N. (2004), Beyond the ivory tower. The scientific consensus on climate change, *Science (New York, N.Y.), 306*(5702), 1686, doi:10.1126/science.1103618.

Oschlies, A., K. G. Schulz, U. Riebesell, and A. Schmittner (2008), Simulated 21st century's increase in oceanic suboxia by CO_2 -enhanced biotic carbon export, *Global Biogeochem. Cycles, 22*(4), n/a-n/a, doi:10.1029/2007GB003147.

O'Shea, M. L., and T. M. Brosnan (2000), Trends in indicators of eutrophication in western Long Island Sound and the Hudson-Raritan Estuary, *Estuaries, 23*(6), 877, doi:10.2307/1353004.

Paerl, H. W. (2006), Assessing and managing nutrient-enhanced eutrophication in estuarine and coastal waters: Interactive effects of human and climatic perturbations, *Ecological Engineering, 26*(1), 40–54, doi:10.1016/j.ecoleng.2005.09.006.

Paerl, H. W. (2009), Controlling eutrophication along the freshwater–marine continuum: Dual nutrient (N and P) reductions are essential, *Estuaries and Coasts, 32*(4), 593–601, doi:10.1007/s12237-009-9158-8.

Paerl, H. W., J. T. Scott, M. J. McCarthy, S. E. Newell, W. S. Gardner, K. E. Havens, D. K. Hoffman, S. W. Wilhelm, and W. A. Wurtsbaugh (2016), It takes two to tango: When and where dual nutrient (N & P) reductions are needed to protect lakes and downstream ecosystems, *Environmental science & technology,* doi:10.1021/acs.est.6b02575.

Pan, L., P. Ding, and J. Ge (2012), Impacts of deep waterway project on morphological changes within the north passage of the Changjiang Estuary, China, *Journal of Coastal Research, 284,* 1165–1176, doi:10.2112/JCOASTRES-D-11-00129.1.

Parker, C. A., and J. E. O'Reilly (1991), Oxygen depletion in Long Island Sound: A historical perspective, *Estuaries, 14*(3), 248, doi:10.2307/1351660.

Paulmier, A., and D. Ruiz-Pino (2009), Oxygen minimum zones (OMZs) in the modern ocean, *Progress in Oceanography, 80*(3-4), 113–128, doi:10.1016/j.pocean.2008.08.001.

Peña, M. A., S. Katsev, T. Oguz, and D. Gilbert (2010), Modeling dissolved oxygen dynamics and hypoxia, *Biogeosciences, 7*(3), 933–957, doi:10.5194/bg-7-933-2010.

Pennock, J. R. (1985), Chlorophyll distributions in the Delaware estuary: Regulation by light-limitation, *Estuarine, Coastal and Shelf Science, 21*(5), 711–725, doi:10.1016/0272-7714(85)90068-X.

Picado, A., J. M. Dias, and A. B. Fortunato (2010), Tidal changes in estuarine systems induced by local geomorphologic modifications, *Continental Shelf Research, 30*(17), 1854–1864, doi:10.1016/j.csr.2010.08.012.

Postma, L., P. M. A. Boderie, J. A. G. van Gils, and J. K. L. van Beek (2003), Component software systems for surface water simulation, in *Computational Science — ICCS 2003, Lecture Notes in Computer Science,* edited by G. Goos et al., pp. 649–658, Springer Berlin Heidelberg, Berlin, Heidelberg.

Prandle, D. (1986), Generalised theory of estuarine dynamics, in *Physics of Shallow Estuaries and Bays, Lecture Notes on Coastal and Estuarine Studies,* edited by J. van de Kreeke, pp. 42–57, American Geophysical Union, Washington, D. C.

Prandle, D. (2003), Relationships between tidal dynamics and bathymetry in strongly convergent estuaries, *J. Phys. Oceanogr., 33*(12), 2738–2750, doi:10.1175/1520-0485(2003)033<2738:RBTDAB>2.0.CO;2.

Pusch, M. (Ed.) (2006), *Stoffdynamik und Habitatstruktur in der Elbe: Mit 39 Tabellen,* XVIII, 385 S., *Konzepte für die nachhaltige Entwicklung einer Flusslandschaft,* vol. 5, Weißensee-Verl., Berlin.

Qian, W., J. Gan, J. Liu, B. He, Z. Lu, X. Guo, D. Wang, L. Guo, T. Huang, and M. Dai (2018), Current status of emerging hypoxia in a eutrophic estuary: The lower reach of the Pearl River Estuary, China, *Estuarine, Coastal and Shelf Science, 205,* 58–67, doi:10.1016/j.ecss.2018.03.004.

Quiel, K., A. Becker, V. Kirchesch, A. Schöl, and H. Fischer (2011), Influence of global change on phytoplankton and nutrient cycling in the Elbe River, *Reg Environ Change, 11*(2), 405–421, doi:10.1007/s10113-010-0152-2.

Rabalais, N., W.-J. Cai, J. Carstensen, D. Conley, B. Fry, X. Hu, Z. Quiñones-Rivera, R. Rosenberg, C. Slomp, E. Turner, M. Voss, B. Wissel, and J. Zhang (2014), Eutrophication-driven deoxygenation in the coastal ocean, *oceanog, 27*(1), 172–183, doi:10.5670/oceanog.2014.21.

Rabalais, N. N., R. J. Díaz, L. A. Levin, R. E. Turner, D. Gilbert, and J. Zhang (2010), Dynamics and distribution of natural and human-caused hypoxia, *Biogeosciences, 7*(2), 585–619, doi:10.5194/bg-7-585-2010.

Rabalais, N. N., R. E. Turner, R. J. Diaz, and D. Justic (2009), Global change and eutrophication of coastal waters, *ICES Journal of Marine Science, 66*(7), 1528–1537, doi:10.1093/icesjms/fsp047.

Rayson, M. D., E. S. Gross, R. D. Hetland, and O. B. Fringer (2016), Time scales in Galveston Bay: An unsteady estuary, *J. Geophys. Res. Oceans, 121*(4), 2268–2285, doi:10.1002/2015JC011181.

Regnier, P., S. Arndt, N. Goossens, C. Volta, G. G. Laruelle, R. Lauerwald, and J. Hartmann (2013), Modelling estuarine biogeochemical dynamics: From the local to the global scale, *Aquat Geochem, 19*(5-6), 591–626, doi:10.1007/s10498-013-9218-3.

Robins, P. E., M. W. Skov, M. J. Lewis, L. Giménez, A. G. Davies, S. K. Malham, S. P. Neill, J. E. McDonald, T. A. Whitton, S. E. Jackson, and C. F. Jago (2016), Impact of climate change on UK estuaries: A review of past trends and potential projections, *Estuarine, Coastal and Shelf Science, 169,* 119–135, doi:10.1016/j.ecss.2015.12.016.

Roegner, G. C., J. A. Needoba, and A. M. Baptista (2011), Coastal upwelling supplies oxygen-depleted water to the Columbia River estuary, *PLoS ONE, 6*(4), e18672, doi:10.1371/journal.pone.0018672.

Roman, M. R., J. J. Pierson, D. G. Kimmel, W. C. Boicourt, and X. Zhang (2012), Impacts of hypoxia on zooplankton spatial distributions in the Northern Gulf of Mexico, *Estuaries and Coasts, 35*(5), 1261–1269, doi:10.1007/s12237-012-9531-x.

Rosenzweig, C., D. Karoly, M. Vicarelli, P. Neofotis, Q. Wu, G. Casassa, A. Menzel, T. L. Root, N. Estrella, B. Seguin, P. Tryjanowski, C. Liu, S. Rawlins, and A. Imeson (2008), Attributing physical and biological impacts to anthropogenic climate change, *Nature, 453*(7193), 353–357, doi:10.1038/nature06937.

Ruiz, J., M. J. Polo, M. Díez-Minguito, G. Navarro, E. P. Morris, E. Huertas, I. Caballero, E. Contreras, and M. A. Losada (2015), The Guadalquivir Estuary: A hot spot for environmental and human conflicts, in *Environmental Management and Governance: Advances in Coastal and Marine Resources, Coastal Research Library,* vol. 8, edited by C. W. Finkl and C. Makowski, pp. 199–232, Springer International Publishing, Cham.

Savenije, H. H. G. (2005), *Salinity and tides in alluvial estuaries,* 1st ed., Elsevier, Amsterdam, Boston.

Scavia, D., J. C. Field, D. F. Boesch, R. W. Buddemeier, V. Burkett, D. R. Cayan, M. Fogarty, M. A. Harwell, R. W. Howarth, C. Mason, D. J. Reed, T. C. Royer, A. H. Sallenger, and J. G. Titus (2002), Climate change impacts on U.S. Coastal and Marine Ecosystems, *Estuaries, 25*(2), 149–164, doi:10.1007/BF02691304.

Schmidtko, S., L. Stramma, and M. Visbeck (2017), Decline in global oceanic oxygen content during the past five decades, *Nature, 542*(7641), 335–339, doi:10.1038/nature21399.

Schöl, A., B. Hein, J. Wyrwa, and V. Kirchesch (2014), Modelling Water Quality in the Elbe and its Estuary: Large scale and long term applications with focus on the oxygen budget of the estuary, *Die Küste, 81,* 203–232.

Schroeder, F. (1997), Water quality in the Elbe estuary: Significance of different processes for the oxygen deficit at Hamburg, *Environmental Modeling and Assessment,* 73–82.

Scully, M. E. (2010), Wind modulation of dissolved oxygen in Chesapeake Bay, *Estuaries and Coasts, 33*(5), 1164–1175, doi:10.1007/s12237-010-9319-9.

Scully, M. E. (2013), Physical controls on hypoxia in Chesapeake Bay: A numerical modeling study, *J. Geophys. Res. Oceans, 118*(3), 1239–1256, doi:10.1002/jgrc.20138.

Sehili, A., G. Lang, and C. Lippert (2014), High-resolution subgrid models: background, grid generation, and implementation, *Ocean Dynamics,* doi:10.1007/s10236-014-0693-x.

Seitzinger, S. P., E. Mayorga, A. F. Bouwman, C. Kroeze, A. H. W. Beusen, G. Billen, G. van Drecht, E. Dumont, B. M. Fekete, J. Garnier, and J. A. Harrison (2010), Global river nu-

trient export: A scenario analysis of past and future trends, *Global Biogeochem. Cycles, 24*(4), n/a-n/a, doi:10.1029/2009GB003587.

Shaffer, G., S. M. Olsen, and J. O. P. Pedersen (2009), Long-term ocean oxygen depletion in response to carbon dioxide emissions from fossil fuels, *Nature Geosci, 2*(2), 105–109, doi:10.1038/ngeo420.

Sharp, J. H. (2010), Estuarine oxygen dynamics: What can we learn about hypoxia from long-time records in the Delaware Estuary?, *Limnol. Oceanogr., 55*(2), 535–548, doi:10.4319/lo.2010.55.2.0535.

Sharp, J. H., C. H. Culberson, and T. M. Church (1982), The chemistry of the Delaware estuary. General considerations1, *Limnol. Oceanogr., 27*(6), 1015–1028, doi:10.4319/lo.1982.27.6.1015.

Sheldon, J. E., and M. Alber (2006), The calculation of estuarine turnover times using freshwater fraction and tidal prism models: A critical evaluation, *Estuaries and Coasts, 29*(1), 133–146, doi:10.1007/BF02784705.

Shen, J., and L. Haas (2004), Calculating age and residence time in the tidal York River using three-dimensional model experiments, *Estuarine, Coastal and Shelf Science, 61*(3), 449–461, doi:10.1016/j.ecss.2004.06.010.

Sherwood, C. R., D. A. Jay, R. Bradford Harvey, P. Hamilton, and C. A. Simenstad (1990), Historical changes in the Columbia River Estuary, *Progress in Oceanography, 25*(1-4), 299–352, doi:10.1016/0079-6611(90)90011-P.

Smith, V. H. (1998), Cultural eutrophication of inland, estuarine, and coastal waters, in *Successes, limitations, and frontiers in ecosystem science,* edited by M. L. Pace and P. M. Groffmann, pp. 7–49, Springer, New York, Barcelona.

Smits, J. G. C., and J. K. L. van Beek (2013), ECO: a generic eutrophication model including comprehensive sediment-water interaction, *PLoS ONE, 8*(7), e68104, doi:10.1371/journal.pone.0068104.

Soetaert, K., P. M.J. Herman, and J. Kromkamp (1994), Living in the twilight: estimating net phytoplankton growth in the Westerschelde estuary (The Netherlands) by means of an ecosystem model (MOSES), *J Plankton Res, 16*(10), 1277–1301.

Stanley, D. W., and S. W. Nixon (1992), Stratification and bottom-water hypoxia in the Pamlico River Estuary, *Estuaries, 15*(3), 270, doi:10.2307/1352775.

Statham, P. J. (2012), Nutrients in estuaries--an overview and the potential impacts of climate change, *The Science of the total environment, 434,* 213–227, doi:10.1016/j.scitotenv.2011.09.088.

Sterner, R. (2011), C: N:P stoichiometry in Lake Superior: freshwater sea as end member, *IW, 1*(1), 29–46, doi:10.5268/IW-1.1.365.

Streeter, H. W., and E. B. Phelps (1925), A study of the pollution and natural purification of the Ohio river.: III. Factors concerned in the phenomena of oxidation and reaeration, *Public Health Bulletin, 146.*

Sweers, H.E. (1976), A nomogram to estimate the heat-exchange coefficient at the air-water interface as a function of wind speed and temperature: a critical survey of some literature, *Journal of Hydrology, 30,* 375–401.

Talke, S. A., H. E. Swart, and V. N. Jonge (2009), An idealized model and systematic process study of oxygen depletion in highly turbid estuaries, *Estuaries and Coasts, 32*(4), 602–620.

Testa, J. M., Y. Li, Y. J. Lee, M. Li, D. C. Brady, D. M. Di Toro, W. M. Kemp, and J. J. Fitzpatrick (2014), Quantifying the effects of nutrient loading on dissolved O2 cycling and hypoxia in Chesapeake Bay using a coupled hydrodynamic–biogeochemical model, *Journal of Marine Systems, 139,* 139–158, doi:10.1016/j.jmarsys.2014.05.018.

Testa, J.M., and W.M. Kemp (2011), Oxygen – Dynamics and Biogeochemical Consequences, in *Treatise on Estuarine and Coastal Science,* pp. 163–199, Elsevier.

Thomann, R. V., and J. A. Mueller (1987), *Principles of surface water quality modeling and control,* XII, 644, HarperCollinsPublishers, New York.

Tomaso, D. J., and R. G. Najjar (2015), Long-term variations in the dissolved oxygen budget of an urbanized tidal river: The upper Delaware Estuary, *J. Geophys. Res. Biogeosci., 120*(6), 1027–1045, doi:10.1002/2014JG002758.

Topcu, D., H. Behrendt, U. Brockmann, and U. Claussen (2011), Natural background concentrations of nutrients in the German Bight area (North Sea), *Environ Monit Assess, 174*(1-4), 361–388, doi:10.1007/s10661-010-1463-y.

Trancoso, A. R., S. Saraiva, L. Fernandes, P. Pina, P. Leitão, and R. Neves (2005), Modelling macroalgae using a 3D hydrodynamic-ecological model in a shallow, temperate estuary, *Ecological Modelling, 187*(2-3), 232–246, doi:10.1016/j.ecolmodel.2005.01.054.

Umlauf, L., and H. Burchard (2003), A generic length-scale equation for geophysical turbulence models, *J Mar Res, 61*(2), 235–265, doi:10.1357/002224003322005087.

van Damme, S., E. Struyf, T. Maris, T. Ysebaert, F. Dehairs, M. Tackx, C. Heip, and P. Meire (2005), Spatial and temporal patterns of water quality along the estuarine salinity gradient of the Scheldt estuary (Belgium and The Netherlands): Results of an integrated monitoring approach, *Hydrobiologia, 540*(1-3), 29–45, doi:10.1007/s10750-004-7102-2.

van Maren, D. S., T. van Kessel, K. Cronin, and L. Sittoni (2015a), The impact of channel deepening and dredging on estuarine sediment concentration, *Continental Shelf Research, 95,* 1–14, doi:10.1016/j.csr.2014.12.010.

van Maren, D. S., J. C. Winterwerp, and J. Vroom (2015b), Fine sediment transport into the hyper-turbid lower Ems River: The role of channel deepening and sediment-induced drag reduction, *Ocean Dynamics, 65*(4), 589–605, doi:10.1007/s10236-015-0821-2.

van Vliet, M. T.H., W. H.P. Franssen, J. R. Yearsley, F. Ludwig, I. Haddeland, D. P. Lettenmaier, and P. Kabat (2013), Global river discharge and water temperature under climate change, *Global Environmental Change, 23*(2), 450–464, doi:10.1016/j.gloenvcha.2012.11.002.

Vaquer-Sunyer, R., and C. M. Duarte (2008), Thresholds of hypoxia for marine biodiversity, *Proceedings of the National Academy of Sciences of the United States of America, 105*(40), 15452–15457, doi:10.1073/pnas.0803833105.

Verity, P. G., M. Alber, and S. B. Bricker (2006), Development of hypoxia in well-mixed subtropical estuaries in the Southeastern USA, *Estuaries and Coasts, 29*(4), 665–673, doi:10.1007/BF02784291.

Vitousek, P. M. (1997), Human domination of earth's ecosystems, *Science, 277*(5325), 494–499, doi:10.1126/science.277.5325.494.

Volta, C., S. Arndt, H. H. G. Savenije, G. G. Laruelle, and P. Regnier (2014), C-GEM (v 1.0): A new, cost-efficient biogeochemical model for estuaries and its application to a funnel-shaped system, *Geosci. Model Dev., 7*(4), 1271–1295, doi:10.5194/gmd-7-1271-2014.

Volta, C., G. G. Laruelle, S. Arndt, and P. Regnier (2016a), Linking biogeochemistry to hydro-geometrical variability in tidal estuaries: A generic modeling approach, *Hydrol. Earth Syst. Sci., 20*(3), 991–1030, doi:10.5194/hess-20-991-2016.

Volta, C., G. G. Laruelle, and P. Regnier (2016b), Regional carbon and CO2 budgets of North Sea tidal estuaries, *Estuarine, Coastal and Shelf Science, 176,* 76–90, doi:10.1016/j.ecss.2016.04.007.

Vriend, H. J. de, Z. B. Wang, T. Ysebaert, P. M. J. Herman, and P. Ding (2011), Eco-Morphological Problems in the Yangtze Estuary and the Western Scheldt, *Wetlands, 31*(6), 1033–1042, doi:10.1007/s13157-011-0239-7.

Wakelin, S. L., Y. Artioli, M. Butenschön, J. I. Allen, and J. T. Holt (2015), Modelling the combined impacts of climate change and direct anthropogenic drivers on the ecosystem of the northwest European continental shelf, *Journal of Marine Systems, 152,* 51–63, doi:10.1016/j.jmarsys.2015.07.006.

Walther, R., C. Cayrol, L. Hamm, A. Delouis, and D. Lehay (2015), Evaluation of an offshore disposal site in the Loire Estuary through field monitoring and 3D numerical modeling, *Int. Conf. Coastal. Eng., 1*(34), 24, doi:10.9753/icce.v34.management.24.

Wan, Y., F. Gu, H. Wu, and D. Roelvink (2014), Hydrodynamic evolutions at the Yangtze Estuary from 1998 to 2009, *Applied Ocean Research, 47,* 291–302, doi:10.1016/j.apor.2014.06.009.

Wang, B., J. Hu, S. Li, and D. Liu (2017), A numerical analysis of biogeochemical controls with physical modulation on hypoxia during summer in the Pearl River estuary, *Biogeosciences, 14*(12), 2979–2999, doi:10.5194/bg-14-2979-2017.

Wang, H., J. Loftis, Z. Liu, D. Forrest, and J. Zhang (2014), The storm surge and sub-grid inundation modeling in New York City during hurricane Sandy, *JMSE, 2*(1), 226–246, doi:10.3390/jmse2010226.

Wang, S. Y., K. Lau, K.-P. Lai, J.-W. Zhang, A. C.-K. Tse, J.-W. Li, Y. Tong, T.-F. Chan, C. K.-C. Wong, J. M.-Y. Chiu, D. W.-T. Au, A. S.-T. Wong, R. Y.-C. Kong, and R. S.-S. Wu (2016), Hypoxia causes transgenerational impairments in reproduction of fish, *Nature communications, 7,* 12114, doi:10.1038/ncomms12114.

Warner, J. C. (2005), Numerical modeling of an estuary: A comprehensive skill assessment, *J. Geophys. Res., 110*(C5), 39, doi:10.1029/2004JC002691.

Webster, I. T., and G. P. Harris (2004), Anthropogenic impacts on the ecosystems of coastal lagoons: Modelling fundamental biogeochemical processes and management implications, *Mar. Freshwater Res., 55*(1), 67, doi:10.1071/MF03068.

Wei, H., Y. He, Q. Li, Z. Liu, and H. Wang (2007), Summer hypoxia adjacent to the Changjiang Estuary, *Journal of Marine Systems, 67*(3-4), 292–303, doi:10.1016/j.jmarsys.2006.04.014.

Weilbeer, H. (2008), Chapter 30 Numerical simulation and analyses of sediment transport processes in the Ems-Dollard estuary with a three-dimensional model, in *Sediment and ecohydraulics: INTERCOH 2005 00,* 1st ed., *Proceedings in marine science,* vol. 9, edited by T. Kusuda, pp. 447–462, Elsevier, Amsterdam, Boston.

Weilbeer, H. (2015), Sediment transport and sediment management in the Elbe Estuary, Germany, *Terra et Aqua, 139,* 11–23.

Weiss, R. F. (1970), The solubility of nitrogen, oxygen and argon in water and seawater, *Deep Sea Research and Oceanographic Abstracts, 17*(4), 721–735, doi:10.1016/0011-7471(70)90037-9.

Welsh, B. L., and F. C. Eller (1991), Mechanisms controlling summertime oxygen depletion in western Long Island Sound, *Estuaries, 14*(3), 265, doi:10.2307/1351661.

Whitehead, P. G., R. L. Wilby, R. W. Battarbee, M. Kernan, and A. J. Wade (2009), A review of the potential impacts of climate change on surface water quality, *Hydrological Sciences Journal, 54*(1), 101–123, doi:10.1623/hysj.54.1.101.

Wild-Allen, K., and J. Andrewartha (2016), Connectivity between estuaries influences nutrient transport, cycling and water quality, *Marine Chemistry, 185,* 12–26, doi:10.1016/j.marchem.2016.05.011.

Wild-Allen, K., J. Skerratt, J. Whitehead, F. Rizwi, and J. Parslow (2013), Mechanisms driving estuarine water quality: A 3D biogeochemical model for informed management, *Estuarine, Coastal and Shelf Science,* doi:10.1016/j.ecss.2013.04.009.

Winterwerp, J. C., J. Vroom, Z.-B. Wang, M. Krebs, E. C.M. Hendriks, D. S. van Maren, K. Schrottke, C. Borgsmüller, and A. Schöl (2017), SPM response to tide and river flow in the hyper-turbid Ems River, *Ocean Dynamics, 67*(5), 559–583, doi:10.1007/s10236-017-1043-6.

Wirtz, K. W. (2011), Non-uniform scaling in phytoplankton growth rate due to intracellular light and CO2 decline, *Journal of Plankton Research, 33*(9), 1325–1341, doi:10.1093/plankt/fbr021.

Wiseman, W.J., N. N. Rabalais, R. E. Turner, S. P. Dinnel, and A. MacNaughton (1997), Seasonal and interannual variability within the Louisiana coastal current: Stratification and hypoxia, *Journal of Marine Systems, 12*(1-4), 237–248, doi:10.1016/S0924-7963(96)00100-5.

Wool, T. A., S. R. Davie, and H. N. Rodriguez (2003), Development of three-dimensional hydrodynamic and water quality models to support total maximum daily load decision process for the Neuse River Estuary, North Carolina, *Journal of Water Resources Planning and Management, 129*(4), 295–306, doi:10.1061/(ASCE)0733-9496(2003)129:4(295).

Wu, R. S. S. (2002), Hypoxia: From molecular responses to ecosystem responses, *Marine pollution bulletin, 45*(1-12), 35–45, doi:10.1016/S0025-326X(02)00061-9.

Wu, S., H. Cheng, Y.J. Xu, J. Li, and S. Zheng (2016), Decadal changes in bathymetry of the Yangtze River Estuary: Human impacts and potential saltwater intrusion, *Estuarine, Coastal and Shelf Science, 182,* 158–169, doi:10.1016/j.ecss.2016.10.002.

Wyrtki, K. (1962), The oxygen minima in relation to ocean circulation, *Deep Sea Research and Oceanographic Abstracts, 9*(1-2), 11–23, doi:10.1016/0011-7471(62)90243-7.

Xu, J., and R. R. Hood (2006), Modeling biogeochemical cycles in Chesapeake Bay with a coupled physical–biological model, *Estuarine, Coastal and Shelf Science, 69*(1-2), 19–46, doi:10.1016/j.ecss.2006.03.021.

Zalasiewicz, J., M. Williams, W. Steffen, and P. Crutzen (2010), The new world of the Anthropocene, *Environmental science & technology, 44*(7), 2228–2231, doi:10.1021/es903118j.

Zarzuelo, C., M. Díez-Minguito, M. Ortega-Sánchez, A. López-Ruiz, and M. Á. Losada (2015), Hydrodynamics response to planned human interventions in a highly altered embayment: The example of the Bay of Cádiz (Spain), *Estuarine, Coastal and Shelf Science, 167,* 75–85, doi:10.1016/j.ecss.2015.07.010.

Zhang, H., and S. Li (2010), Effects of physical and biochemical processes on the dissolved oxygen budget for the Pearl River Estuary during summer, *Journal of Marine Systems, 79*(1-2), 65–88, doi:10.1016/j.jmarsys.2009.07.002.

Zhang, H., L. Zhao, Y. Sun, J. Wang, and H. Wei (2017), Contribution of sediment oxygen demand to hypoxia development off the Changjiang Estuary, *Estuarine, Coastal and Shelf Science, 192,* 149–157, doi:10.1016/j.ecss.2017.05.006.

Zhang, J., D. Gilbert, A. J. Gooday, L. Levin, S. W. A. Naqvi, J. J. Middelburg, M. Scranton, W. Ekau, A. Peña, B. Dewitte, T. Oguz, P. M. S. Monteiro, E. Urban, N. N. Rabalais, V. Ittekkot, W. M. Kemp, O. Ulloa, R. Elmgren, E. Escobar-Briones, and A. K. van der Plas (2010), Natural and human-induced hypoxia and consequences for coastal areas: Synthesis and future development, *Biogeosciences, 7*(5), 1443–1467, doi:10.5194/bg-7-1443-2010.

Zhang, Y., and A. M. Baptista (2008), SELFE: A semi-implicit Eulerian–Lagrangian finite-element model for cross-scale ocean circulation, *Ocean Modelling, 21*(3-4), 71–96, doi:10.1016/j.ocemod.2007.11.005.

Zhu, Z.-Y., J. Zhang, Y. Wu, Y.-Y. Zhang, J. Lin, and S.-M. Liu (2011), Hypoxia off the Changjiang (Yangtze River) Estuary: Oxygen depletion and organic matter decomposition, *Marine Chemistry, 125*(1-4), 108–116, doi:10.1016/j.marchem.2011.03.005.

Zimmerman, J. T. F. (1988), Estuarine residence times, in *Hydrodynamics of estuaries,* edited by B. Kjerfve, pp. 75–84, CRC Press, Boca Raton.

Acknowledgement – Danksagung

Frank Böker, Ilse and Erwin Holzwarth, Stefan Holzwarth, Michelle Jeuken, Frank Kösters, Günther Lang, Arjen Markus, Marie Naulin, many others, Holger Rahlf, Elisabeth Rudolph, Peter Schade, Ulrike Schiller, Aissa Sehili, Rita Seiffert, Susanne Spohr, my parents Elisabeth and Reinhard Stracke, Denise Wehr, Holger Weilbeer, Norbert Winkel, Kai Wirtz.
I am very thankful for your various ways of support during the time of my dissertation. As I don't want to rank you – because all of you provided a piece of support that finally made it possible to complete the dissertation – I simply give your names in alphabetical order. And I know that you know in which way you helped me.

A special thank, however, goes to Henning, Franka and Arne. As my children, you never cared about my work, though you always accepted that I had to go there. By naturally ignoring the importance of a dissertation, you helped me in keeping life's priorities: a full fridge is more satisfying than a full hard disk, reading two more pages of our bedtime story is more exciting than writing two more sentences for my manuscript, and your scratched arm hurts worse than bloodstains on my shirt for a meeting.

Eidesstattliche Erklärung

Hiermit erkläre ich, dass die vorliegende Arbeit mit dem Titel „Implications of direct anthropogenic pressures on dissolved oxygen dynamics in a well-mixed estuary“ von mir selbstständig angefertigt wurde. Bis auf zitierte Referenzen und Beratung meiner Betreuer wurden keine weiteren Quellen verwendet und die Arbeit ist nach Inhalt und Form meine eigene Arbeit. Diese Arbeit ist unter Einhaltung der Regeln guter wissenschaftlicher Praxis der Deutschen Forschungsgemeinschaft entstanden. Sie wurde weder im Rahmen eines Prüfungsverfahrens an anderer Stelle vorgelegt noch veröffentlicht oder zur Veröffentlichung eingereicht. Ich erkläre mich einverstanden, dass diese Arbeit an die Bibliothek des GEOMAR und die Universitätsbibliothek der CAU weitergeleitet wird.

Hamburg, 08.06.2018

(Ingrid Holzwarth)